Research Paper

GEOSPHERE

GEOSPHERE, v. 15, no. 4

https://doi.org/10.1130/GES02052.1

17 figures; 3 tables; 1 set of supplemental files

CORRESPONDENCE: jason@gps.caltech.edu

CITATION: Saleeby, J., and Saleeby, Z., 2019, Late Cenozoic structure and tectonics of the southern Sierra Nevada–San Joaquin Basin transition, California: Geosphere, v. 15, no. 4, p. 1164–1205, https://doi.org/10.1130/GES02052.1.

Science Editor: Shanaka de Silva
Associate Editor: Cathy Busby

Received 7 August 2018
Revision received 24 December 2018
Accepted 9 April 2019

Published online 13 June 2019

Late Cenozoic structure and tectonics of the southern Sierra Nevada–San Joaquin Basin transition, California

Jason Saleeby and Zorka Saleeby

Division of Geological and Planetary Sciences, California Institute of Technology, Pasadena, California 91125, USA

ABSTRACT

This paper presents a new synthesis for the late Cenozoic tectonic, paleogeographic, and geomorphologic evolution of the southern Sierra Nevada and adjacent eastern San Joaquin Basin. The southern Sierra Nevada and San Joaquin Basin contrast sharply, with the former constituting high-relief basement exposures and the latter constituting a Neogene marine basin with superposed low-relief uplifts actively forming along its margins. Nevertheless, we show that Neogene basinal conditions extended continuously eastward across much of the southern Sierra Nevada, and that during late Neogene–Quaternary time, the intra-Sierran basinal deposits were uplifted and fluvially reworked into the San Joaquin Basin. Early Neogene normal-sense growth faulting was widespread and instrumental in forming sediment accommodation spaces across the entire basinal system. Upon erosion of the intra-Sierran basinal deposits, structural relief that formed on the basement surface by the growth faults emerged as topographic relief. Such "weathered out" fossil fault scarps control much of the modern southern Sierra landscape. This Neogene high-angle fault system followed major Late Cretaceous basement structures that penetrated the crust and that formed in conjunction with partial loss of the region's underlying mantle lithosphere. This left the region highly prone to surface faulting, volcanism, and surface uplift and/or subsidence transients during subsequent tectonic regimes. The effects of the early Neogene passage of the Mendocino Triple Junction were amplified as a result of the disrupted state of the region's basement. This entailed widespread high-angle normal faulting, convecting mantle-sourced volcanism, and epeirogenic transients that were instrumental in sediment dispersal, deposition, and reworking patterns. Subsequent phases of epeirogenic deformation forced additional sediment reworking episodes across the southern Sierra Nevada–eastern San Joaquin Basin region during the late Miocene break-off and west tilt of the Sierra Nevada microplate and the Pliocene–Quaternary loss of the region's residual mantle lithosphere that was left intact from the Late Cretaceous tectonic regime. These late Cenozoic events have left the high local-relief southern Sierra basement denuded of its Neogene basinal cover and emergent immediately adjacent to the eastern San Joaquin Basin and its eastern marginal uplift zone.

INTRODUCTION

The southern Sierra Nevada is widely known for its deep-level exposures of large- volume Cretaceous batholithic rocks (Nadin and Saleeby, 2008), while the San Joaquin Basin is widely known for its Neogene deep-marine conditions that produced prolific hydrocarbon reserves (Hoots et al., 1954). Rarely in the literature are the late Cenozoic geologic features of these two adjacent regions discussed in any depth together. The late Cenozoic features of these two regions speak to a number of significant issues in tectonics and geomorphology. These include: (1) the Earth's surface responses to geologically rapid changes in the distribution of mantle lithosphere loads; (2) the stability of cover strata–basement transition zones and the time scales over which profound geomorphic changes can occur between basinal and upland areas; and (3) the importance of basement structures in controlling cover strata faulting and the creation of sediment accommodation spaces. The transition between the Sierra Nevada basement uplift and the southeastern San Joaquin Basin is particularly well suited to pursue these issues because the various rock assemblages that record basement structures as well as sedimentary facies relationships track northward into broadly correlative assemblages that lack the tectonic overprints of interest.

The San Joaquin Basin lies nested within the southern Great Valley tectonomorphic province of central California. Together, the Great Valley and Sierra Nevada constitute a semi-coherent microplate that moves within the San Andreas–Walker Lane dextral transform system (Argus and Gordon, 1991; Unruh et al., 2003). Regional relief generation and erosion of the Sierra Nevada are linked to subsidence and sedimentation in the Great Valley by regional west tilt along an axis that runs along the western Sierra Nevada Foothills (Fig. 1 inset). For much of the Sierra Nevada north of 37°N, regional west tilt produces a gentle west-sloping ramp whereby Tertiary strata of the Great Valley lap eastward onto Sierran basement, and low-relief interfluve areas of the basement uplift separate deeply incised west-flowing river channels (Unruh, 1991; Clark et al., 2005). In parallel, the basement surface of the Great Valley (north of 37°N) assumes a relatively simple west slope beneath Cretaceous and Cenozoic strata, reaching a depth of ~16 km along the western margin of the Great Valley (Wentworth et al., 1995). The east-west profile of the buried basement surface and its eastward continuation with the west-sloping interfluve surface represent the idealized regional structural form of the Sierran microplate (Unruh, 1991). This regional structural form to first order was inherited from the Cretaceous Great Valley forearc basin and Sierra Nevada magmatic arc, with the Great Valley transitioning into an intermontane basin with the Late Cretaceous termination of the Sierran arc and the Cenozoic emergence of the Coast Ranges to the west (Davis and Lagoe, 1988; Lettis and Unruh, 1991; Nadin and Saleeby, 2008).

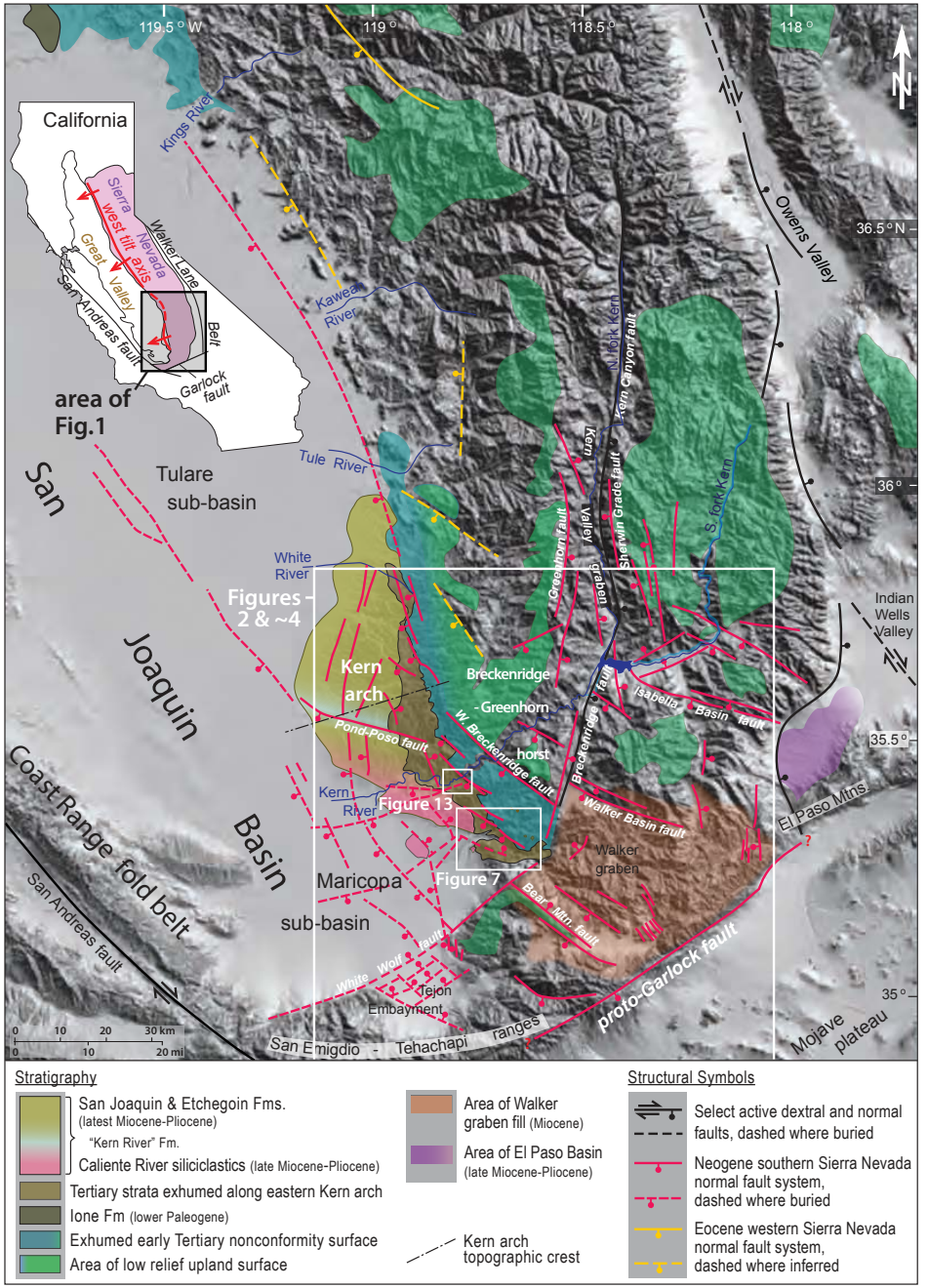

Figure 1. Regional structure and geomorphic map of the southern Sierra Nevada and adjacent Great Valley region emphasizing the Neogene southern Sierra fault system (red), which constitutes southern Sierra basement scarps, and mainly buried growth faults in the San Joaquin Basin. Additional basement scarps inferred to be early Cenozoic in age are shown in yellow, and principal faults of active plate juncture system are shown in black. Outlines of more detailed maps shown in white boxes. Sources: Bartow (1984), Unruh et al. (2003), Clark et al. (2005), Mahéo et al. (2009), Blythe and Longinotti (2013), Saleeby et al. (2013b, 2016), Sousa et al. (2016a), Figure 2, and this study.

The southern Sierra Nevada and adjacent Great Valley province (south of 37°N) are distinct in regional structure and geomorphology from the microplate to the north. In the south, both regional and local topographic relief of the Sierran uplands and structural relief on the basement surface in the Great Valley are significantly greater (Saleeby et al., 2013a, 2013b). This is a result of multiple phases of Cenozoic high-angle, mainly normal faulting (Hake, 1928; Fox, 1929; Nugent, 1942; Mahéo et al., 2009; Sousa et al., 2016a; Chapman et al., 2017) and superposed Pliocene–Quaternary epeirogenic uplift and subsidence (Le Pourhiet and Saleeby, 2013; Saleeby et al., 2013a). Additionally, the Mesozoic arc-forearc system along the southern reaches of the microplate underwent profound tectonic disruptions in Late Cretaceous time entailing whole crust-scale thrust faulting, large-magnitude crustal extension, and profound basement exhumation (Nadin and Saleeby, 2008; Nadin et al., 2016; Chapman et al., 2010, 2012, 2017). The Late Cretaceous tectonic overprint on the southern Sierra Nevada and adjacent Great Valley had a profound effect on the crustal responses to subsequent tectonic regimes, resulting in Cenozoic structural overprints that contrast the southern and northern microplate. In terms of superposed Cenozoic features, the most significant is a system of distinct fault-controlled topographic steps in the southern Sierra basement (Hake, 1928; Mahéo et al., 2009; Sousa et al., 2016a), formation of the Neogene, chiefly marine, San Joaquin Basin (Hoots et al., 1954; Bandy and Arnal, 1969; Bartow and McDougall, 1984), and areas of coupled anomalous uplift and subsidence currently expressed as the Kern arch and Tulare sub-basin within the San Joaquin Basin (Saleeby et al., 2013a). The map distribution of these features is shown on Figure 1.

In this paper, we focus primarily on late Cenozoic structural and related geomorphic features, particularly along the eastern San Joaquin Basin–western Sierra Nevada transition. We assert that rapidly evolving phases in tectonic forcing operated over the region in late Cenozoic time, entailing both plate tectonic and more localized epeirogenic geodynamic regimes. Structural inheritance is shown to have operated at a wide range of scales through Cenozoic time. We utilize surface and subsurface structural and stratigraphic mapping, geomorphic analysis, and both U/Pb zircon and Ar/Ar dating of Cenozoic volcanic rocks that sit in key structural-stratigraphic positions. We also apply to our structural analysis a large body of low-temperature thermochronometric data that have been published for the southern Sierra basement and for strata sampled in the southeastern San Joaquin Basin subsurface (Clark et al., 2005; Saleeby et al., 2007; Mahéo et al., 2009; Blythe and Longinotti, 2013; Cecil et al., 2014; Sousa et al., 2016a, 2016b).

CENOZOIC STRUCTURAL FRAMEWORK OF THE SOUTHERN SIERRA NEVADA AND EASTERN SAN JOAQUIN BASIN

The late Cenozoic tectonics of the southern Sierra Nevada–eastern San Joaquin Basin region produced distinct structural domains that include the Kern arch, the Tulare and Maricopa sub-basins, the Walker and Edison grabens, and the Breckenridge-Greenhorn horst (Figs. 1 and 2). Cenozoic high-angle faulting is widespread across each of these structural domains. On Figures 1 and 2, we differentiate several classes of Cenozoic faults. Principal members of the mainly Neogene southern Sierra fault system are shown in red on Figure 1 and in black on Figure 2. These include basement fault scarps and growth faults in the Basin, which include high-angle planar normal faults and vertical dip-slip and transfer faults (Fox, 1929; Nugent, 1942; Mahéo et al., 2009; Reid, 2009; Saleeby et al., 2013a, 2016; this study). The White Wolf, Breckenridge, and Garlock zones underwent significant high-angle normal displacements as part of the integrated southern Sierra system (Davis, 1983; Saleeby et al., 2009a, 2013a; Blythe and Longinotti, 2013). Shown in black on Figure 1 are principal active faults of the current plate juncture system. These include the San Andreas fault and dextral and normal faults of the Indian Wells–Owens Valley area, which constitute part of the Walker Lane belt (Unruh et al., 2003; Fig. 1 inset). Active faulting on Figure 2 is shown in red and includes the dextral San Andreas and sinistral Garlock faults, normal faults of the Kern Canyon–Breckenridge system, and reverse, thrust, and sinistral faults of the Tehachapi–San Emigdio fold-thrust belt (Goodman and Malin, 1992; Li et al., 1992; Malin et al., 1995; Gordon and Gerke, 2009; Nadin and Saleeby, 2010; Brossy et al., 2012; Goebel et al., 2016; Chapman et al., 2017; Davis and Namson, 2017). Shown in yellow on Figure 1 are faults and scarps of the early Cenozoic western Sierra fault system, most clearly expressed between 36°N and 37°N (Hake, 1928; Sousa et al., 2016a, 2016b).

We start our analysis with the Kern arch, which most clearly distinguishes the study region from regions to the north along the Sierran microplate.

Quaternary Kern Arch

We have integrated published and new structural, stratigraphic, and geomorphic data to define a broad arch-like uplift that formed during the Quaternary along the southeastern San Joaquin Basin between ~35.3°N and 36°N; we call this uplift the Kern arch (Mahéo et al., 2009; Saleeby et al., 2009a, 2013a, 2013b, 2016). Regionally, the arch resembles a WSW-plunging extremely open anticline, but, at local scales, attitude variations of low W-dipping beds are more strongly influenced by widespread high-angle faulting. The structural crest and the topographic crest of the arch coincide along an ~N80°E axis (Figs. 1 and 2). Structural relief across the arch can only be approximated due to its superpositioning over previously highly faulted strata with significant lateral thickness and facies changes. Based on Quaternary sediment exhumation constraints discussed below and on the elevation of denuded upper Pliocene shallow-marine strata, structural relief along the eastern margin of the arch is ~1800 m. Exhumation resulting from surface and rock uplift along the arch has exposed Tertiary strata of the southeastern San Joaquin Basin (Fig. 2).

Much of the Kern arch is covered by a thin veneer of pebble-to-boulder-size clast accumulations and soils that mask nearly pervasive vertical and high-angle normal faults of lower Miocene to Quaternary age (Fox, 1929; Nugent,

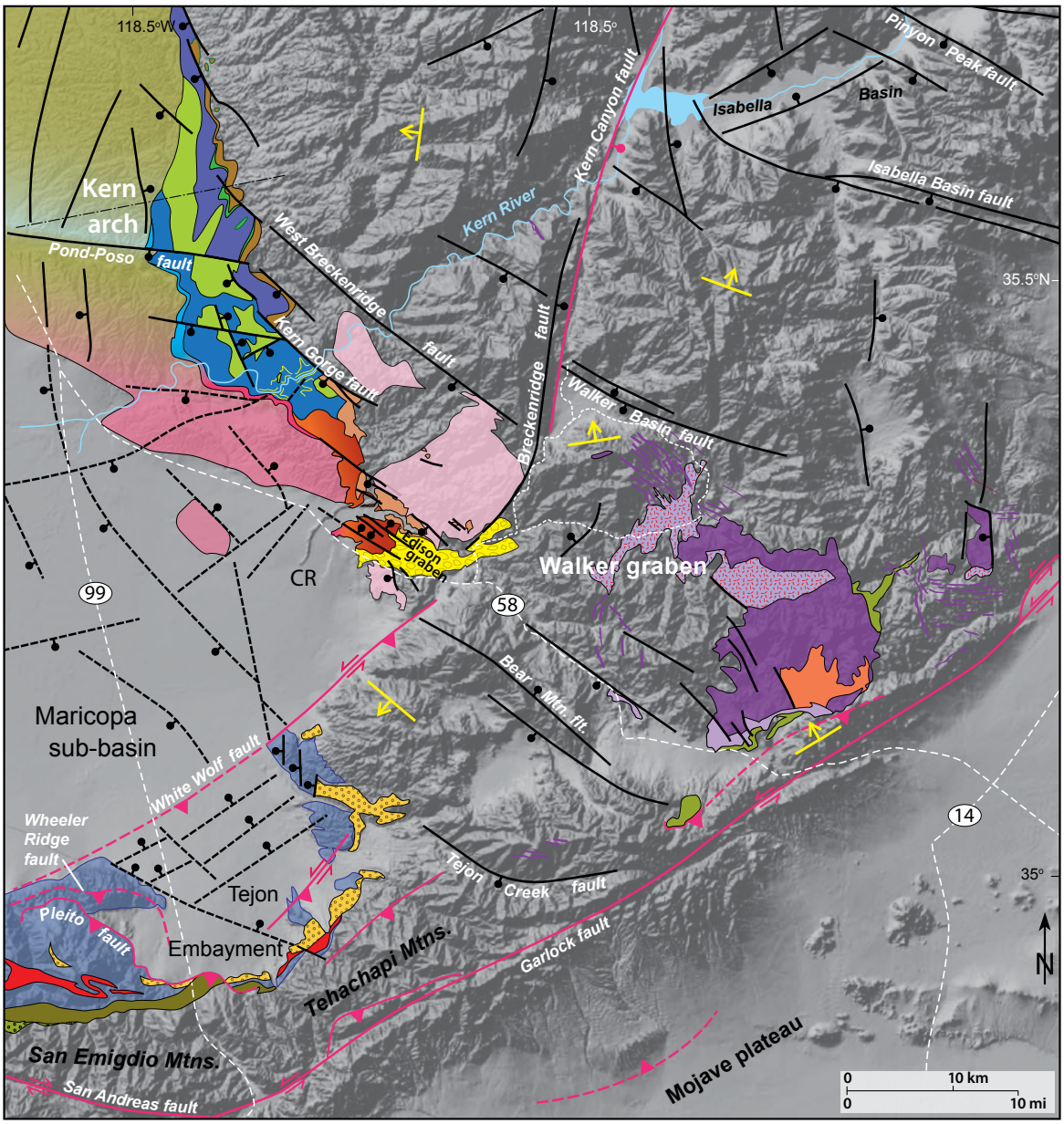

Figure 2. Structure map with selected faults of the Neogene southern Sierra fault system (black), and main active faults (red), which cut the southernmost Sierra Nevada and adjacent San Joaquin Basin. Selected Neogene sedimentary and volcanic (Fig. 3) and Late Cretaceous batholithic units also shown as discussed in text. Sources: Michael (1960), Dibblee and Louke (1970), Bartow (1984), Hirst (1986), Ross (1989), Goodman and Malin (1992), Chapman and Saleeby (2012), Chapman et al. (2017), and this study.

1942; Mahéo et al., 2009; Saleeby et al., 2009a, 2013a, 2013b). Both Fox (1929) and Nugent (1942) recognized that such faulting controls the local trellis-like drainage pattern of the arch. They also recognized that the arch is entirely under erosion and lacks surficial alluvial fans sourced from the Sierra Nevada. In contrast, multiple levels of "alluvial" terraces, mantled by "fan" deposits, are shown on published maps across the arch (Bartow, 1984; Bedrossian et al., 2012). Below we argue that these (mainly strath) terraces are mantled by locally derived coarse erosional lags resulting from rapid Quaternary erosion of the arch along its low-relief surface as it ascended from the eastern margin of the San Joaquin Basin.

Uplift and exhumation of the Kern arch is intimately related to recent surface uplift of the adjacent western Sierra Nevada (Mahéo et al., 2009; Saleeby et al., 2009a, 2013a; Nadin and Saleeby, 2010). Sierran basement adjacent to the Kern arch is broken into a wedge-shaped horst that has been named the Breckenridge-Greenhorn horst (Fig. 1), denoting Breckenridge Mountain and the Greenhorn Mountains, which formed from the elevated footwall blocks along the W-up Kern Canyon–Breckenridge-Greenhorn fault system. The southwest margin of the horst is defined by NW-striking, NE-up normal faults such as the Kern Gorge and West Breckenridge faults (Figs. 1 and 2). Numerous additional E- to NE-up normal faults and subordinate antithetic SW-up normal faults cut the Kern arch section downslope from exposed basement of the horst (Nugent, 1942; Saleeby et al., 2013a, 2013b). The antithetic faults, working in conjunction with the principal NE-up faults are important trap structures for numerous oil pools of the arch (Nugent, 1942; Reid, 2009). Kilometer-scale W-up displacement along the Kern Canyon–Breckenridge-Greenhorn fault system (Figs. 1 and 2) has imparted a west tilt to the low-relief interfluve surface of the horst, which mimics the west tilt of the greater Sierran microplate to the north.

Stratigraphic and subsurface thermochronometric data discussed below show that the Kern arch has ascended over the past 1–2 m.y., and that profound exhumation resulting from this rock and surface uplift regime has stripped the easternmost sediments of the southern San Joaquin Basin off the adjacent Sierran basement uplift (Saleeby et al., 2013a, 2013b; Cecil et al., 2014; Fig. 1). Seismicity and high-angle faulting are associated with the broad uplift of the arch, but the principal high-angle faults that cut strata of the arch and are responsible for stratigraphic growth in the basin date back to at least early Miocene time (see below).

Cenozoic High-Angle Fault Systems

In our discussions below on the Kern arch subsurface, we present data indicating significant growth of vertical and high-angle normal faults during early Neogene sedimentation. A major thrust of our research in the region has also been in the study of topographic scarps in the adjacent basement; we interpret these scarps as an eastward continuation of the Kern arch subsurface faults, now exhumed of once overlying Neogene strata. Structural and geomorphic data are integrated below with published low-temperature thermochronometric data to aid in the resolution of fault offsets (in exposed basement) that can be plausibly related to the normal growth faults in the Kern arch subsurface.

A first-order geomorphic feature of the Sierran microplate is the regional expression of a low-relief upland surface that is preserved primarily along large interfluve areas and slopes westward to continue as the basement nonconformity beneath Tertiary strata along the eastern Great Valley (Clark et al., 2005; Cecil et al., 2006; Mahéo et al., 2009; Sousa et al., 2016a). This surface was deeply incised by major west-flowing river channels in the Late Cretaceous and Eocene (House et al., 2001; Sousa et al., 2016a). The river channels developed along the western margin of an expansive orogenic plateau that along its western margin encompassed the early Sierran uplift (Nevadaplano) and predated Basin and Range extensional faulting (DeCelles, 2004; Busby and Putirka, 2009; Henry and John, 2013). The low-relief upland surface is shown to parallel regional apatite (U-Th/)He isochronal cooling surfaces of the Cretaceous Sierra Nevada batholith, for which age-elevation relationships indicate slow exhumation of the batholith from latest Cretaceous to mid-Tertiary time at a rate of ~0.05 mm/yr. Distortions and disruptions of the coherency in the regional age-elevation patterns in apatite-He ages are used to measure structural relief superposed across the geomorphic surface by Cenozoic high-angle faulting and related footwall tilting (Mahéo et al., 2009; Blythe and Longinotti, 2013; Sousa et al., 2016a). We use this relationship in our analysis of Cenozoic faulting and in our correlation of exposed basement structure with subsurface structure within the San Joaquin Basin.

Surface and subsurface structure mapping in the area of Figure 2 enlightened by measured disruptions in the regional age-elevation patterns in apatite-He ages have been used to define a primarily Neogene high-angle fault system named the southern Sierra fault system (Mahéo et al., 2009; Saleeby et al., 2013a, 2013b, 2016; Cecil et al., 2014). This system consists of a rectilinear network of NW-, N-S-, and NE-striking planar high-angle normal and vertical faults that mutually cut each other (Figs. 1 and 2). There are many more small offset faults and fault zones in the system than those shown on Figures 1 and 2. Along the eastern San Joaquin Basin, many of these faults show evidence of early Neogene and some additional early Tertiary growth (discussed below).

The southern Sierra fault system is responsible for imparting a series of topographic scarps across the southern Sierra basement, rendering local topographic relief variation that is lacking in the Sierran microplate to the north. Distinct internal topographic scarps have long been known to contrast the southern reaches of the Sierran microplate from those to the north. Hake (1928) first drew attention to a number of these scarps and hypothesized their origin by high-angle faulting. Most of the scarps recognized by Hake are north of the Figure 2 area (Fig. 1), many between 36°N and 37°N. Subsequently, Warhaftig (1965) hypothesized a solely surface weathering mechanism for the production of the scarps; this mechanism has gone untested until recently. Sousa et al. (2016a) used focused low-temperature thermochronometry across one of Hake's principal fault scarps (solid yellow line in Fig. 1), in conjunction with the regional age-elevation patterns in apatite-He ages in order to test Hake's versus Warhaftig's contrasting interpretations. Sousa et al. (2016a) show this scarp

to correspond to a fault with kilometer-scale vertical offset of late Eocene age (40–45 Ma). Basement scarps that are typically more pronounced than those recognized by Hake characterize the southern Sierra south of 36°N. Our work presented below in conjunction with that of Mahéo et al. (2009) and Blythe and Longinotti (2013) indicates mainly early Neogene normal-sense growth along these scarps. The discovery of both Neogene and late Eocene phases of faulting along these basement scarps further contrasts the southern and northern reaches of the Sierran microplate.

Normal faults of the southern Sierra system in many localities follow major Late Cretaceous basement structures. Most fundamental is the Kern Canyon–Breckenridge–White Wolf zone, which functioned as a major dextral transfer zone linked to differential large-magnitude extension and exhumation during the Late Cretaceous (Nadin and Saleeby, 2008; Saleeby et al., 2008; Chapman et al., 2012; Nadin et al., 2016). Our mapping, in conjunction with low-temperature thermochronometery (Mahéo et al., 2009), shows that the Kern Gorge fault, and at least part of the West Breckenridge fault, are precisely superposed on Late Cretaceous composite shear fabrics consisting of high-temperature mylonite and lower-temperature brittle shear fractures. Much of the basement from the Isabella Basin region to the Tejon Embayment, east and southeast of the Kern Canyon–White Wolf zone (Fig. 2), is cut by domainal sets of NW-striking greenschist- to clay-grade tensile and dilational shear fractures (Wood and Saleeby, 1998; Nadin and Saleeby, 2008; Chapman et al., 2012). Neogene normal faults such as the Pinyon Peak, Isabella Basin, Walker Basin, Bear Mountain, and Tejon Creek (Fig. 2) follow these older basement structures. In our closing tectonic analysis, we further pursue the relationships between the Late Cretaceous basement structures and Neogene normal faulting and their uniqueness to the southernmost Sierran microplate.

Neogene Grabens

One of the outstanding expressions of the southern Sierra fault system was the production of a series of grabens that served as localized accommodation spaces during the Neogene, and in particular, during the early to middle Miocene. The graben fills have been differentially eroded over late Miocene–Quaternary time with the regional uplift of the southern Sierra Nevada and Kern arch (Mahéo et al., 2009; Saleeby et al., 2016). Along the eastern margin of the Kern arch, we define a range-front graben system that runs southeastward from where the Kern River exits the western Sierra to the area of the White Wolf fault (Fig. 2). The NW-striking Kern Gorge fault and related splays form the east-bounding E-up structures, and less conspicuous parallel W-up normal faults to the west form the west-bounding structures of the graben system. We name the southeastern segment of the range-front graben system the Edison graben, which formed an important accommodation space and structural channel for sediment transport in the Neogene (Saleeby et al., 2016).

The Walker graben is a complex, structurally controlled accommodation space that developed within Sierran basement principally in early and middle Miocene time (Mahéo et al., 2009; Saleeby et al., 2009a, 2016; Blythe and Longinotti, 2013). It formed as a volcanically active graben that hosted the lower and middle Miocene Cache Peak volcanic center (Michael, 1960; Dibblee and Louke, 1970; Saleeby et al., 2016). The graben fill is internally faulted, tilted, and partially eroded off its Sierran basement. The extent of the fill, beyond its current erosional remnants, is broadly constrained by stratigraphic, geomorphic, and low-temperature thermochronometry, as detailed below. The graben is bounded by a complex array of high-angle normal faults and normal-fault–controlled tilt blocks (Figs. 1 and 2). To the northwest, the W-up Breckinridge fault and the N-up Walker Basin fault form the northwest sector of the graben. To the south, the north-tilted footwall block of the N-up proto–Garlock fault forms the south wall of the graben (Blythe and Longinotti, 2013; Saleeby et al., 2016). The southwest margin of the graben is bounded by the SW-up Bear Mountain fault, which controls west tilt on the Bear Mountain basement block. The surface of this tilted basement block extends southwestward beneath the Neogene section of the Tejon Embayment (Figs. 1 and 2). The northwest margin of the Bear Mountain block is bounded by the White Wolf fault, which during the Neogene functioned as a SE-up normal fault (Davis, 1983; Saleeby et al., 2013a). The intersection zone between the White Wolf and Breckenridge faults formed a structural-topographic saddle that linked strata of the Walker graben to that of the southeastern San Joaquin Basin (Figs. 1 and 2).

We also draw attention to other apparent Neogene age grabens to the north of the Walker graben; these grabens either did not fill with much sediment or lost most of whatever fill existed to recent erosion along the medial reaches of the Kern River. Kinematically related to the northern boundary of the Walker graben is the Isabella Basin half graben that was controlled by NE-up motion on the Isabella Basin and Pinyon Peak faults, which are interpreted to be part of the same fault set as the Walker Basin fault (Fig. 2). To the northwest of Isabella Basin is the Kern Valley graben, controlled by the W-up Greenhorn fault and the E-up Sherwin Grade fault (Fig. 1). The axial area of the Kern Valley graben hosts active W-up scarps of the Kern Canyon fault system between ~35.7°N and 36.2°N (Nadin and Saleeby, 2010; Brossy et al., 2012; Figs. 1 and 2). Based on regional fault kinematic patterns and the geomorphic state of the principal graben-forming faults, we infer that the Isabella Basin and Kern Valley grabens formed in the Neogene along with the Walker and Edison grabens, although early Cenozoic displacements along the graben-bounding faults cannot be excluded.

Tehachapi–San Emigdio Fold-Thrust Belt

The southern end of the Sierran microplate is bounded by (1) a complex structural zone consisting of the late middle Miocene to Quaternary sinistral Garlock fault and (2) along the western segment of the Garlock fault, a zone of active ~N-S shortening above blind thrusts that root into the Garlock and San Andreas faults. We call these blind thrusts the Tehachapi–San Emigdio fold-thrust belt (Nilsen et al., 1973; Davis and Lagoe, 1988; Li et al., 1992; Bawden,

2001; Gordon and Gerke, 2009; Chapman and Saleeby, 2012; Goebel et al., 2016; Davis and Namson, 2017; Fig. 2). Stratigraphic relationships within the Tejon Embayment (Hirst, 1986; Goodman and Malin, 1992; this study) and along the northern forelimb of the thrust belt to the west (Davis and Lagoe, 1988; Gordon and Gerke, 2009; Chapman and Saleeby, 2012) indicate that much or all of the topographic relief resulting from fold-thrust deformation was generated in latest Pliocene(?)–Quaternary time. These relationships include: (1) the presence of fine-grained upper Pliocene shallow-marine–lagoonal strata of the San Joaquin Formation laying in conformable stratigraphic succession within the northern forelimb of the belt; (2) unconformably overlying deeply dissected, actively tilting lower Pleistocene alluvial fan deposits that contain clast populations that were derived from distinctive basement rocks that are exposed south of the Garlock–San Andreas fault intersection zone (J. Saleeby and A.D. Chapman, 2010, personal commun.); and (3) seismic-reflection data that show much of the foredeep deposition occurred over the past 1 m.y. (Gordon and Gerke, 2009, their figure 5). Active ~N-S shortening within the basement along the fold-thrust belt is expressed by the 2015 M = 4.7 and 1952 M = 7.8 reverse-sense earthquakes with epicenters near the White Wolf fault within the Tejon Embayment (Bawden, 2001; Goebel et al., 2016). It is not known whether the principal slip patches for these events were on the White Wolf fault proper or adjacent blind basement thrusts like those deduced by Gordon and Gerke (2009) and Davis and Namson (2017).

The geological youthfulness of the Tehachapi–San Emigdio fold-thrust belt bears on the offset history of the White Wolf fault and the subsidence history of the Maricopa sub-basin. The Maricopa sub-basin is commonly assumed to be the foredeep to active north-directed thrust motion along the White Wolf fault (e.g., Stein et al., 1988). However, the extraordinary thickness of Neogene strata that lie in the sub-basin was deposited during the White Wolf fault's SE-up normal displacement phase, prior to the late Pliocene–Quaternary initiation of the fold-thrust belt (Hirst, 1986; Davis, 1983; Gordon and Gerke, 2009; Saleeby et al., 2013a; Davis and Namson, 2017; and below). We also emphasize that the White Wolf fault originated as a major basement structure in the Late Cretaceous in continuity with the Kern Canyon fault system (Nadin and Saleeby, 2008; Saleeby et al., 2009b; Chapman et al., 2012). It was remobilized as a Neogene normal fault and then again as a Quaternary N-directed reverse fault. The "foredeep" position of the Maricopa sub-basin relative to the White Wolf fault is fortuitous.

STRUCTURAL AND STRATIGRAPHIC LINKAGES BETWEEN THE SOUTHEASTERN SAN JOAQUIN BASIN AND THE WALKER GRABEN

Stratigraphic Framework

Figure 3 shows generalized stratigraphic columns for the Kern arch and Tejon Embayment of the southeastern San Joaquin Basin and rocks of the Cache Peak volcanic center within the Walker graben fill. Table 1 gives an overview of the lithologic character and depositional environments for the stratigraphic units shown in Figure 3. Our focus is on the use of the stratigraphy for structure mapping, both surface and subsurface in the Kern arch area, and for the establishment of regional facies relations and paleogeographic patterns. Because the Neogene section of the Kern arch is dominated by alluvial, fluvial, and deltaic facies, paleontological age data are sparse. To supplement the sparse set of published age constraints, we present new U-Pb zircon and Ar-Ar plagioclase data on key volcanic rock intervals. As discussed below, these new data point to a lower Miocene chronostratigraphic "horizon" between the Walker graben fill and the southern Kern arch in the form of a volcanic ash sequence that was erupted over an ~2 m.y. span. The ash layers are numerous, reach up to 3 m of thickness proximal to the volcanic center, and occur locally as more distal deposits within Kern arch strata. Below, we cover the new age data and the stratigraphic settings of their sample sites.

Lower Miocene Chronostratigraphic "Horizon"

A primary focus of our field studies has been the detailed relations along the basement nonconformity that is exposed along the eastern margin of the Kern arch. Fortunately, we have found felsic ash beds that are useful for time-stratigraphic applications at numerous locations at or very near the base of the Tertiary section along the nonconformity. We have sampled such ashes at ten locations and have recovered microphenocryst zircon populations from six of these that could be dated by U-Pb techniques (map locations on Figs. 4 and 7). We have also found that the Neogene strata that lie above the ash-bearing strata located south of the crest of the Kern arch contain abundant pebbles, cobbles, and boulders that were derived from the Cache Peak volcanic center. This led us to search for possible correlative explosive felsic volcanic units in the Cache Peak eruptive stratigraphy. We have found likely correlative felsic ash-flow, air-fall, and water-laid tuffs within the proximal zone of the Cache Peak center and more distally within siliciclastic strata that lie near the base of the Walker graben fill.

The Cache Peak volcanic center consists of an andesitic to basaltic stratocone complex that also includes abundant silicic pyroclastic, dome, and hypabyssal rocks (Michael, 1960; Dibblee and Louke, 1970; Quinn, 1987; Coles et al., 1997; Saleeby et al., 2016). Proximal and distal eruptives from the center are interbedded with siliciclastic strata of the Kinnick and Bopesta formations (Fig. 3B). Lower-level ignimbrites from the Cache Peak volcanic center produced extensive ash-flow and air-fall deposits that are interbedded with the Kinnick Formation. We recovered zircon from two felsic eruptives at locations as deep in the volcanic section as accessibility would permit and also a felsic hypabyssal unit that cuts basement. To these, and to the six ashes from the Kern arch that yielded microphenocryst zircon, we employed laser ablation–inductively coupled plasma mass spectrometry (LA-ICP MS) techniques to determine U-Pb ages of zircon grains that are interpreted as eruptive ages. Analytical

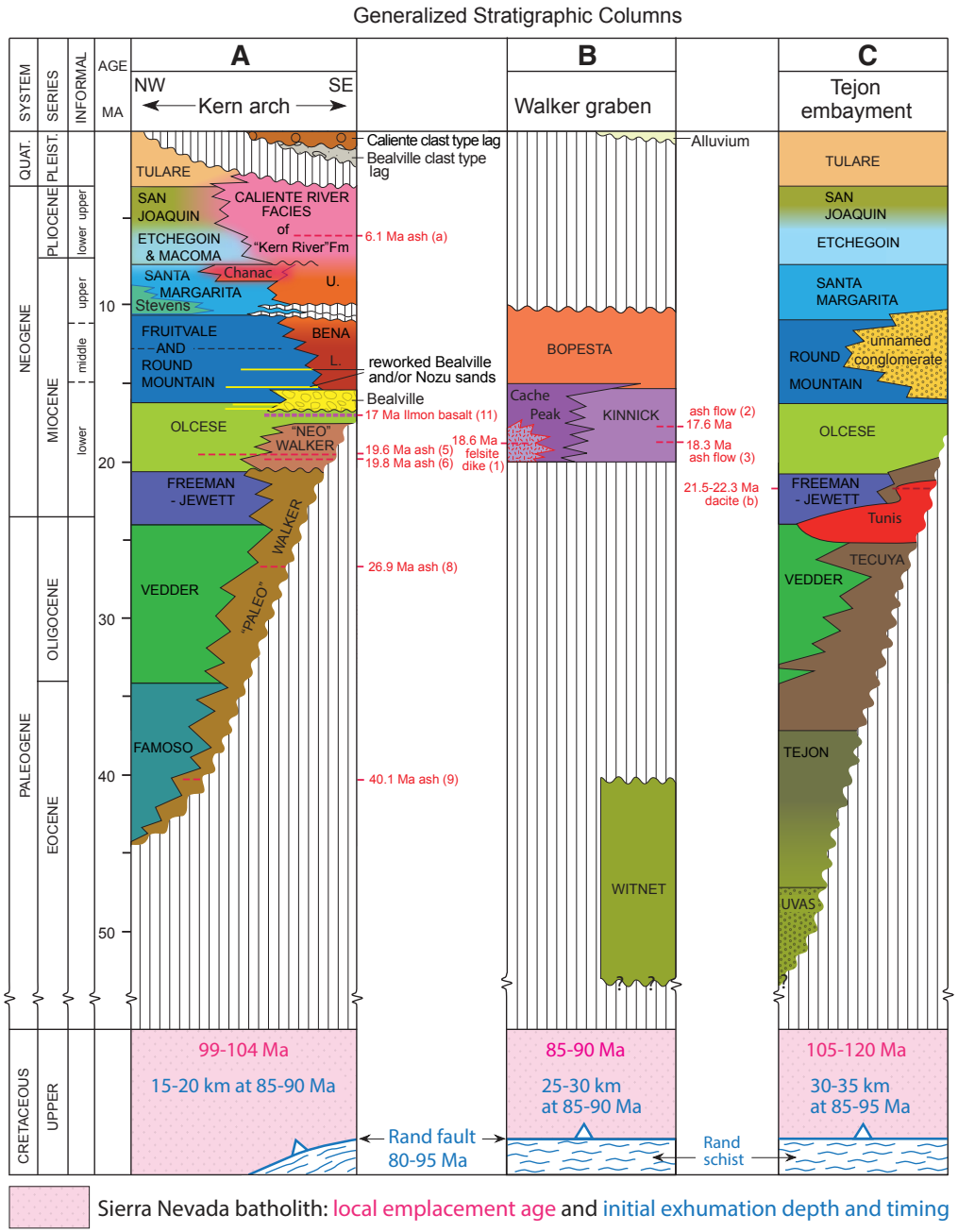

Figure 3. Generalized stratigraphic columns for formal and informal stratigraphic units designated in maps and structure sections of this study. Sources given in Table 1. Select ages for volcanic intervals given as sample numbers from Table 2 and Figure 4, and for (A): Baron et al. (2007) and (B) Nilsen et al. (1973). For more aerially extensive overview of San Joaquin Basin stratigraphy, see Hosford Scheirer and Magoon (2003). Basement relations are derived from Wood and Saleeby (1998), Saleeby et al. (2007), and Chapman et al. (2012, 2017). (A) Kern arch including proximal areas of Tulare and Maricopa sub-basins; (B) Walker graben remnant inlier exposures; and (C) Tejon Embayment along footwall of Pleito-Wheeler Ridge thrust system.

TABLE 1. LITHOLOGIC AND DEPOSITIONAL ENVIRONMENT OVERVIEW OF STRATIGRAPHIC UNITS SHOWN IN FIGURE 3

Unit	Overview	Sources
Kern arch and Tejon embayment		
Tulare	Alluvial and fluvial sand, gravel, and lacustrine mud	5, 20, 24
San Joaquin	Shallow-marine and estuary silt, mud, and fine sand	5, 19, 24, 33
Etchegoin	Shallow-marine sand and silt	5, 19, 24, 33
Kern River	Fluvial, alluvial; and deltaic gravel, sand, and mud	4, 5, 7, 23, 33
Chanac	Fluvial and deltaic gravel and sand	5, 6, 8, 27, 33, 36
Santa Margarita	Shallow-marine sand	1, 2, 5, 6, 13, 16, 17, 18, 24, 25
Stevens	Submarine fan sand and mud	15, 16, 33
Upper Bena	Alluvial and fluvial sand and gravel	5, 6, 33, 37
Lower Bena	Shallow-marine sand and mud and Cache Peak–derived marine mud flow	5, 6, 12, 33, 37
Bealville	Chaotic boulder fan and bedded terrestrial and marine debris flows	12, 32, 37
Nozu	Marine sands and grits with high detrital biotite modes	6, 8, 21, 37
Monterey	Bathyal marine diatomite, chert, siltstone, and shale	3, 5, 6, 13, 14, 15, 17, 18, 25
Fruitvale and Round Mountain	Upper bathyal marine mud, silt, fine sand, shale, and diatomite	1, 2, 3, 5, 6, 8, 27, 28, 29, 32
Unnamed Conglomerate	Alluvial to shallow-marine cobble and boulder conglomerate	13, 17, 18, 37
Olcese	Shallow-marine sand and gravel, with mid-level alluvial unit	5, 6, 27, 28, 33, 37
Tunis-Tecuya	Alluvial and shallow-marine sand and gravel; and mid-level section of basalt, dacite, and rhyolite	13, 14, 25, 34
(Neo)Walker	Fluvial and alluvial sand and gravel	5, 6, 12, 33, 37
Freeman-Jewett	Marine silt and shale with lower level sands	3, 5, 6, 8, 26
Vedder	Shallow-marine and alluvial sand	5, 6, 35
Famoso	Marine sand	6, 31, 35
(Paleo)Walker	Fluvial and alluvial sand and gravel	5, 6, 27, 28, 37
Tejon	Marine sand, shale, and silt; local conglomerate	9, 13, 25
Uvas	Marine sand and boulders deposited in supra-detachment basin	9, 13
Walker graben		
Bopesta	Fluvial and alluvial sand and gravel with volcanic interbeds	11, 22, 30
Kinnick	Felsic ash and tuff, alluvial and fluvial sand and gravel, lacustrine mud with volcanic interbeds	10, 11, 22, 30, 33, 37
Cache Peak	Basal silicic pyroclastic sequence, basalt and andesite flows, dacite domes, plugs, and hypabyssal stocks and dikes, with local lenses of upper Kinnick and lower Bopesta siliciclastics	10, 11, 22, 30, 33, 37
Witnet	Fluvial and deltaic sands and gravels deposited in supra-detachment basin	9, 11, 22, 37

Sources: 1—Addicott, 1965; 2—Addicott, 1970; 3—Bandy and Arnal, 1969; 4—Baron et al., 2007; 5—Bartow, 1992; 6—Bartow and McDougall, 1984; 7—Bartow and Pittman, 1983; 8—Calloway, 1990; 9—Chapman et al., 2012; 10—Coles et al., 1997; 11—Dibblee and Louke, 1970; 12—Dibblee and Warne, 1986; 13—Goodman and Malin, 1992; 14—Gordon and Gerke, 2009; 15—Harrison and Graham, 1999; 16—Hewlett and Jordon, 1993; 17—Hirst, 1986; 18—Hirst, 1988; 19—Klausing and Lohman, 1964; 20—Lettis and Unruh, 1991; 21—MacPherson, 1977; 22—Michael, 1960; 23—Miller, 1986; 24—Miller, 1999; 25—Nilsen et al., 1973; 26—Olson, 1988; 27—Olson, 1990; 28—Olson et al., 1986; 29—Pyenson et al., 2009; 30—Quinn, 1987; 31—Reid, 1988; 32—Saleeby et al., 2013b; 33—Saleeby et al., 2016; 34—Sharma et al., 1991; 35—Tye et al., 1993; 36—Wilson and Prothero, 1997; 37—this study.

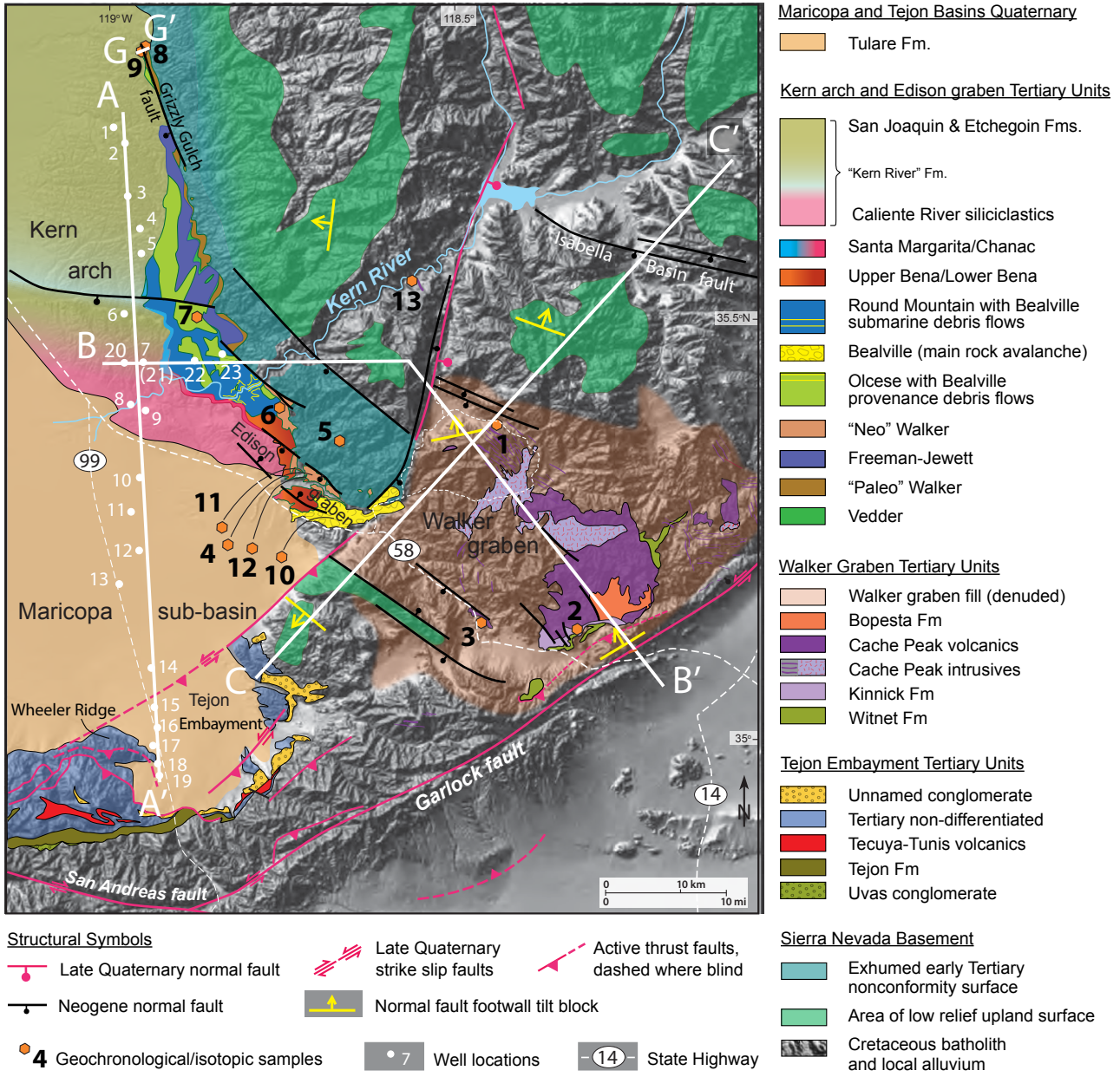

Figure 4. Generalized geologic map emphasizing upper Cenozoic units and selected geomorphic features of the southern Sierra Nevada and adjacent San Joaquin Basin, showing regional cross-section lines, well locations used for subsurface study, and locations and numbers for geochronology and geochemistry samples. Derived from Figure 2.

data are presented in Supplemental Item 1[1]. Between 64 and 94 zircon grains were analyzed for each sample, for which 10–47 grains constituted cognate microphenocrysts, and the remaining grains were xenocrysts that were entrained from batholithic basement and/or Kinnick siliciclastic strata. The age patterns of the xenocrystic grains were discussed in Saleeby et al. (2016) in the context of basement age patterns and detrital-zircon age patterns in Neogene strata of the region. We focus here on eruptive age constraints and on their time stratigraphic implications.

Age and location data for zircon microphenocrysts recovered from the basal Cache Peak volcanic center and for ash deposits laying adjacent to the Kern arch basement nonconformity are given in Table 2. We focus here on samples 1 through 7, all of which yield early Miocene ages. Samples 1 through 3 are from the Cache Peak volcanic center, and 4 through 7 are from the eastern margin of the Kern arch. The ages for samples 1 through 7 were derived from the means of zircon $^{206}Pb/^{238}U$ ages (Supplemental Items 1 and 2 [footnote 1]). Poor precisions of the $^{207}Pb/^{235}U$ zircon ages prohibited the use of concordia plots for samples 1 through 7. We interpret the $^{206}Pb/^{238}U$ mean ages as good approximations for eruptive ages of samples 1 through 7.

The entire age range for samples 1 through 7 is 17.7–19.8 Ma. We also note that this is within the 20–16 Ma magnetostratigraphic age range determined for proximal rocks of the Cache Peak center (Coles et al., 1997). We adopt an age range of 15–20 Ma for the Cache Peak center based on these data, the stratigraphic positions of samples 2 and 3, and also on the 15–20 Ma age range determined for numerous detrital-zircon grains dated from Neogene siliciclastic strata from the eastern San Joaquin Basin, which also contains Cache Peak center-derived conglomerate clasts (Saleeby et al., 2016). In the $^{206}Pb/^{238}U$ age distribution plots of Supplemental Item 2, there is a small subset of grains with ages that range back to ca. 25 Ma (eight out of 187 total grains); these grains are deleted from the age means but have analytical uncertainties that are comparable to those of the grains that are used in the means. We defer the interpretation of these aberrant-aged grains to our discussion of the tectonics of early Miocene volcanism.

Turning attention back to the eruptive ages for samples 1–7 (Table 2), note that samples 1 and 2 are from proximal areas of the Cache Peak center. Sample 1 is a thick dacite dike that is part of a voluminous felsic hypabyssal complex that extends off the northern margin of the volcanic center. This particular dike was sampled from the hypabyssal complex for its structural relationships that are discussed below under "syndepositional faulting." Sample 2 is from a clast-free ash-flow tuff (Fig. 5A) from basal ignimbrites that lie in the Kinnick Formation. Accessibility restrictions prohibited the mapping and sampling of the basal zone of this sequence; therefore, the ca. 17.6 Ma interpreted eruption age of this sample represents the medial stages of the basal Cache Peak ignimbrite eruptions. Sample 3 consists of a distal ash-flow tuff that lies in the westernmost outlier exposure of the Kinnick Formation. Here, the Kinnick consists of lacustrine strata containing dozens of distinct tuff beds (Fig. 5B) with multiple ash-flow tuffs lying along the base of the section nonconformable above basement. Sample 3 is from one of the higher-level ash flows within the lacustrine section (Fig. 5C). Coarse basement-derived debris flows lie with erosional unconformity above the dated ash flow. The debris flows are discussed further below. Accessibility restrictions also prohibited the study and sampling of the lower levels of the ash flows; thus, this location also provides age data on the medial phases of Cache Peak lower-level ignimbrite eruptions. Sample 3 yields an interpreted eruption age of ca. 18.3 Ma.

Ash layers dated along the eastern margin of the Kern arch are useful for both stratigraphic correlations and for analysis of the timing of growth faulting. Samples 4 through 6 are from the lower levels of the Walker Formation (Figs. 3A and 4), south of the lower Kern River Gorge area. Sample 4 is from the upper of two distinct, ~2–4-m-thick fluvially reworked ash beds that were deposited within the easternmost Edison graben (Saleeby et al., 2016; Fig. 6B). Figure 5D shows the lower of the two beds, which only yielded basement-derived xenocrystic zircon, consistent with a high concentration of basement clasts. Additionally, there are numerous other thinner, fluvially reworked ash beds within the Walker section of this area. Sample 4, which contains only sparse exotic clasts, yielded an interpreted eruption age of ca. 17.8 Ma (Table 2). Sample 5 is from the lowermost levels of an erosional outlier of the Walker Formation, exposed upslope from the Edison graben where the basal Tertiary nonconformity surface has been denuded over an extensive area (Fig. 4). Sample 5 yields an interpreted eruption age of ca. 19.6 Ma (Table 2). Sample 6 is from a fluvial, or shallow-marine, reworked ash layer from the lower (Neo)

TABLE 2. DATA AND LOCATION OVERVIEW FOR U/Pb ZIRCON AND Ar/Ar PLAGIOCLASE GEOCHRONOLOGICAL SAMPLES AND BULK-ROCK Sr AND Nd ISOTOPIC SAMPLES

Sample	Latitude (°N)	Longitude (°W)	Age (Ma)
1. Cache Peak dacite dike	35.38113	118.41273	18.63 ± 0.55
2. Kinnick Formation ash-flow tuff	35.18637	118.34263	17.57 ± 0.13
3. Kinnick Formation distal ash flow	35.17139	118.47639	18.34 ± 0.20
4. Walker Formation fluvial reworked tuff	35.33849	118.71859	17.75 ± 0.35
5. Basal Walker Formation outlier air-fall ash	35.37001	118.67561	19.56 ± 0.30
6. Walker Formation fluvial reworked ash	35.41344	118.75229	19.79 ± 0.27
7. Olcese Formation shallow-marine reworked tuff	35.51287	118.90165	19.47 ± 0.59
8. Basal Walker Formation reworked ash	35.82053	118.93980	26.94 ± 0.20
9. Basal Walker Formation reworked ash	35.81923	118.94182	40.10 ± 0.27
10. Bealville Formation biotite tonalite clast	35.27860	118.69050	98.66 ± 0.53
11. Ilmon pillow basalt	35.34253	118.74543	17.0 ± 0.20*
			Sr_i and εNd(t)
11. Ilmon pillow basalt	35.34253	118.74543	0.704414 + 4.74
12. Ilmon basalt massive flow interior	35.33317	118.72782	0.703769 + 4.62
13. Lower Kern River basaltic dike	35.58322	118.53305	0.704730 + 1.91

*Average of Ar/Ar plagioclase isochron and stepwise-heating ages; average is used for samples 11, 12, and 13 Sr_i and εNd(t) age corrections (Supplemental Files 3, 4, and 5 [see text footnote 1]). Other age entries are U/Pb zircon ages (Supplemental Files 1 and 2).

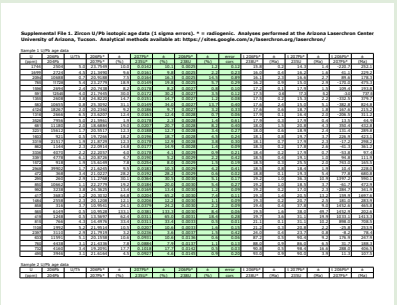
Supplemental File 1. Zircon U/Pb isotopic age data (1 sigma errors). * = radiogenic. Analyses performed at the Arizona Laserchron Center University of Arizona, Tucson. Analytical methods available at: https://sites.google.com/a/laserchron.org/laserchron/

[1]Supplemental Files. Geochronological data tables and age plots, and structure section displaying subsurface stratigraphic picks. Please visit https://doi.org/10.1130/GES02052.S1 or access the full-text article on www.gsapubs.org to view the Supplemental Files.

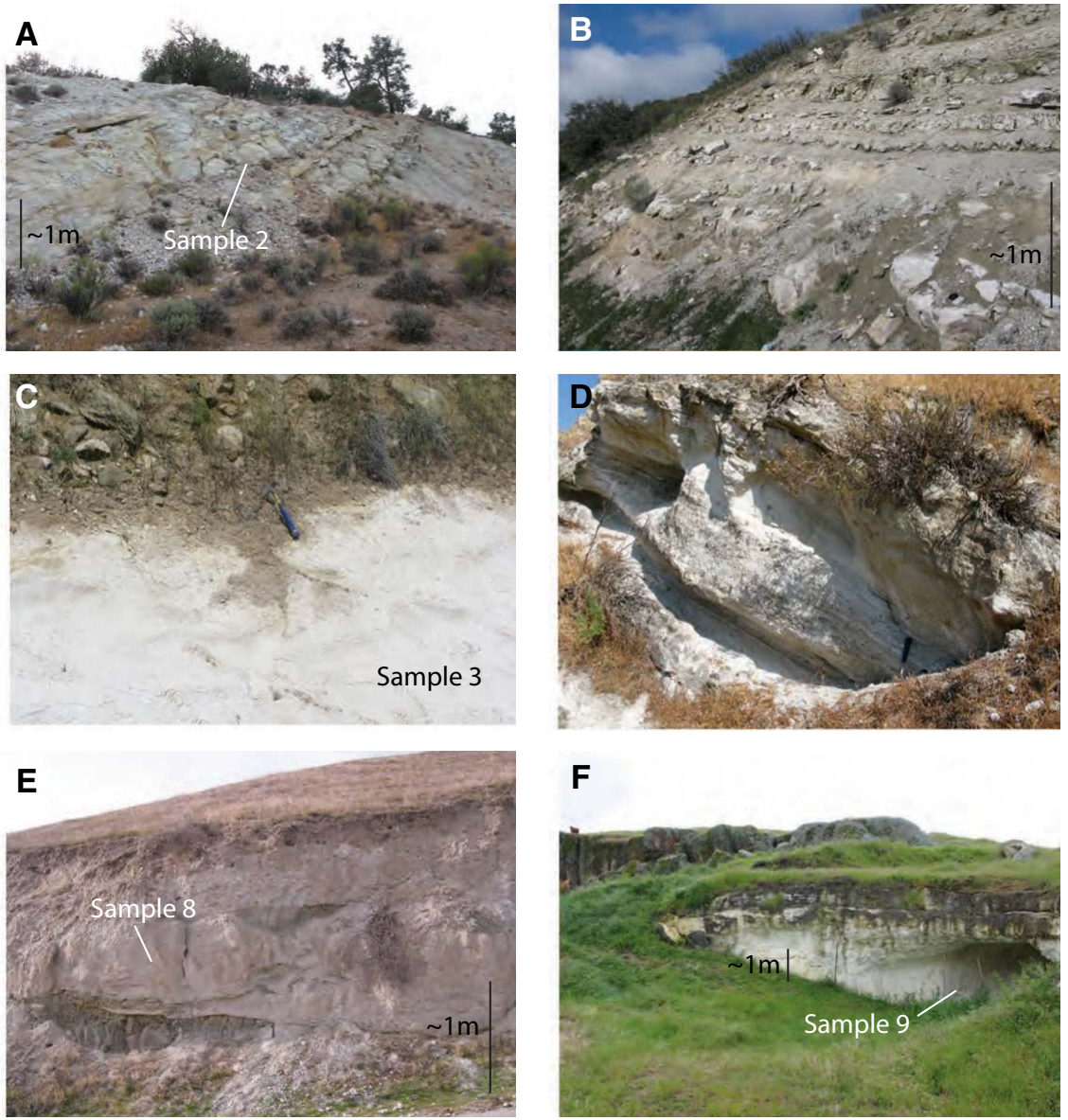

Figure 5. Field photos of volcanic ashes from the Walker graben fill and the eastern margin of the Kern arch. (A) Basal ignimbrite sequence of Cache Peak center within the Kinnick Formation consisting of air-fall and ash-flow tuffs showing sample 2 location; (B) western Kinnick Formation outlier showing sequence of water-laid tuffs and lacustrine mud and fine sand; (C) western Kinnick Formation outlier showing sample 3 ash-flow tuff with overlying basement-derived debris flow; (D) fluvially reworked ash within lower Miocene Walker Formation of Edison graben fill; (E) fluvially reworked ash of sample 8 location within Oligocene Walker Formation of northern Kern arch; (F) silicic ash of sample 9 location at base of upper Eocene Walker Formation of northern Kern arch.

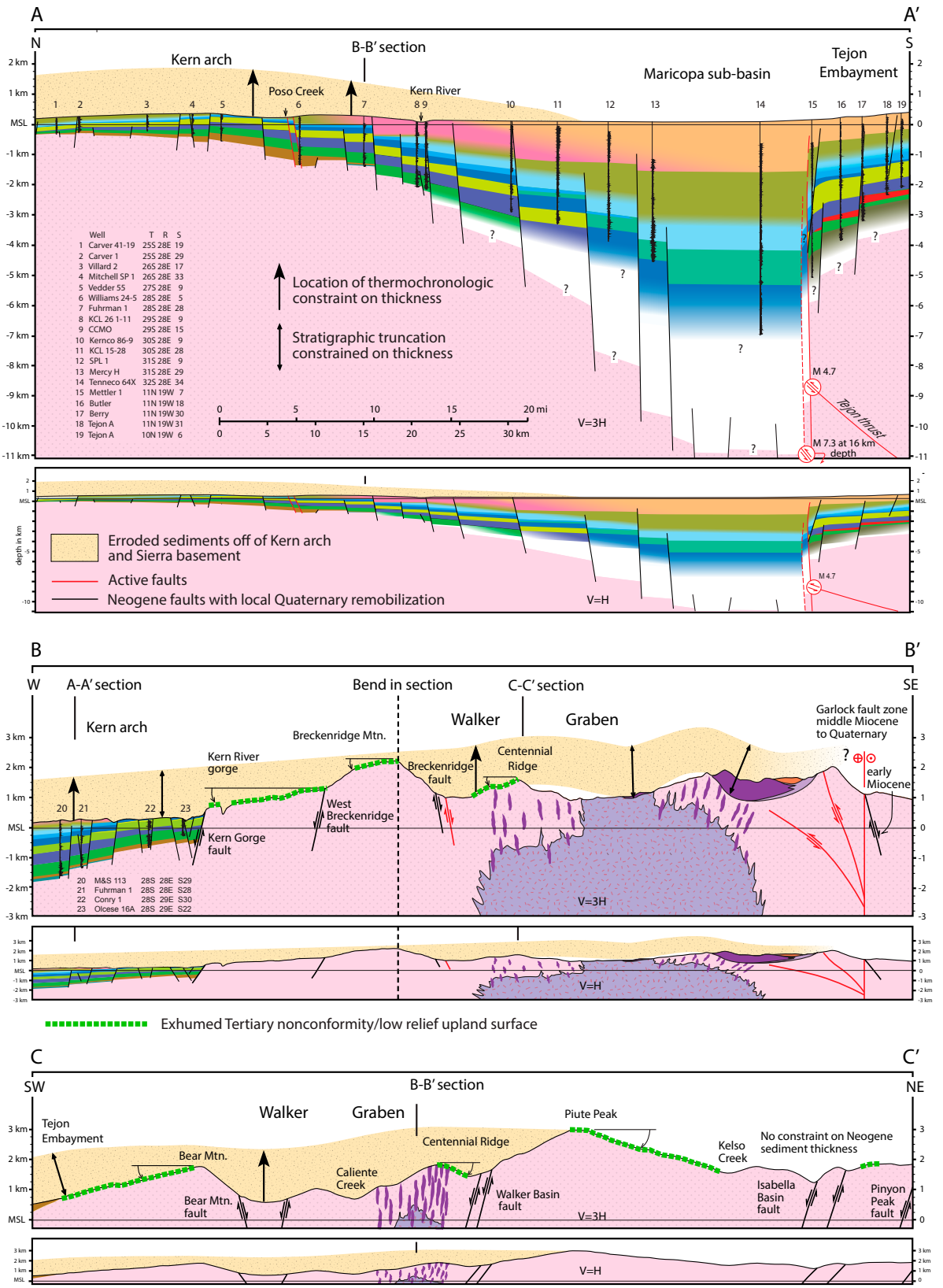

Figure 6. Regional structure sections along the southeastern San Joaquin Basin and across the southernmost Sierra Nevada. Surface traces shown on Figure 4. (A) North-south section across Tejon Embayment footwall of Pleito-Wheeler Ridge fault system, Maricopa sub-basin and southern Kern arch. Subsurface structure based on wells indicated, wells studied in Saleeby et al. (2013a, Fig. 8), and seismic-reflection data (Black Coral Inc., 2008, personal commun.); (B) Northwest-southeast section across Garlock fault, Walker graben, Breckenridge Mountain horst, and Kern arch. Subsurface structure based on wells indicated, and those in Mahéo et al. (2009, figure 9), Saleeby et al. (2009a, figure 3), and Saleeby et al. (2013a, figure 5). Surface geology based on Michael (1960), Dibblee and Louke (1970), Mahéo et al. (2009), Chapman et al. (2017), and this study; (C) northeast-southwest section across eastern margin of Tejon Embayment, Walker graben, Piute Range tilt block, and Isabella Basin margin (after Bartow, 1984; Mahéo et al., 2009; Blythe and Longinotti, 2013; this study). V=H—vertical scale equals horizontal scale; V=3H—vertical scale equals 3× horizontal scale.

Walker Formation farther north, where it interfingers with the shallow-marine Olcese Formation (Figs. 3 and 4). It yields an interpreted eruption age of ca. 19.8 Ma. Farther north, sample 7 was taken from a reworked ash layer within the shallow-marine Olcese Formation (Fig. 4). It yielded an interpreted eruption age of ca. 19.5 Ma (Table 1).

Bartow and McDougall (1984) report a 21.4 ± 0.6 Ma age for an "ash-flow tuff" from the section in which our 17.8 Ma sample 4 occurs. These authors did not include detailed sample location data, and we have only observed fluvially reworked ashes in this section. These authors also report 21.8 ± 0.6 Ma sanidine and 21.8 ± 0.6 Ma plagioclase K/Ar ages and a 15.5 Ma zircon fission-track age from a pumice clast within the middle Olcese. Detailed sample location data were not provided for this sample either. These authors discount these K/Ar ages in favor of the 15.5 Ma fission-track age. Such a young age for the Olcese is inconsistent with our samples 4–7 data and with our observations of the Olcese and (Neo)Walker being at least in part in facies relationship (Fig. 3A).

Distal ash-flow and air-fall deposits derived from the early explosive phases of the Cache Peak volcanic center were channeled into the Edison and other range-front grabens and fell across exhumed basement of the graben system's eastern wall, most to be reworked under fluvial and shallow-marine conditions. Surface and subsurface mapping of the Edison graben fill reveals the presence of a greater number and thicker beds of ashes within both the Walker and Olcese formations relative to adjacent correlative stratigraphy outside the bounds of the graben. We interpret this to reflect the importance of the Edison graben as a localized accommodation space, as well as the eastern end of the graben projecting into the structural-topographic saddle of the Breckenridge–White Wolf (faults) intersection zone, which provided a breach in the western wall of the Walker graben (Figs. 1 and 2). Structural and/or stratigraphic relations of samples 4 and 6 within graben fill sections, in conjunction with the sample 5 tuff that lie directly on upland exposed basement, suggest that graben growth initiated in the early Miocene, near the time of the initiation of the Cache Peak volcanic center. The occurrence of coarse conglomerates (boulder beds) capping the distal eruptive stratigraphy of the westernmost Kinnick outlier section (Fig. 5C) further indicates fault scarp growth in the region at this time, a subject developed further below.

Additional ash layers were discovered along the base of the Walker Formation at the northern terminus of the Walker outcrop belt (samples 8 and 9; Figs. 4, 5E, and 5F). These layers yielded U-Pb zircon ages of 26.9 Ma and 40.1 Ma, respectively (Table 2; Supplemental Items 1 and 2 [footnote 1]) and are accordingly discussed below under "early Cenozoic activity along the southern Sierra fault system."

Regional Structure Sections

A number of structure sections have been published for the transitions between the Kern arch and both the Walker graben and Breckenridge-Greenhorn horst (Mahéo et al., 2009; Saleeby et al., 2009a, 2013a, 2016). In Figure 6, we expand on these sections in some detail using well log and core data from the southern San Joaquin Basin, as well as surface mapping across the Kern arch and adjacent Sierran basement. These regional structure sections show the generalized geometry of the southern Sierra fault system and its role in creating both Neogene sediment accommodation spaces and relief on the subsurface and exposed basement surface. Also shown are normal-fault footwall tilt blocks that are demarked by the exhumed Tertiary nonconformity and low-relief upland surface tilts. The traces of the Figure 6 structure sections (Fig. 4) were chosen in order to display basin structure from the Kern arch southward across the Maricopa sub-basin and adjacent Tejon Embayment margin (Fig. 6A) and generally west to east across the Basin margin and the adjacent Sierran uplift (Figs. 6B and 6C). We have drawn the Figure 6A section to the east of active thrust lateral ramps within the cover strata in order to emphasize the Neogene normal offset relationships of the White Wolf fault (Figs. 4 and 6A). We also show on Figure 6 that a substantial thickness of Neogene strata has been eroded off the Kern arch and adjacent Sierran basement. We utilize low-temperature thermochronometry (Mahéo et al., 2009; Blythe and Longinotti, 2013; Cecil et al., 2014) in conjunction with structural and stratigraphic relations to constrain the spatial thickness patterns of the eroded strata.

Neogene Sediment Burial across the Southern Sierra Nevada Region

Structure sections extending across the Kern arch and adjacent Sierra Nevada and Walker graben suggest that up to ~1.8 km of Neogene strata once covered much of the region and have been largely removed by erosion in the Quaternary (Mahéo et al., 2009; Saleeby et al., 2009a, 2013a, 2016; Fig. 6). Here we utilize published low-temperature thermochronometry interfaced with structural and stratigraphic relations in order to reconstruct the former thickness of Neogene strata that once rested on the Kern arch and adjacent Sierran basement. These data are also used to reconstruct the paleorelief patterns across the basement surface during early Neogene time. The paleorelief patterns are, in turn, interpreted in the context of Neogene faulting. Several aspects of low-temperature thermochronometry are leveraged against structural and stratigraphic relations in order to constrain the amount of paleorelief on the basement and sediment overburden that existed in the Neogene. First, there is the relationship between the regional low-relief upland surface and the coherency in the regional primary age-elevation patterns in apatite-He ages for the Sierran basement regions that have remained undisturbed through their rock and surface uplift history. Disruptions in this relationship may be used for the approximations of high-angle fault offsets and fault block tilts (Mahéo et al., 2009; Blythe and Longinotti, 2013; Sousa et al., 2016a). This relationship may also be used to determine basement domains that have escaped notable Cenozoic deformation and/or sediment burial (House et al., 2001; Clark et al., 2005). Second, there are distinct signatures in the dispersion of apatite-He ages, as a function of U and Th concentrations that occur due

to reheating within or below a given sedimentary section (age-effective U concentration relationship of Shuster et al., 2006; Flowers et al., 2007, 2009). This relationship may be used to reconstruct the depth of sediment burial of the underlying basement or the depth of burial within a given sedimentary section for detrital-apatite populations.

In Figure 6, sediment thickness reconstructions that utilize this relationship are based on nominal values for the geothermal gradient of ~25 °C/km, apatite-He closure temperature of ~60 °C, and partial He retention between 40 °C and 60 °C (Wolf et al., 1996; Flowers et al., 2009; Mahéo et al., 2009; Cecil et al., 2014). The fact that erosional truncations of stratigraphic sections from both the Kern arch and the Walker graben are comparable to erosional thickness values derived from the apatite-He data (Fig. 6) lends confidence to the thickness reconstructions based on the apatite-He data.

In Figure 6B, we show a section that extends NW-SE from the SE-facing Garlock fault scarp across the Breckenridge fault and then bends to an E-W trace to the medial reaches of the Kern arch. This section shows NW tilt of the northwest wall of the Garlock fault, which is also expressed in the dip of the nonconformity along the base of the lower Paleogene Witnet Formation (after Dibblee and Louke, 1970; Saleeby et al., 2016; Chapman et al., 2017). The NW tilt has been accentuated by Quaternary blind thrusts of the Tehachapi–San Emigdio belt; however, a north-south transect across the north wall of the Garlock fault utilizing coupled zircon and apatite fission-track and apatite-He ages shows this tilting to be primarily early Miocene in age and linked to proto–Garlock fault normal displacements (Blythe and Longinotti, 2013). This phase of normal faulting clearly predates the middle to late Miocene initiation of left slip along the Garlock fault (Monastero et al., 1997; Andrew et al., 2014) and accounts for the SE-facing topographic scarp of the Garlock fault. The southward pinch-out pattern of thicker Cache Peak lava flows within the Kinnick and lower Bopesta formations shown on structure sections of Michael (1960) and Dibblee and Louke (1970) suggests that the NW tilt of the Garlock fault footwall ponded at least the lower levels of the Walker graben fill. The total thickness of the fill (Fig. 6B) indicates that it overtopped the proto–Garlock fault scarp and extended into the northern Mojave plateau region.

The Figure 6B section traverses the core of the Cache Peak volcanic center and, then, farther to the northwest, a complex zone of Cache Peak hypabyssal intrusions. Continuing northwestward, deeply weathered basement of the Centennial Ridge tilt block is crossed, and, then, farther northwest, the scarp of the W-up Breckenridge fault is crossed. The section bends to an E-W trace in the Breckenridge Mountain summit area. The west slope of Breckenridge Mountain preserves the low-relief upland surface with an ~9° W tilt, interpreted as footwall tilting along the Breckenridge fault (Mahéo et al., 2009). The section continues westward across the Kern Gorge fault, where the thickness of exhumed overburden shows that the entire scarp was buried by sediments in the Neogene.

In Figure 6C, we show a section that extends NE-SW between the Tejon Embayment and Isabella Basin. This section displays in profile NW-striking normal faults and related tilt blocks. Three footwall tilt blocks are defined as the Piute block (controlled by the Isabella basin fault), the Centennial Ridge block (controlled by the Walker Basin fault), and the Bear Mountain block (controlled by the Bear Mountain fault). The Walker Basin and Bear Mountain faults were important graben-bounding faults in the early Neogene. Widespread deep weathering of the graben floor basement between these faults, as well as disturbance patterns in apatite-He ages from the intervening basement, indicates sediment burial of ~1.8 km (Mahéo et al., 2009). This overburden thickness is similar to the Kinnick-Bopesta stratigraphic thickness measured adjacent to the Cache Peak vent complex, which in aggregate may have been in excess of 2 km (Michael, 1960; Dibblee and Louke, 1970; Quinn, 1987). In addition to the deep weathering profile across the basement of this region, interpreted as in situ weathering beneath the Neogene nonconformity, isolated outcrops of Neogene volcanic (or hypabyssal) rocks across the Centennial Ridge block further attest to the basement of this region having been covered by the Walker graben volcanogenic fill.

The thickness of Neogene strata that have been removed by Quaternary erosion across the Kern arch and adjacent Sierran basement is approximated by the yellow band on Figure 6. The thickness of this overburden in the region east of the Breckenridge fault (Fig. 6B) is constrained by stratigraphic thicknesses measured in the Kinnick-Bopesta section and disturbance patterns in apatite-He ages from the basement. For the area west of Breckenridge Mountain, this is based on the up-dip projections of eroded Neogene strata of the Kern arch, as well as low-temperature thermochronometry of subsurface samples utilizing disturbance patterns in detrital apatite-He ages, vitrinite reflectance, and low-grade metamorphic minerals in deep core samples (Cecil et al., 2014). Many of the principal members of the southern Sierra fault system appear to have undergone substantial growth in the early Neogene and then sediment burial throughout the Neogene, to be subsequently exhumed in the Quaternary. This is suggested by the fact that the elevated footwall areas of the Kern Gorge, West Breckenridge, Breckenridge, Walker Basin, Bear Mountain, and proto–Garlock faults retain the regional apatite-He age-elevation patterns of their low-relief upland surface, albeit tilted, while adjacent hanging-wall basement exposures yield (reheated) significantly disturbed apatite-He ages (Clark et al., 2005; Mahéo et al., 2009; Blythe and Longinotti, 2013; Cecil et al., 2014). We interpret this to indicate that these basement fault scarps experienced substantial early Neogene growth and that sediment burial of the scarps accelerated through the Neogene prior to their Quaternary erosional denudation. We now focus on the more detailed age relationships of these and related scarps.

EARLY AND MIDDLE MIOCENE SYNDEPOSITIONAL FAULTING

Overview

The thickness of Neogene sediment overburden that once sat above southern Sierra basement (Fig. 6) carries a number of important implications, including the stratigraphic continuity between the Walker graben fill and strata

of the southeastern San Joaquin Basin (Saleeby et al., 2016), as well as the spatial and temporal patterns of superposed Quaternary rock uplift and related erosion (Mahéo et al., 2009; Cecil et al., 2014). In this section, we further pursue the generation of relief on the basement surface during the Neogene and its influence on sediment provenance, dispersal, and accumulation. We focus primarily on the generation of basement relief along the current western Sierra range front, adjacent to the Kern arch. Of particular interest is the lack of, or retarded development of, Quaternary alluvial fans currently built along the base of the kilometer-scale basement scarps of the range front. This relationship is amplified by the fact that only a small proportion of siliciclastic sediment that comprises the Neogene section across the Kern arch has a western Sierra provenance (Saleeby et al., 2016). We assert that only through a detailed understanding of the Neogene sediment provenance, dispersal, and accumulation patterns for strata of the Kern arch can the history of faulting, subsidence, and uplift be meaningfully pursued. Critical insights are gained by the analysis of cover strata-basement relationships along the erosionally truncated Tertiary section of the Kern arch. Cover strata-basement relationships are further clarified by the use of well log and core data where significant thicknesses of Tertiary strata remain adjacent to the current erosional edge of the Kern arch section.

Structural Relationships of the Partially Exhumed Edison Graben

The Edison graben has been differentially exhumed to progressively deeper levels to the southeast, where it projects southeastward into the intersection zone between the Breckenridge and White Wolf faults (Figs. 2 and 7). Along with the structural saddle of this fault intersection zone, the Edison graben formed an important structural channel for Neogene fluvial sediments that were sourced from the Walker graben and transported into the southern San Joaquin Basin (MacPherson, 1977; Saleeby et al., 2016). Figure 7 is a geologic map across the eastern part of the Edison graben, and Figure 8 is a series of structure sections across the map area. The principal faults that form the graben consist of NW-striking, NE-up normal faults that step basin down from the Kern Gorge and West Breckenridge faults (Fig. 2) and the subsurface Edison fault zone, a complex zone of numerous subsurface, mainly SW-up, normal faults that die out to the southeast. The Edison fault zone, which is simplified in Figures 7 and 8, consists of many more normal-fault splays than shown.

Subsurface stratigraphic thickness variations and fault offsets shown in the Figure 8 D–D′ and E–E′ structure sections suggest that growth faulting started during the deposition of the upper Oligocene–lowermost Miocene Vedder sands and Freeman-Jewett silts and was most significant during the deposition of the lower and middle Miocene Olcese sands and Round Mountain silts, all under marine conditions. Growth faulting within the graben appears to have begun waning during the deposition of the upper Miocene shallow-marine and terrestrial units. Note that on the Figure 8 sections, the buried Edison basement high has more structural relief than can be accounted for by Neogene growth faulting, indicating early Tertiary and/or Late Cretaceous paleorelief on the buried basement surface. We return to this subject below.

The exposed stratigraphy within the southeastern part of the Edison graben (Fig. 7) further indicates rapid relief generation on the basement surface in early and middle Miocene time, as recorded by the Bealville fanglomerate. Dibblee and Warne (1986) recognized the syntectonic depositional setting of this unit, inferring that it was derived from the footwall of the Edison fault. This does not stand up to detailed field inspection. The "Edison fault" contact that these workers show passing at a highly oblique angle through the California State Route 58 road cut is a nonconformity with Bealville boulder-cobble conglomerate laying on Sierran basement (Figs. 9A and 9B). The Edison fault zone within the Figure 7 map area is shown by surface and subsurface data to have been in a state of growth but depositionally buried by the Bealville fanglomerate.

The Bealville fanglomerate consists of non-sorted pebbles to large boulders (up to 3 m diameter) of proximal Sierran basement commonly dispersed in an isotropic matrix composed of fragmented clast material broken down to sand-size polycrystalline and individual igneous mineral grains (Figs. 9C–9E). Clasts are commonly grooved, and partially faceted, as well as partially rounded. Much of the deposit lacks bedding and resembles rock avalanche deposits with matrix materials consisting of rock flour derived directly from the essentially monolithologic clast population (McSaveney and Davies, 2006). Megabreccia deposits interpreted as principally rock avalanche in origin occur immediately above lower Miocene Walker Formation along erosional surfaces (Figs. 7 and 8 F–F′). Debris flows consisting of the Bealville clast assemblage extend into the Olcese, Round Mountain, and lower Bena marine units, and sands and grits of the Nozu within the Round Mountain Formation record further reworking of Bealville debris into deeper marine conditions (Figs. 7 and 8 D–D′). The clast population in the lower part of the Walker Formation is distinct, lacking local western Sierra provenance. Cobbles of the Bealville clast type abruptly appear in fluvial channel conglomerates in the middle levels of the (local) Walker Formation, and debris flows consisting of only Bealville-type clasts occur in the (local) uppermost Walker, just below the Bealville rock avalanche facies (Fig. 9F). We interpret these fluvial conglomerates and subsequent debris flows as the initial accelerating stages of relief generation in the Bealville source area, which led up to the climax avalanche event(s). Submarine debris flows within the Olcese, Round Mountain, and lower Bena formations are interpreted to have been reworked off of the avalanche apron, with some possibly being direct submarine runouts of avalanching.

Since the work of Dibblee and Warne (1986), the basement of the region has been mapped and studied petrologically and geochronologically in some detail, providing the data necessary to resolve the Bealville source area (Saleeby et al., 1987, 2007, 2008; Ross, 1989; Pickett and Saleeby, 1993, 1994). The pertinent basement units are shown in Figures 2 and 7. The Bealville clasts consist of distinct mixtures of basement lithologies that can be accurately linked to specific source areas. Most notable is the distinct southern lobe of the ca. 99 Ma Tonalite of Mount Adelaide (Fig. 2), which consists of typical Mount Adelaide coarse euhedral biotite tonalite, but in this lobe, the tonalite is cut by dikes

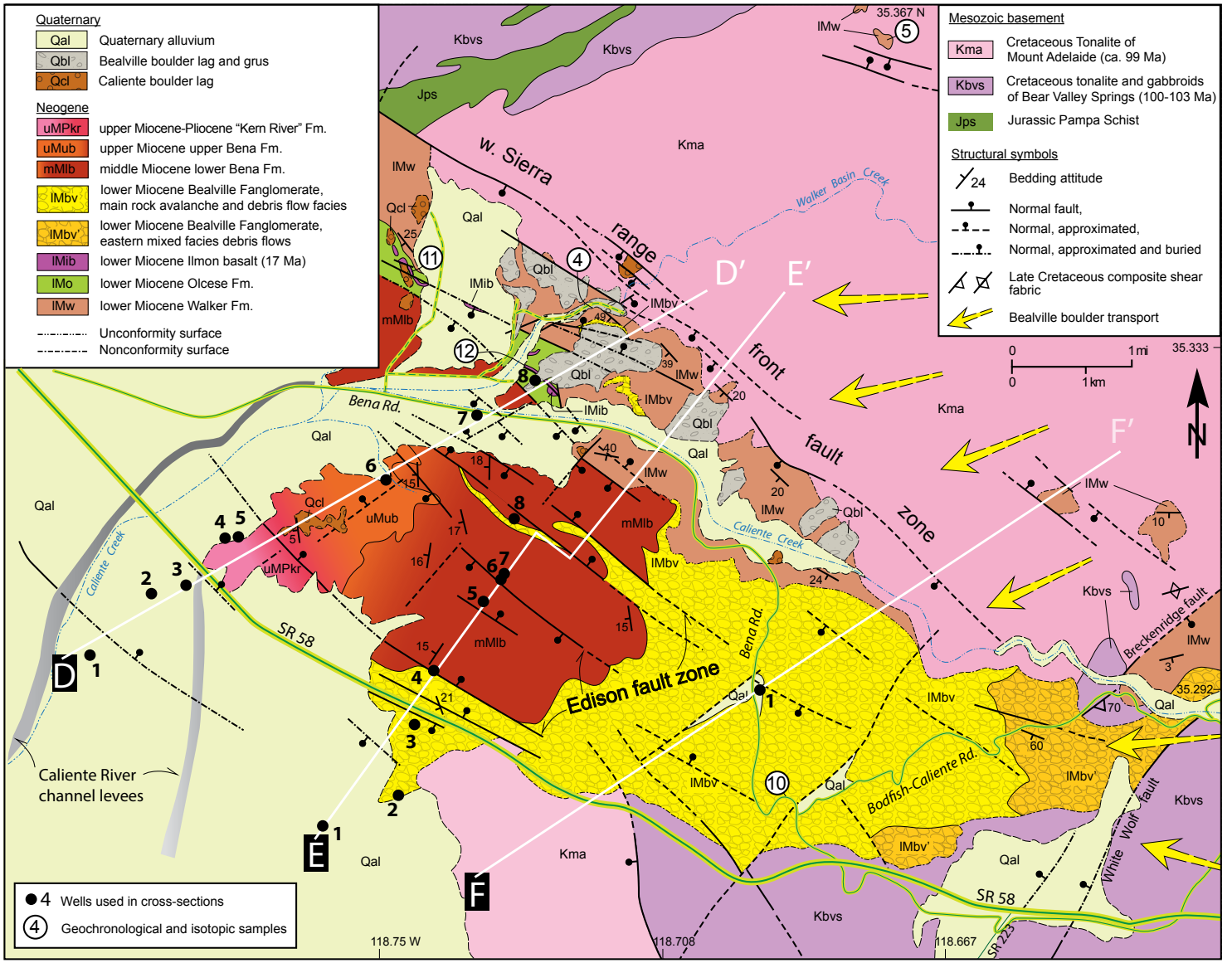

Figure 7. Geologic map of the Edison graben area, based on mapping of this study modified after Dibblee and Warne (1986). Locations of structure section lines shown for Figure 8.

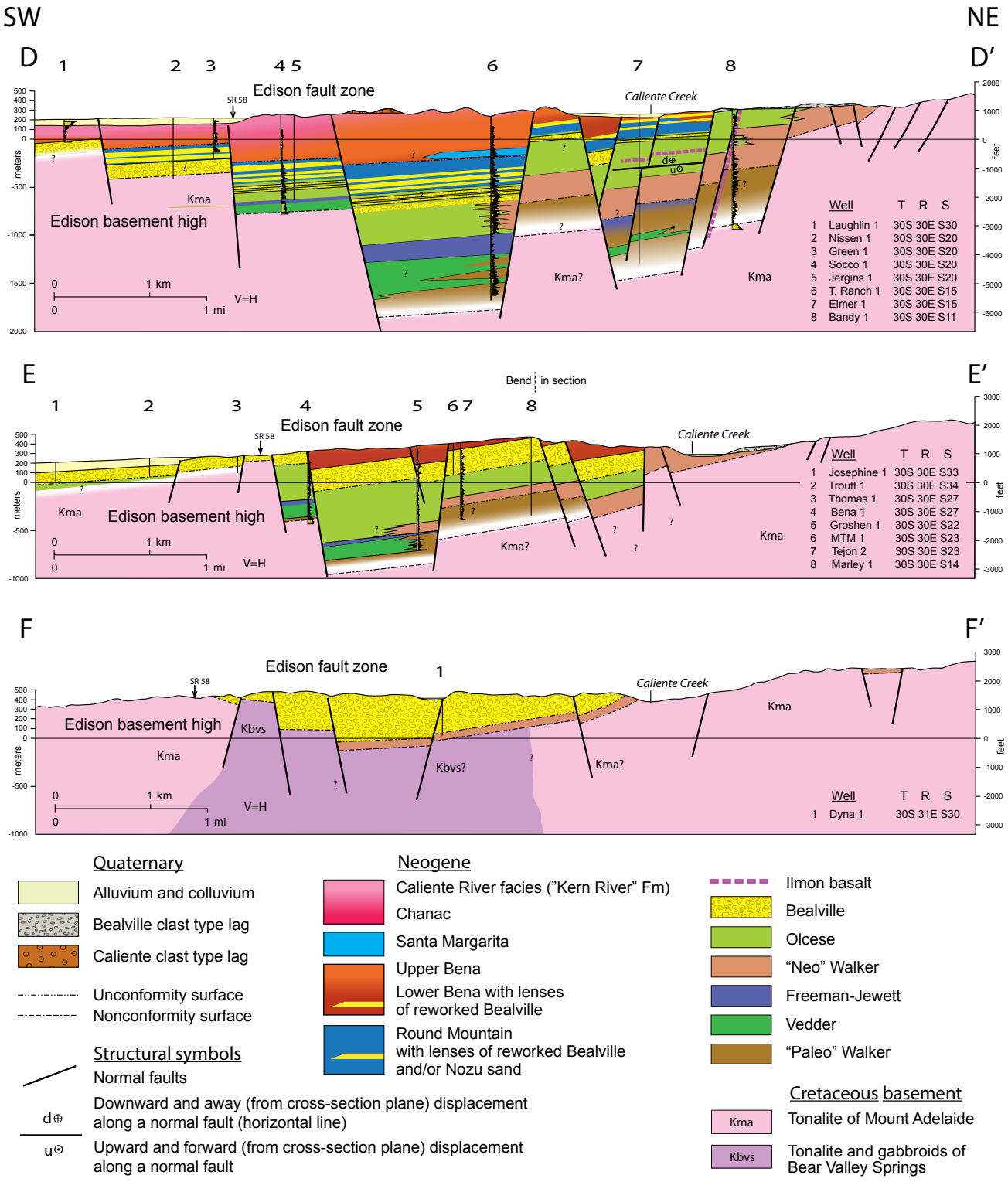

Figure 8. Structure sections across Edison graben, based on surface mapping of Figure 7 and well log and core data as indicated. V=H—vertical scale equals horizontal scale.

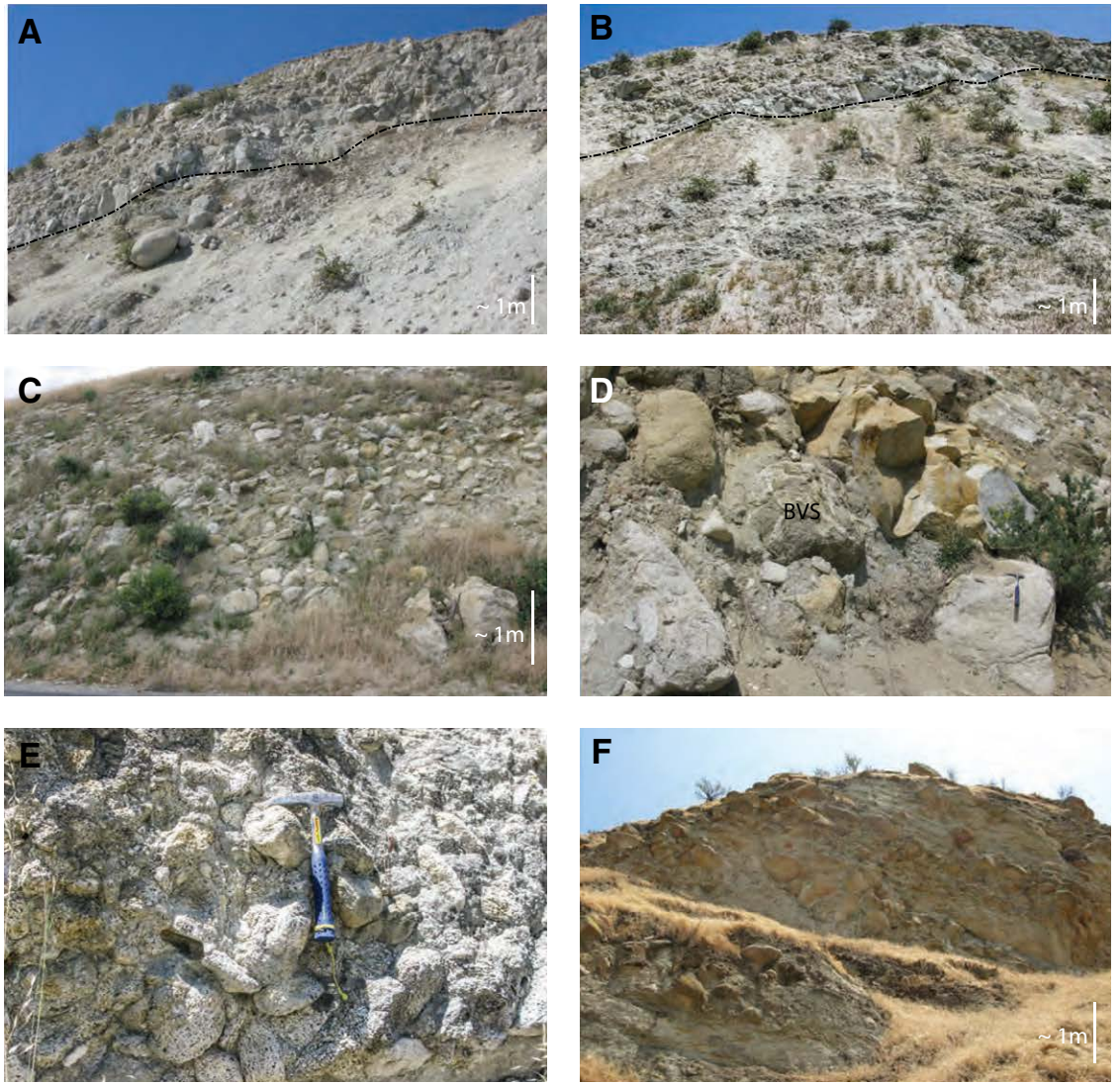

Figure 9. Field photographs of Bealville Fanglomerate. (A) Clast-supported boulder bed laying nonconformable on shattered Tonalite of Mount Adelaide in road cut along north side of State Route 58. Note boulder and cobble float laying on basement downslope from nonconformity that is demarked by dot-dash line. (B) Same nonconformable contact between Bealville clast-supported megabreccia and basement as in frame (A), but farther east along contact. This frame shows shattered basement structure. (C) Road cut along Bena Road (sample 10 location, Fig. 7) showing main facies of Bealville Fanglomerate that is characterized by non-sorting, lack of bedding, and clast-supported texture. (D) Road cut along Bodfish–Caliente Road ~2 km east of sample 10 location (C) showing clast-supported main rock avalanche facies of Bealville but with introduction of Bear Valley Springs mafic tonalite boulders (BVS). (E) Close-up of clast-supported cobble cluster situated between larger boulders of Figure 9C showing that matrix consists wholly of granulated igneous grains derived from clasts. Sharp tip of hammer oriented above clast taken as sample 10. (F) Debris-flow beds within upper Walker Formation immediately below Bealville Fanglomerate along Caliente Creek (Fig. 7). Boulders consist wholly of Tonalite of Mount Adelaide but contrast in color from those of (A) through (E) due to staining by debris-flow mud matrix.

and small cupolas of medium- to coarse-grained leucotonalite and/or low-K granodiorite. In the Figure 9E photograph of the main facies of the Bealville, we indicate a clast for which we have determined a 98.7 ± 0.5 Ma U-Pb zircon age (sample 10, Table 2; Supplemental Items 1 and 2 [footnote 1]). This age is within error of multiple U-Pb zircon ages published for the Mount Adelaide tonalite (Saleeby et al., 1987, 2008). We interpret the ca. 99 Ma zircon date on the sample 10 clast as additional support for our Bealville provenance correlation to the southern lobe of the Mount Adelaide; this correlation was originally based on map and mesoscale petrographic observations.

Both the northern and southern lobes of the Tonalite of Mount Adelaide are intruded into the petrographically distinct 100–103 Ma Tonalite of Bear Valley Springs. Adding to the uniqueness of the basement assemblages of this area is the occurrence of a 95–98 Ma aplite and pegmatite dike swarm within the Bear Valley Springs unit, specifically in the area east of its contact with the southern lobe of the Mount Adelaide (Saleeby et al., 1987, 2008; Ross, 1989). The clast population of the Bealville fanglomerate, in the area of the Edison graben, tracks spatially with the basement units mapped directly upslope to the northeast and east (Fig. 7). The main facies is nearly monolithologic with derivation from the southern lobe of the Mount Adelaide exposed directly upslope to the northeast (Fig. 2). Eastward, the clast population changes to include the Bear Valley Springs unit (Fig. 9D), as well as increasing proportions of the aplite and pegmatite dike rock clasts. Continuing eastward, the eastern Bealville facies lacks large boulders, and the unit becomes entirely debris flow in origin. This also can be correlated to basement-source features. The Bear Valley Springs unit upslope to the east of the eastern Bealville facies is texturally degraded and hydrated due to its position within the Late Cretaceous Kern Canyon–White Wolf ductile shear zone (Figs. 1 and 7). The Bear Valley Springs unit of this area is texturally incapable of generating a high concentration of boulders, as observed in the eastern Bealville facies.

The source area for the Bealville Fanglomerate is uniquely determined to have been in the hanging-wall areas of the ~60° intersection zone between the Breckenridge and West Breckenridge faults (Figs. 1, 2, and 7). We infer that rapid relief generation on these faults resulted in the catastrophic production of the Bealville fanglomerate by rock avalanche and debris-flow mechanisms. Basement relief patterns shown in Figure 6B indicate that both the Breckenridge and West Breckenridge faults generated kilometer-scale scarps. The hanging walls of such an intersection zone between two large normal faults, as well as part of the intersection zone having been superposed across a preexisting basement damage zone, provided a highly fragmented and high local relief area that was prone to catastrophic collapse and the shedding of rock debris into the adjacent, actively subsiding Edison graben.

The timing of the Bealville catastrophic (rock avalanche) event(s) is constrained by the ca. 17.8 Ma ash age determined within the Walker Formation, which lies immediately below the main facies Bealville (sample 4, Fig. 7; Table 2) and the overlying middle Miocene lower Bena Formation (Figs. 7 and 8 E–E′ and F–F′). Submarine debris flows that represent direct runouts from the main avalanche facies, as well as debris reworked from the main facies, occur to the northwest, within the upper Olcese, lower Bena, and Round Mountain formations (Figs. 3, 7, and 8 D–D′). These debris-flow beds appear to both predate and postdate the ca. 17 Ma eruption of the Ilmon Basalt (sample 11, Fig. 7; Table 2), which is discussed below under "syn-igneous" faulting.

Even though the Bealville is a distinct sedimentary unit, it is not unique to the early Neogene of the southern San Joaquin Basin–Sierra Nevada region. Boulder beds laying directly above the volcanic ash-lacustrine sequence of the Kinnick Formation outlier, inclusive of the sample 3, ca. 18.3 Ma, ash-flow tuff (Fig. 5C), consist of the 100–103 Ma Tonalite of Bear Valley Springs and are devoid of metasedimentary rock fragments for which local sources are abundantly exposed as pendants laying nonconformably beneath the outlier section. Field observations of the coarse clast population indicate that the most likely basement source is in the area of the Bear Mountain fault scarp to the southwest (Figs. 2 and 6C). Lower Miocene coarse boulder beds ("unnamed conglomerate") also occur in the shallow-marine section of the Tejon Embayment (Nilsen et al., 1973; Goodman and Malin, 1992; Figs. 2 and 3C). Field inspections educated by widespread basement rock thin-section petrography (Saleeby et al., 1987, 2007) suggest that the source area for the unnamed conglomerate is in the footwall area of the Tejon Creek fault (Fig. 2).

In summary, there is abundant stratigraphic evidence for rapid generation of basement relief along normal faults in the early to middle Miocene along the eastern San Joaquin Basin–southern Sierra Nevada transition. We now look to distinct early Miocene igneous assemblages whose structural settings indicate similar age normal faulting in the region.

Syn-Igneous Normal Faulting

We now focus on early Neogene igneous rocks of the region for which field relations and age data further reveal the significance of widespread early Neogene normal faulting. We focus first on relationships within the Edison graben. The structural and stratigraphic setting of the Ilmon basalt (Figs. 7 and 8 D–D′) places its eruption within the time interval of initial Bealville fanglomerate deposition and debris-flow reworking, an event inferred above to have been forced by significant normal displacements along the Breckenridge and West Breckenridge faults. The structural and textural states of the Ilmon basalt, in their own right, indicate active faulting in the area during Bealville deposition. The Ilmon basalt consists of faulted pillow breccia and hyaloclastite and massive flow and/or feeder dike rock. Pillow breccia and hyaloclastite alone suggest a high bathymetric relief eruption environment, and the faulted state of the basalt (Fig. 7) further suggests that such relief was generated by active faulting during eruption. Ilmon basalt pillow breccia and hyaloclastite form an up to ~5-m-thick bed within Olcese sandstone and ash (Fig. 10A), which is in both depositional and fault contact with the Walker Formation and in fault contact with the lower Bena Formation (Fig. 7). Sample 11 was taken from the most pristine pillow interior that we could identify (Fig. 10B). Groundmass phases consist of plagioclase, olivine, and subordinate clinopyroxene, with

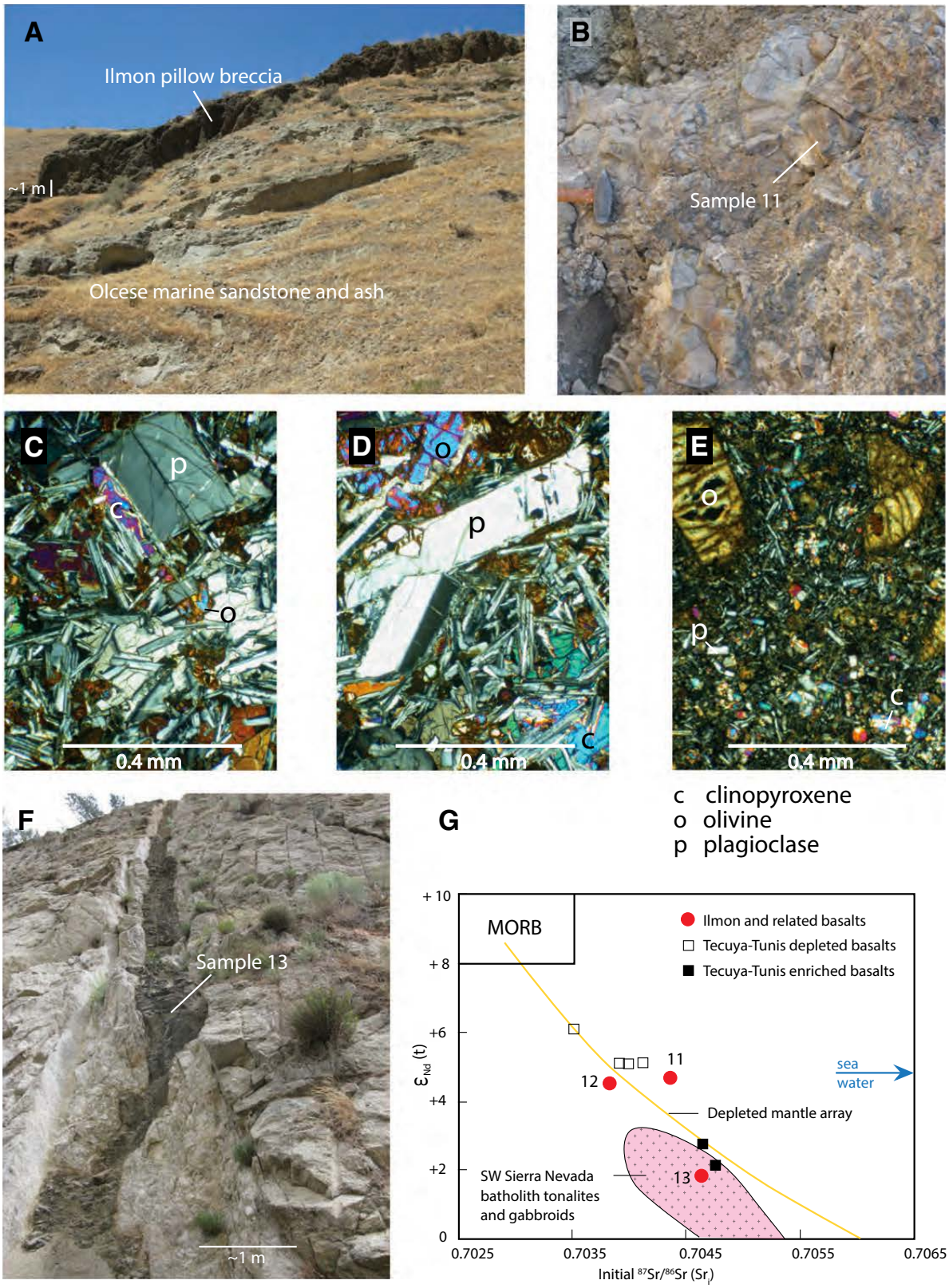

Figure 10. Field, petrographic, and geochemical features of early Miocene mafic igneous rocks. (A) Ilmon basaltic pillow breccia and hyaloclastite bed within shallow-marine Olcese Formation. (B) Close-up of Ilmon basalt showing isolated pillow from which interior was sampled (11) for geochronology and geochemistry. (C) Pillow interior photomicrograph from sample 11 showing plagioclase, olivine, and clinopyroxene. (D) Photomicrograph from sample 12 massive basalt showing groundmass and phenocrystic plagioclase, olivine, and clinopyroxene. (E) Photomicrograph of sample 13 basaltic dike rock showing groundmass and phenocrystic olivine, plagioclase, and clinopyroxene. (F) Field setting of olivine phyric basaltic dike rock of sample 13 emplaced into and sheared along with brittle damage zone of high-angle normal fault in basement of upper Kern River Gorge. (G) Sr_i-εNd(t) plot with depleted mantle array curve after Hoffman (2004) showing plots of basalt samples 11–13 (Supplemental Item 5 [text footnote 1]) as well as plots of basalt samples from the Tunis-Tecuya volcanics of the Tejon Embayment–San Emigdio Mountains (Sharma et al., 1991); and the field of southwestern Sierra Nevada batholith samples (Kistler and Ross, 1990; Pickett and Saleeby, 1994). MORB—mid-ocean ridge basalt.

plagioclase also forming microphenocrysts (Fig. 10C). We performed Ar/Ar laser probe analysis on plagioclase (Supplemental Item 3 [footnote 1]). Supplemental Item 4 shows stepwise-heating and isochron plots for sample 11. Stepwise heating yielded a plateau age of 17.18 ± 0.10, and the isochron age is at the margin of analytical uncertainty of the plateau age at 16.85 ± 0.11 Ma. We interpret the age of the basalt to be ca. 17 Ma (Table 2).

Southeastward ~2 km from the sample 11 site, the Ilmon basalt lies along a high-angle fault, and together these are cut by smaller diagonal high-angle faults (Figs. 7 and 8 D–D′). The basalt here consists of massive dike and/or flow interior rock as well as hyaloclastite. Sample 12 was taken from massive basalt of this location for geochemical comparison to the sample 11 pillow interior and additional dikes discussed below. Sample 12 is petrographically similar to sample 11 (Figs. 10C and 10D). The structural relations of the basalt at this location further indicate active faulting within the Edison graben at ca. 17 Ma.

Basalts of early to middle Miocene age appear to be widespread but, for the most part, of small volume throughout the southern San Joaquin Basin and adjacent western Sierra Nevada. Exceptions include the Tunis-Tecuya volcanics of the Tejon embayment (Sharma et al., 1991) and the Cache Peak volcanics (Michael, 1960; Dibblee and Louke, 1970), where volumetrically significant basalt occurs along with abundant more felsic volcanic rocks. The more widely dispersed basalts are encountered in well logs and cores from sites not included on our cross sections. Also, small isolated exposures and float clasts of Ilmon-like basalt occur in other scattered locations along the southeastern Kern arch and southern reaches of the Breckenridge-Greenhorn horst, but rarely can primary field relations be observed due to poor exposure. One exception is a well-exposed olivine phyric dike that was emplaced and sheared along a small normal fault that cuts basement along the upper part of the lower Kern River Gorge (sample 13, Figs. 2, 4, 10E, and 10F). Plagioclase phenocryst grain size and alteration are such that a meaningful date could not be obtained, but petrographic and geochemical data suggest that the dike is consanguineous with the Ilmon basalt (Table 2 and discussions below). As shown in Figure 10F, the basalt dike was emplaced into and deformed along with the brittle damage zone of a steeply dipping normal fault.

Radiogenic Sr and Nd isotopic measurements were made for the two Ilmon basalt samples (11 and 12) and the sample 13 dike (Table 2; Supplemental Item 5). The three samples lie roughly on the depleted mantle Sr-Nd array (Fig. 10G). Compositions of the sample 11 pillow appear to be displaced off the array by interaction with seawater. Assuming that sample 12 preserves the most pristine primary isotopic composition and that the three samples are consanguineous, sample 13 appears to have been displaced off the array by interaction with batholithic host rocks. Inasmuch as all three samples were emplaced through (and into sample 13) such batholithic rocks, it is possible that samples 11 and 12 have been displaced a more limited extent down and slightly off of the depleted mantle array. Figure 10G also shows basalt Sr-Nd data from the Tunis-Tecuya volcanics of the Tejon embayment (Sharma et al., 1991; Fig. 2). These data suggest a similar pattern of pristine initial compositions with non-uniform contamination by seawater and batholithic host rocks. We return to the tectonic and petrogenetic significance of these relationships below. In summary, we interpret the petrographic and isotopic similarities, along with the field settings of the sample 11, 12, and 13 basalts, to indicate their emplacement along dilatational normal faults at ca. 17 Ma.

The igneous emplacement and contemporaneous shearing out of dikes along early Miocene dilational normal faults and fissures are well expressed for the northern exposures of the hypabyssal complex of the Cache Peak volcanic center. The generalized structure of this complex is shown on Figure 2 as a myriad of NW-striking, steeply dipping dikes, which coalesce southward into dike-on-dike and massive hypabyssal rock. Many of the dikes show strong plastic flow along their margins consistent with normal-sense shear and dilation during igneous emplacement. The dike swarm dies out sharply northward across the Walker Basin fault (Figs. 2 and 6 C–C′). Dike density along the northwest ~6 km extent of the dike swarm is such that the host basement has been effectively extended by a factor of two in a NE-SW direction. Proximal basement of the Centennial Ridge tilt block to the northwest of the dike swarm is highly shattered and hydrated, thereby inhibiting quality exposure. This poorly exposed track of basement rock as well as the more massive hypabyssal rocks to the southeast of the dike swarm in some fashion accommodated the extensional strain imposed by the dike swarm. As discussed earlier, sample 1 (Fig. 4) was taken from the interior of one of the larger dikes, and it yielded a ca. 18.6 Ma U-Pb zircon age (Table 2; Supplemental Items 1 and 2). The structural and petrographic uniformity of the dikes of the swarm lead us to interpret this as the approximate age of the swarm (medial early Miocene), as well as its NW-SE–directed synemplacement extensional deformation.

Summary

Above, we have leveraged a number of lines of inquiry ranging from surface and subsurface structure mapping, sedimentology, stratigraphy, geochronology, and low-temperature thermochronometry in order to demonstrate widespread normal faulting of early Neogene age throughout the southern Sierra Nevada and adjacent San Joaquin Basin region. An important component of this faulting was focused in early to middle Miocene time, particularly in the time interval of 18.6–17 Ma. Such faulting provided dilational normal-shear surfaces for depleted mantle-derived basaltic and more evolved felsic magmas to ascend into as dikes and also created the sediment accommodating spaces of the Walker and Edison grabens, as well as the area that subsequently became the Maricopa sub-basin.

EARLY CENOZOIC ACTIVITY ALONG THE SOUTHERN SIERRA FAULT SYSTEM

The western Sierra fault system was defined above as a series of generally E-up topographic scarps mainly between 36°N and 37°N (Hake, 1928), one of

which has been documented to have undergone ~1000 m of E-up normal displacement in middle to late Eocene time (40–45 Ma; Sousa et al., 2016a). The aerial distribution of these scarps merges with scarps of the southern Sierra fault system (Fig. 1), raising the possibility of early Cenozoic activity on some members of the mainly Neogene southern Sierra system. This is consistent with our observation that some faults of the system within the San Joaquin Basin produced structural relief on the basement surface in excess of that which can be accounted for by Neogene growth faulting. This is displayed in the D–D′, E–E′, and H–H′ structure sections (Fig. 8; Supplemental Item 6). Early Cenozoic activity on Neogene growth faults that are well displayed in the Maricopa sub-basin on Figure 6 A–A′ is further suggested by the depth to basement beneath the sub-basin. Unfortunately, lower Cenozoic strata are not penetrated by deep wells of the sub-basin.

Evidence that high-angle normal faulting similar to that of the late Eocene western Sierra fault system extended into the Kern arch area is provided by the ages and structural settings of volcanic ash samples 8 and 9, which were taken from the base of the northern exposures of the (Paleo-)Walker Formation (Fig. 4). Figure 11 is a structure section (G–G′) through the sample 8 and 9 sites. The section shows the sample 8 reworked ash of ca. 26.9 Ma age (Table 2; Supplemental Items 1 and 2 [footnote 1]) along the base of the Walker Formation, nonconformable on basement within the Grizzly Gulch fault zone. This high-angle normal fault zone offsets the contact between the Walker Formation and the basement, and southward forms a west-facing basement scarp. Progressing westward along the section trace across the fault zone at a position ~7 m topographically lower than the sample 8 site lies the sample 9 felsic tuff of ca. 40.1 Ma age (Table 2; Supplemental Items 1 and 2), likewise nonconformable on basement along the base of the Walker Formation. The basement nonconformity of this region corresponds to the southern exposed limit of an extensive pre-late Eocene paleo-pediment surface that runs along the western Sierra Foothills between ~36°N and 37°N (Sousa et al., 2016b; Fig. 1). As such, it has extremely low local relief, except for distinct paleo-monadnocks that have been reexhumed with the erosion of late Cenozoic strata along the eastern edge of the Basin. At ~36.7°N, the paleo-pediment surface emerges northward from beneath a thin alluvial cover to continue northward as the basal nonconformity surface beneath the lower Paleogene Ione Formation (Fig. 1), similar to the relationships of Figure 11. The sample 8 and 9 ashes do not have local sources and most likely represent distal air-fall and fluvial reworked ash deposits whose likely source areas are discussed below.

The relationships exhibited in Figure 11 are most readily explained by the initial deposition of the 40.1 Ma tuff across the basement pediment surface prior to or during E-up motion on the Grizzly Gulch fault zone. This could correspond with the 40–45 Ma age constraints for faulting along the western Sierra system (Sousa et al., 2016a), assuming that the Grizzly Gulch fault originated as part of the system. Subsequent to tuff deposition, E-up motion elevated the eastern fault wall enough to promote the erosional stripping of the tuff. Walker terrestrial sedimentation proceeded across the western wall, punctuated by the deposition of the 26.9 Ma ash, which lapped across the eastern wall that was denuded of its Walker section and basal 40.1 Ma tuff. Walker terrestrial sedimentation continued but was interrupted by a phase of erosion prior to deposition of the lower Miocene Olcese Formation. During this erosional phase, much of the western wall 26.9 Ma ash was eroded and reworked. Subsequent to Olcese sedimentation, a period of non-sedimentation,

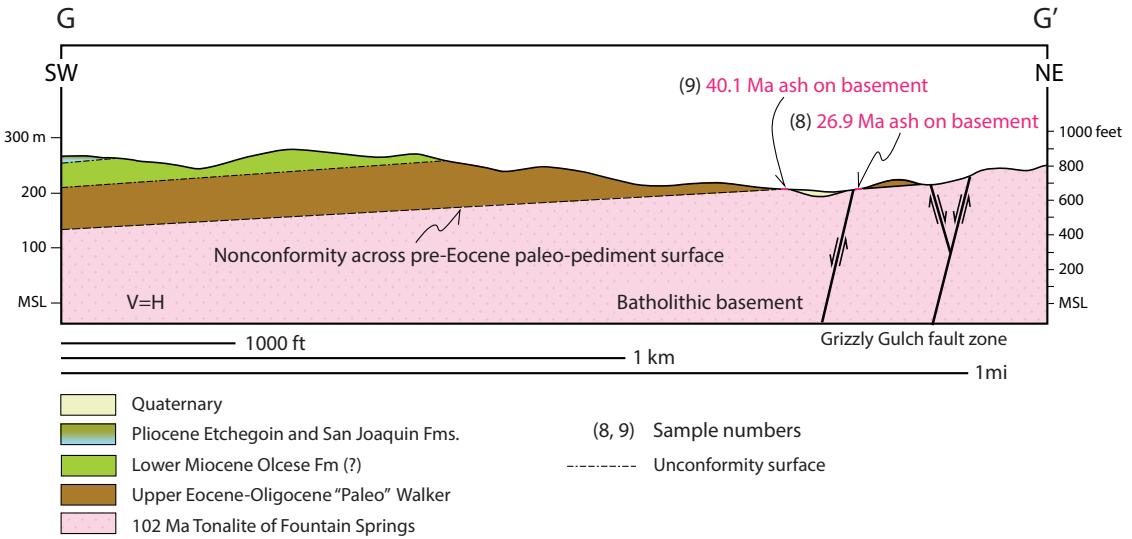

Figure 11. Structure section across cover strata-basement contact of northern Kern arch showing structural and stratigraphic relationships of geochronological samples 8 and 9. Location of section line shown on Figure 4. Tertiary stratigraphy based on this study and Saleeby et al. (2016), paleopediment surface after Sousa et al. (2016b), and basement after Saleeby and Sharp (1980). V=H—vertical scale equals horizontal scale; MSL—mean sea level.

or cycles of sedimentation and erosion, occurred prior to Pliocene deposition of the Etchegoin and San Joaquin formations. Quaternary uplift and erosion of the Kern arch exposed the Figure 11 relationships.

Cenozoic sedimentation along the eastern margin of the southern San Joaquin Basin, as exposed along the Kern arch, was sensitive to surface uplift and subsidence, which produced a spatially complex stratigraphic succession with numerous hiatuses. The erosional phases recorded in Figure 11 appear to be part of a broader erosional regime that affected the eastern San Joaquin Basin and southern Sierra region in the late Paleogene (Olson et al., 1986; Saleeby et al., 2016). This is well established along the eastern edge of the Kern arch, as well as in the area of the Walker graben. From the White River area southward, the base of the exposed Walker Formation decreases in age from late Eocene to Oligocene adjacent to the lower Kern Gorge. Exposures south of the Kern Gorge are entirely lower Miocene (Fig. 2), except in graben floors along the adjacent subsurface (Fig. 8 D–D′ and E–E′). The relationships integrated above for the Figures 6 A–A′, 8 D–D′ and E–E′, and 11 G–G″ structure sections indicate Eocene to Oligocene activity along at least some members of the primarily Neogene southern Sierra fault system.

EARLY NEOGENE SEDIMENT BURIED STRUCTURAL RELIEF ON THE BASEMENT DENUDED AS LATE QUATERNARY TOPOGRAPHIC RELIEF

Select members of the southern Sierra Nevada fault system were discussed above in order to establish an important phase of early to middle Miocene displacement, which controlled regional patterns in stratigraphy, sediment accumulation, and geomorphology. A number of these faults have generated kilometer-scale structural relief on the basement, and according to the Figure 6 structure sections, a number of these fault scarps were buried by Neogene strata during and/or shortly after they formed. Because the rocks constituting the basement scarps are much more resistant to erosion than the Neogene strata that once buried them, the footwall areas of the scarps have weathered out as topographic scarps as the sedimentary overburden was eroded off. This has led to the early Neogene structural relief of the basement faults to emerge as Quaternary topographic relief. This appears to be a significant geomorphic feature of the southern Sierra, south of 35.7°N. In this section, we focus on the Kern Gorge fault as an excellent example of this process, and then we apply these findings in a more general fashion to some of the other significant faults of the system.

Kern Gorge Fault Scarp

The Kern Gorge fault scarp constitutes the local range front of the western Sierra Nevada in the lower Kern River area, with the Kern River Gorge incised steeply through its footwall. It is exceptional due to (1) its abrupt local relief relative to that of the adjacent Kern arch and (2) the state of preservation of part of the principal fault surface. In his treatise on Basin and Range geology, Gilbert (1928) showcased the Kern Gorge fault as a type example of a Basin and Range normal fault scarp. Figure 12A shows a view to the southeast along the Kern Gorge fault scarp with the lower Kern River Gorge incised steeply through its footwall. The principal fault surface is preserved immediately adjacent to the river gorge and is offset by NE-striking, high-angle faults to the south of the gorge (Fig. 13). The scarp exhibits up to ~700 m of NE-up normal displacement, which diminishes rapidly to zero both to the southeast and northwest (Fig. 2). Southeastward along the fault, range-front normal fault displacements step over by a series of relay ramps to the NE-up normal fault set that controls the northeast margin of the Edison graben (Figs. 2 and 7). Northwestward along the fault, normal displacements step over by a relay ramp to additional NE-up range-front normal faults. At both terminations of the Kern Gorge fault, the respective relay ramps preserve the current erosional truncation of the Kern arch Neogene section, as well as its basement nonconformity, with interfluve surfaces of the footwall approximating the exhumed nonconformity surface (Figs. 1 and 4). This indicates that the Neogene section once extended across the fault's footwall (Fig. 6B). The Kern gorge fault is mapped as a late Quaternary fault on the Fault Activity Map of California (Jennings and Bryant, 2010). Under closer examination, however, the principal scarp appears to have grown in the early Neogene, or perhaps earlier, with its current expression representing a fault-line scarp.

Figures 12 and 13 show a number of important features of the Kern gorge fault. On the Figure 12A oblique view along the scarp, hanging-wall rocks in the foreground consist of middle Miocene bathyal marine Round Mountain Formation juxtaposed against footwall diorite and mafic tonalite of the Bear Valley Springs suite. As displayed on Figure 12A, and mapped on Figure 13, there is a paucity of alluvial aprons extending off the basement scarp across the footwall. Close field examination of the footwall and proximal hanging wall, interpreted in the light of the amount of Neogene sediment eroded off of the area (Fig. 6B), indicates that the surface trace of the Kern Gorge fault is a locally sheared buttress nonconformity that developed across the fault scarp by deposition of the Walker, Olcese, and Round Mountain formations (Fig. 13). In some areas of minimal erosional modification of the scarp, there are remnants of non- to feebly-sheared siliciclastic sediments derived from these Miocene units amalgamated onto the fault scarp surface. We interpret the Kern gorge fault to have begun growth at least by the early Miocene and to have continued to grow at least through (Neo-)Walker and Olcese deposition, based on penecontemporaneous folding in these units adjacent to the Kern Gorge and subsidiary faults (Fig. 13). Round Mountain deposition may have completely postdated fault displacement, with its weak to nil deformation fabric adjacent to the fault resulting from differential compaction. Maximum structural relief on the fault was attained prior to the Pliocene burial of the hanging-wall section by ~1800 m of strata that have been eroded off the eastern margin of the Kern arch in the Quaternary (Cecil et al., 2014). Accordingly, apatite-He ages in basement of the elevated footwall area escaped the disturbance effects of sediment burial since enough relief was generated

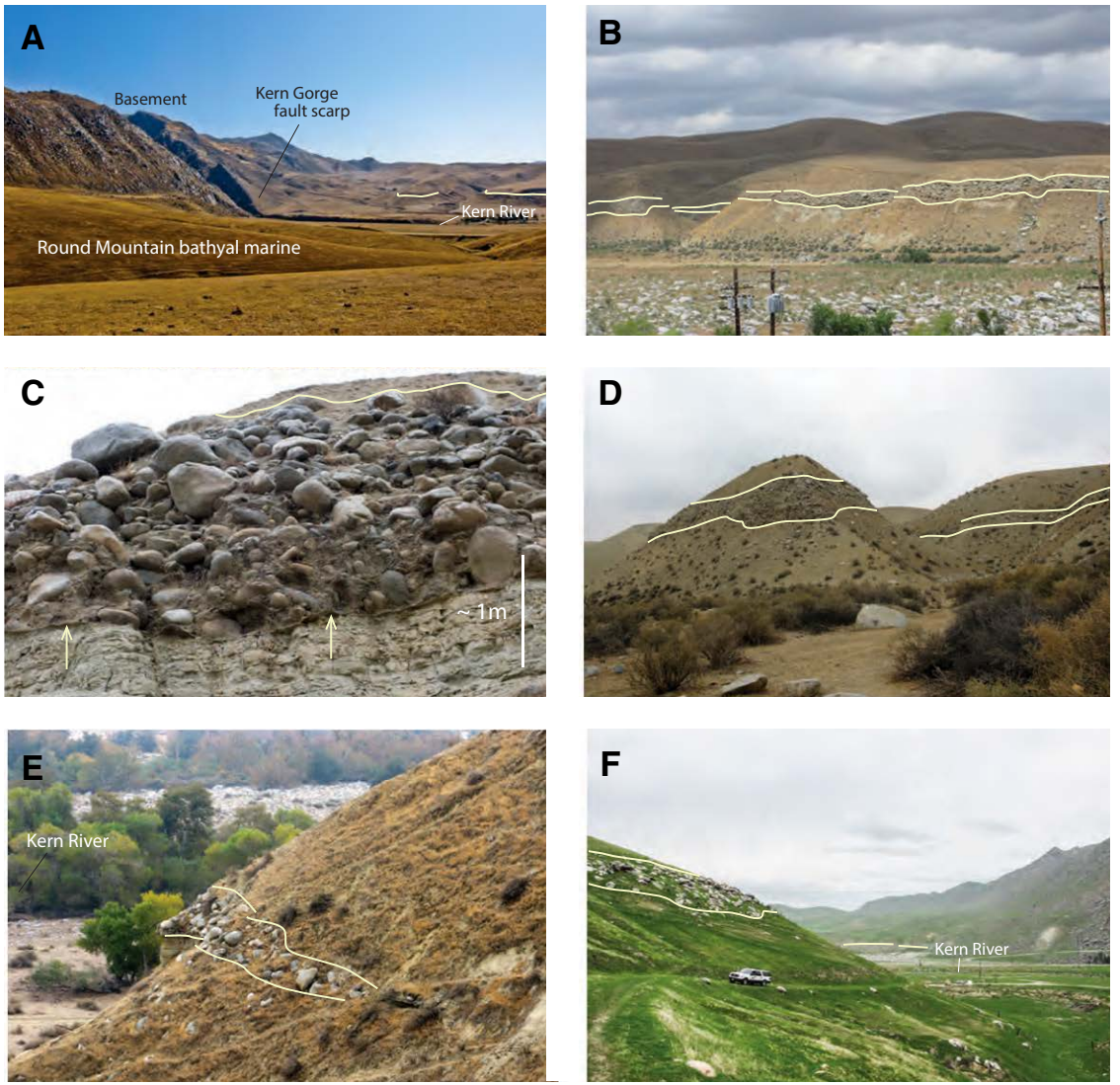

Figure 12. Field photographs taken across hanging-wall area of Kern Gorge fault. (A) View southeast along Kern Gorge fault-line scarp with mafic intrusives of Bear Valley Springs batholithic suite in footwall and middle Miocene Round Mountain Formation in hanging wall (foreground). Yellow lines in background trace Bealville boulder bed within Round Mountain Formation. (B) View to northwest of erosionally modified strath terrace along main Kern River channel showing in yellow lines distinct tonalite boulder bed of Bealville submarine debris-flow facies lying stratigraphically within diatomaceous silty shale of the Round Mountain Formation. Note Bealville boulder lags on slope below boulder bed and lying in Kern River channel in foreground. (C) Close-up of part of the boulder bed shown in Figure 12B showing crude inverse grading and gypsum-bearing seam along the base of the boulder bed denoted by arrows. Upper contact of boulder bed with Round Mountain siltstone (shown by yellow line). (D) View north into sharp gullies cut into strath terrace and stratigraphic sequence of Figure 12B showing that Bealville boulder bed (outlined by yellow lines) lies within stratigraphic sequence. Note boulder lag in foreground. (E) View southwestward within sharp gulley cut into strath terrace of Figure 12B showing boulder bed (outlined by yellow lines) pinching out northward. Note Bealville boulder lags lying in main Kern River channel in upper left and on slope immediately below boulder bed. (F) View north from south side of river gorge showing boulder bed (outlined by yellow lines) laying at distinctly higher topographic level than to the north of the river channel (single yellow line) and the distinctly coarser size of the constituent boulders as compared to boulders along the north side of the river channel (vehicle for scale).

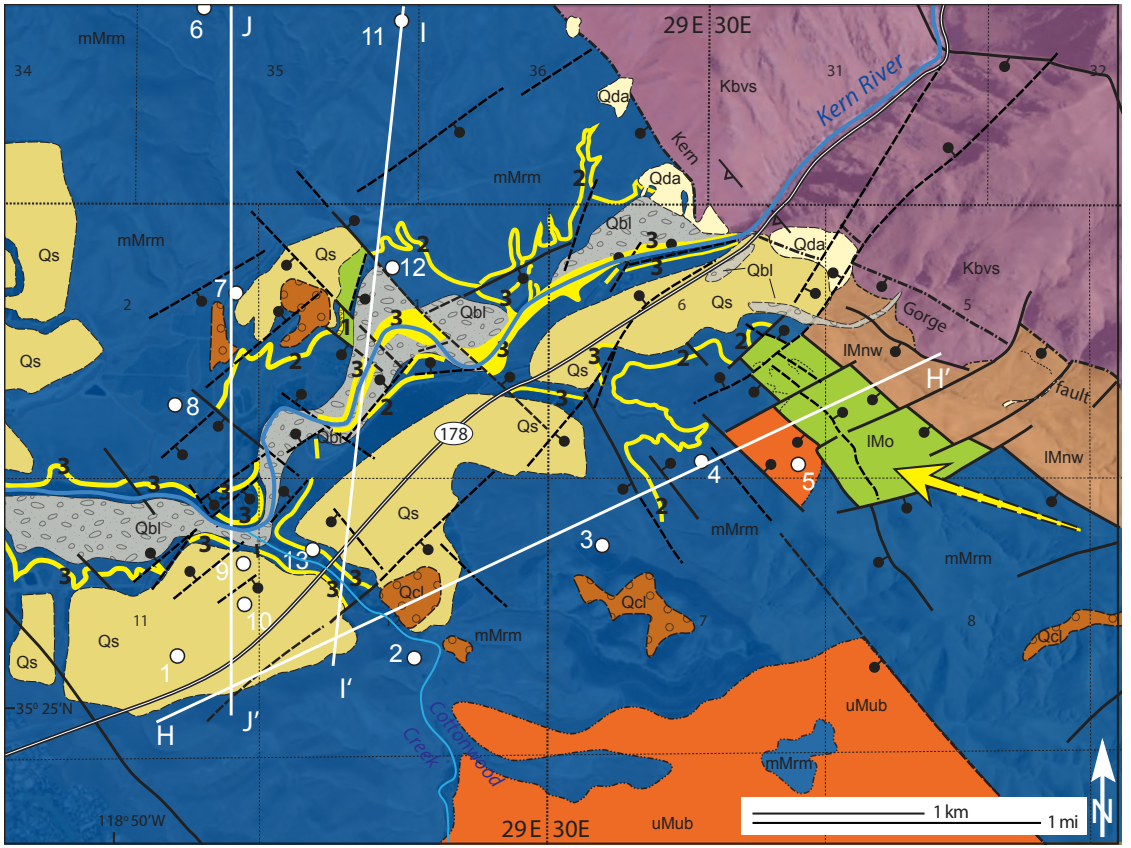

Figure 13. Geologic map of the Sierra Nevada range front area where the lower Kern River Gorge exits the range (this study). Cross sections for lines H–H′, I–I′, and J–J′ are in Supplemental File 6 (text footnote 1). Apparent dips of bedding are ~5° SW along H–H′ and 2°–5° S along I–I′ and J–J′.

on the footwall to elevate the basement surface above the apatite-He partial retention zone (Mahéo et al., 2009).

Important stratigraphic relationships of the Kern gorge fault hanging wall are expressed by a series of distinct boulder beds that lie within strath terraces along the trunk channel and in hills to the south of the Kern River (Fig. 13). Figure 12B is a view to the northwest from the south side of the Kern River channel. The boulder bed runs along the terrace near but beneath its surface. This bed is traditionally interpreted as part of a Kern River terrace deposit (Bartow and Pittman, 1983; Bartow, 1984; Bedrossian et al., 2012). Our surface and subsurface mapping shows that this boulder bed lies stratigraphically within the lower part of the middle Miocene Round Mountain Formation (Fig. 13 and Supplemental File 6 [footnote 1]). Figure 12C shows a close-up along the outcrop face of Figure 12B, where a clear depositional contact is displayed between the boulder bed and Round Mountain diatomaceous silty shale. An insoluble residue seam lies along the contact that locally contains gypsum. Figure 12D is located farther westward along the exposure face shown in Figure 12A, where the boulder bed is incised by sharp gullies that display in three dimensions the boulder bed that lies within the Round Mountain Formation. A photograph taken nearby (looking southward out of a sharp gully toward the trunk channel of the Kern River; Fig. 12E) shows the boulder bed pinching out northward within Round Mountain diatomaceous shale. Subsurface data in the Figure 13 map area (Supplemental File 6) show this bed to be the middle of three such beds within the Round Mountain Formation. The lower of the three beds lies along the Olcese–Round Mountain contact. These boulder beds are numbered accordingly in Figure 13 and in the sections of Supplemental File 6. The highest-level (number 3) bed is dropped down to the topographic level of the Kern River channel by NE-striking normal faults that form a small graben (Fig. 13). Dense boulder lags laying in the Kern channel as displayed in Figures 12B and 12E are in situ bed number 3 exhumed along the river channel and winnowed of matrix mud and sand. The distinctive number 2 boulder bed (Figs. 12B–12E) is faulted up to a higher topographic level and exposed in the hills south of the Kern channel (Figs. 12F and 13).

Mesoscopic observations of the Round Mountain boulder bed (number 2) reveal its origin. As displayed in Figures 12B–12D, there is a crude inverse grading to this bed. By comparison of these photos with Figure 12F, taken from the south side of the river gorge, both the average and largest sizes of the constituent clasts decrease from south to the north, across the modern Kern trunk channel. These observations indicate a southerly source for the boulders by debris-flow mechanisms not related to the modern Kern River channel. Furthermore, the boulders from this bed are distinct from the Bear Valley Springs tonalite and diorite, which constitute the proximal footwall of the Kern Gorge fault. The position of the boulder bed within a bathyal marine section, along with the presence of a gypsum-bearing basal seam, indicates submarine deposition.

Boulders constituting the beds that lie within the Round Mountain Formation in the Figure 13 map area consist of the same distinct tonalitic assemblage that constitutes the Mount Adelaide southern lobe (Fig. 2) and the Bealville fanglomerate (Figs. 7 and 8). We interpret the Figure 13 boulder beds as marine debris-flow runouts that were directly linked to Bealville deposits of the Edison graben where such submarine debris flows occur in the Olcese, Round Mountain, and lower Bena formations (Fig. 8 D–D′ and E–E′). As on Figure 7, we show on Figure 13 the diagrammatic transport direction for the coarse debris by a yellow arrow. We suspect that Bealville boulder transport into the Figure 13 map area followed the relay ramp between the Kern Gorge fault and the normal fault system that formed the eastern margin of the Edison graben. Note the relative position of these features relative to the southern lobe of the Tonalite of Mount Adelaide on Figure 2.

The analysis presented above for the stratigraphy of the terraces laying along the hanging wall of the Kern gorge fault leads us to interpret them as differentially eroded strath terraces that were cut into lower and middle Miocene marine strata—not Quaternary Kern River terraces. The oldest of the remnant terraces lies immediately adjacent to the Kern gorge fault in the left foreground of Figure 12A. The youngest rests along the south side of the Kern trunk channel where the channel crosses into the hanging wall. Some flat top hilltops in the right background of Figure 12A could also be erosional remnants of older strath surfaces.

On Figure 6 B–B′, we show ~1800 m of missing Neogene strata above the hanging wall of the Kern gorge fault based on erosional truncations of the Kern arch section and disturbance patterns of apatite-He ages from nearby down-hole detrital samples (Cecil et al., 2014). Similar erosional truncations and both basement and detrital apatite-He age disturbance patterns from wells drilled into the sections adjacent to both the northwest and southeast relay ramps of the Kern gorge fault show similar ~1750–1800 m erosional values (Mahéo et al., 2009; Cecil et al., 2014). In contrast, the footwall basement surface from the Kern gorge fault lacks any sign of disturbance, indicating that it did not reach the apatite-He partial retention zone by sediment burial. We interpret this to indicate that structural relief on the fault grew during and/or shortly before sediment burial, resulting in the preservation of the regional primary apatite-He age-elevation relationship in the basement, indicative of a reduced sediment overburden.

Principal Faults of the Walker Graben

Normal fault structural relief that was sufficient in the Neogene to place elevated footwall basement high enough to shield its primary age-elevation patterns in apatite-He ages from sediment burial disturbance is preserved for the West Breckenridge, Breckenridge, Walker Basin, Bear Mountain, and proto-Garlock faults, as well as the Kern Gorge fault (Clark et al., 2005; Mahéo et al., 2009; Blythe and Longinotti, 2013). Each of these faults, except the proto-Garlock, is characterized by sparse to nil footwall debris draped across hanging-wall areas. In the case of the proto-Garlock fault, its hanging wall has been disrupted and sinistrally displaced ~64 km by the late Miocene to Quaternary Garlock fault (Monastero et al., 1997; Andrew et al., 2014). A near lack of hanging-wall alluvium is well displayed along the Kern Gorge fault (Figs. 12A

and 13). In the case of the Breckenridge fault, the paucity of footwall-derived alluvium is likewise extraordinary (Fig. 14). Similarly, the Walker Basin fault is devoid of footwall-derived alluvium. Both the Breckenridge and Walker Basin faults are mapped as imbricate normal faults, with modest late Quaternary W-up displacements documented along the eastern trace of the Breckenridge fault (Brossy et al., 2012). The basement floor of Walker Basin corresponds to a tilted segment of the regional low-relief upland surface (Fig. 6B and 6C) that is partly covered by fine-grained siliciclastic sediments of unknown age, or stratigraphic affinity. A core sample from an unspecified but "relatively shallow" depth from the center of the basin (obtained from W.D. Kleck, personal commun., 2013) consists of indurated gray-green siltstone suggestive of lacustrine conditions akin to those recorded in the Kinnick Formation (Fig. 5B). The low-relief basement surface beneath the basin locally emerges to the west and north as a pediment surface along the hanging walls of the Breckenridge and Walker Basin faults and southward as the low-relief basement surface of the Centennial Ridge tilt block (Figs. 6C and 14). The emergence of the Centennial Ridge basement surface adjacent to the Breckenridge basement scarp has localized the course of Walker Basin Creek where it exits the floor of Walker Basin, which is primarily under erosion, and not sedimentation. We attribute the paucity, or lack of, footwall-derived debris along the faults of Figure 14 to have resulted from much, or all, of their growth occurring under the actively accumulating Walker graben fill in early and middle Miocene time.

The early Neogene structural relief on the basement of the Kern Gorge and Walker graben-bounding faults has in Quaternary time been exhumed as topographic relief, rendering the high local relief pattern that distinguishes southern Sierra topography from the rest of the Sierran microplate to the north.

Coarse Erosional Lags across the Kern Arch

Published maps of the Kern arch, particularly adjacent to the modern Kern River channel, show extensive areas of low topographic relief, including terrace tops, as dissected Quaternary alluvial fans (Bartow, 1984; Bedrossian et al., 2012). These workers made no reference to the constituent clast populations of the mapped alluvial fan deposits. Furthermore, their fan stratigraphy appears to have been largely influenced by the erroneous assignment of the middle Miocene Bealville submarine debris flow exposed along the lower Kern strath terrace (Figs. 12 and 13) as a Kern River terrace deposit. Surficial deposits formerly mapped as Quaternary alluvial fans and/or Kern River terrace deposits consist of two distinct clast assemblages: (1) southern lobe of the Tonalite of Mount Adelaide, introduced into the Miocene stratigraphy as Bealville clasts; and (2) a mixture of Cache Peak volcanic rocks and southeastern Sierra Nevada batholithic and metamorphic pendant rock types referred to in aggregate as the "Caliente River clast type" (Saleeby et al., 2016), or for sake of brevity here, "Caliente clasts." Conspicuously missing from such surficial deposits are the well-mapped and well-dated batholithic rock types from the western Sierra including the Breckenridge-Greenhorn horst, the Kern River drainage, and the Tehachapi Range (Saleeby et al., 1987, 2007, 2008; Ross, 1989, 1995; Nadin and Saleeby, 2008; Chapman et al., 2012).

The Neogene stratigraphy of the Kern arch, from its topographic crest southward, was mainly marine facies until late Miocene time, when it transitioned into mainly fluvial-deltaic facies, and then, in the Pliocene, alluvial braided stream facies (Bandy and Arnal, 1969; Bartow and Pittman, 1983; Miller, 1986; Olson, 1988; Saleeby et al., 2016). Quaternary exhumation of the Kern arch removed

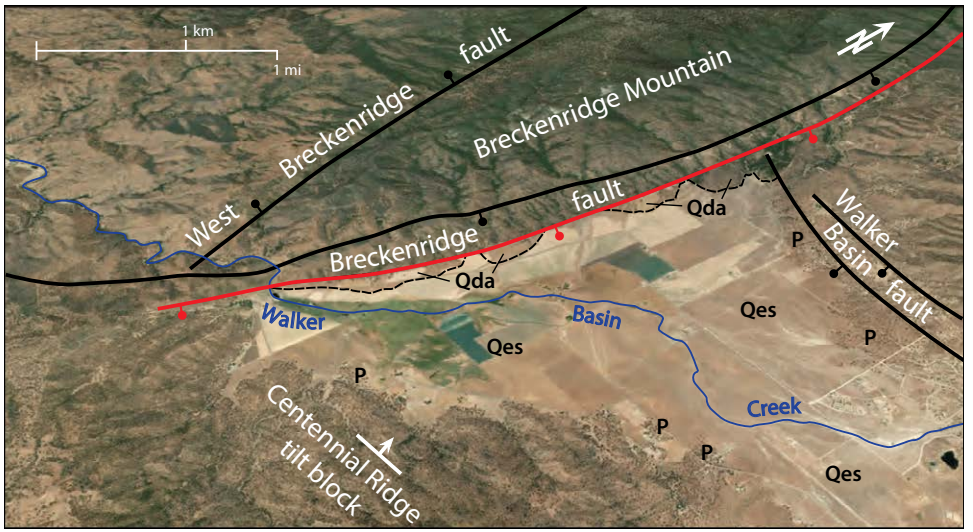

Figure 14. Google Earth oblique image northwestward into Walker Basin, which forms the northwest sector of the Walker graben; image also shows the intersection zone of Breckenridge and Walker Basin faults. Black faults are primarily early Neogene in age (this study), and red fault is late Quaternary (Brossy et al., 2012). View shows near absence of footwall debris extending onto hanging-wall areas of Breckenridge and Walker Basin faults. Qda—Quaternary footwall-derived debris apron; Qes—Quaternary erosion surface with shallow fluvial reworking of surficial debris; P—basement pediment surface.

up to ~1800 m of the mainly fluvial and alluvial strata (Cecil et al., 2014; Saleeby et al., 2016) by fluvial erosion along a low-relief, actively emerging, epeirogenic uplift (Le Pourhiet and Saleeby, 2013; Saleeby et al., 2013a). Other than possibly the trunk channel of the lower Kern River, the fluvial system that has eroded the arch through Quaternary time has done so under very low stream power conditions. Under such conditions, the conglomerate clasts that have been eroded out of the Neogene section have been transported primarily in the vertical direction, to be concentrated as coarse surficial lags as the finer sediment was winnowed out by local sheet flow and stream action. The process outlined above for production of coarse erosional lags across the Kern arch can be observed at a local scale by the most recent Kern River incision into its strath terrace as it exits the range front. The Figure 12B and 12E photographs across the hanging-wall river channel show 100% Bealville boulders choking the modern river channel. Many of these boulders still lie close to their middle Miocene stratigraphic position, which by chance, coincides with the base of the modern Kern channel (boulder bed 3, Fig. 13; Supplemental File 6 [footnote 1]). Along the north side of the channel, boulders derived from bed 2 have been displaced vertically into the channel as fine-grained sediment of the Round Mountain have been eroded along the terrace wall (Figs. 12B–12E). The south to north decrease in the average and largest Bealville clast size, as observed in the boulder beds (see above), is also preserved in the boulder lag, signaling the dominant vertical transport direction in boulder reworking, even within the trunk Kern channel. In contrast to the hanging-wall channel, the footwall basement channel is cluttered with proximal dioritic footwall boulders. The boundary between the two channel lag facies is precisely at the Kern Gorge fault, showing that even the main channel of the lower Kern River lacks the stream power to move large boulders over appreciable distances at recent time scales.

The propensity for the Bealville fanglomerate to form coarse erosional lags is also well expressed in the "type" Bealville map area (Fig. 7). Figure 15A is a photograph viewing west along Walker Basin Creek, where it exits its basement channel (Fig. 7). The steep north slope of Walker Basin Creek in this area consists of normal fault footwall basement that is mantled by Bealville boulder lag and/or grus derived from it. The lag is visible on Figure 15A, particularly the large boulder that lies along the skyline. The position of the Bealville lag on the elevated footwall here shows that the Bealville extended upslope toward the Bealville boulder source, stratigraphically above the Walker Formation, which also remains as small erosional outliers on the sloping basement surface (Fig. 7). As clearly shown on Figure 15A, Bealville lag has dropped topographically down into the Walker Basin Creek channel similar to that which is observed along the lower Kern River channel (Figs. 12B and 15A). Figure 7 shows that Bealville boulder lag is widespread above Walker Formation in the area where Walker Basin Creek exits the basement, as well as along Caliente Creek.

The position of the Bealville lag laying on basement and Walker Formation in the upper central part of Figure 7 indicates that the Bealville once extended upslope to the north and west of the main Bealville deposit. This is significant both in indicating that the Bealville source rests upslope to the north and east of the main deposit and in placing part of the main deposit in a position where it could run out to the northwest across the relay ramp between the range front and Kern Gorge faults (Fig. 4) to find submarine depositional settings along the Kern Gorge fault (Fig. 13). Furthermore, not visible on Figure 15A, but immediately upslope from the Bealville mapped lag, is a small area of Caliente clast lag that lies directly on basement (Fig. 7). The relative topographic levels of these two distinct lags mimic the vertical positions of

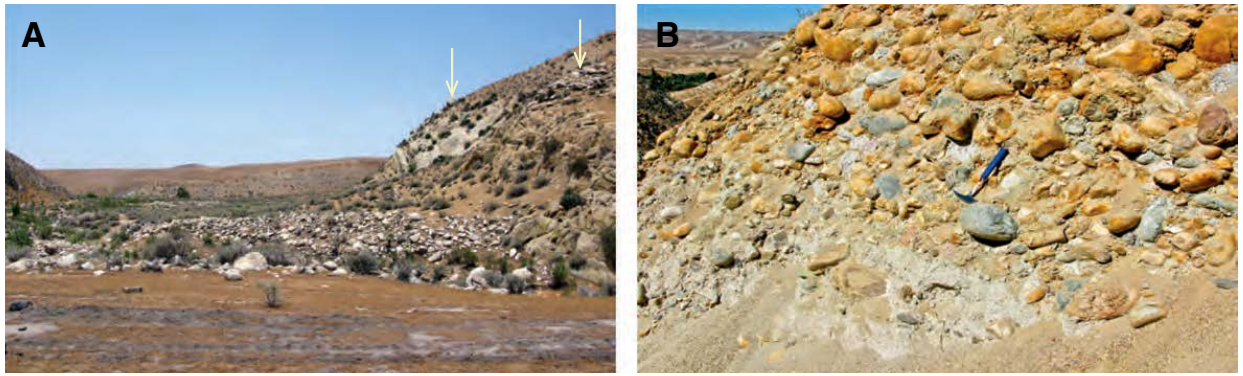

Figure 15. Photographs of erosional lags on Kern arch. (A) View westward out of Walker Basin Creek in Figure 7 map area showing lag deposits derived from the Bealville Fanglomerate on floor of canyon; lag deposits extending in background part way up strath terrace cut into Walker Formation (Fig. 7); and boulders and cobbles laying on sloping basement surface to upper right indicated by arrows. (B) Caliente lag across faulted contact between Chanac and Kern River formations ~6 km west of Kern Gorge fault. Cobbles consist of dacite (orange) and andesite (maroon) derived from Cache Peak volcanic center as well as various plutonic rocks from southeastern Sierra Nevada batholith.

their source beds within the Neogene section and indicate that the Miocene section extended upslope across currently exposed basement. The relative topographic levels of the two lags in this area also express the importance of vertical relative to horizontal transport of the coarse debris during erosional stripping of the finer matrix detritus.

The Caliente River was a major late-middle Miocene to Pliocene fluvial system that was sourced from the Walker graben and was channeled into the southeastern San Joaquin Basin through the structural saddle between the Breckenridge and White Wolf faults and then farther into the Basin through the Edison graben (Saleeby et al., 2016). The Caliente River clast type is expressed in conglomeratic units of the upper Bena, Chanac, and Kern River formations (Fig. 3A), whose detrital-zircon age patterns match age patterns of the Walker graben fill and basement exposures of its floor and walls (Saleeby et al., 2016). The clast assemblage also uniquely matches the Cache Peak volcanic center and proximal basement of the Walker graben floor and walls. Definitive features of these lags are displayed in the Figure 15B field photo. The clasts consist of a mixture of felsic, andesitic, and basaltic volcanic rocks that petrographically match the Cache Peak volcanic center, as well as batholithic and metamorphic rocks that match southeastern Sierra Nevada basement. The lags typically lack bedding features, and their sandy matrix material is typically non-compacted and locally inclusive of plant debris.

Erosional lags consisting of Caliente clasts are widespread across the Kern arch south of the Pond-Poso fault (Fig. 2), which matches the distribution of the Caliente clast-bearing Neogene units (Saleeby et al., 2016). To clarify the Figure 3A stratigraphic relations, large areas of the Kern arch north of the Pond-Poso fault (Figs. 1 and 2) were mapped as "Kern River Formation" (Bartow, 1984) and are reinterpreted as shallow-marine and estuary strata of the Etchegoin and San Joaquin formations, which were in facies relationships with fluvial and deltaic strata of the southern "Kern River Formation." Paleocurrent and provenance data on the southern "Kern River Formation" show that it formed primarily as a braided plain sourced from the Caliente River trunk channel that exited the range in the area of the Edison graben to the southeast (Miller, 1986; Saleeby et al., 2016; Fig. 2). Alluvial, fluvial, and deltaic strata of the Chanac and upper Bena Formations are likewise restricted to the southern Kern arch, being sourced from the trunk Caliente channel. The restriction of the Caliente clast lag deposits to the area where their clasts occur in the source Neogene units reflects the dominance of vertical versus lateral transport of the constituent clasts as they were eroded from their source units. Many of the lags appear to form terrace tops, but these terraces are straths cut into Neogene bedrock; they are not alluvial fans nor are they river-built terraces. These findings are essential for proper tectonic analysis of the Quaternary Kern arch.

TECTONIC FORCING AND PALEOGEOGRPAHIC EVOLUTION

The southern Sierra Nevada and adjacent San Joaquin Basin share a closely related tectonic history that was profoundly affected by both plate tectonics and more localized forces arising from geologically rapid redistributions in underlying mantle lithosphere loads. Bundled within this evolutionary history are the effects of structural inheritance that operated at different scales for the region's brittle crust and mantle lithosphere. In this section, we review both the tectonic and paleogeographic evolution of the region with a focus on late Cenozoic time. Tectonic forcing is manifest at multiple scales by regional rock and surface uplift, regional subsidence, and by more local-scale production of surface relief by faulting. The evolution of the mantle lithosphere beneath the southern Sierra region had profound effects both on the structural inheritance and surface dynamics that governed the late Cenozoic tectonics of the region. We begin our analysis with a brief overview of this subject.

Mantle Dynamics and Crustal Deformation

Figure 16 shows important features that relate to the Late Cretaceous and late Cenozoic evolution of the mantle lithosphere beneath the southern Sierra Nevada–San Joaquin Basin region. We focus first on the southern portion of the figure, which has structure contours constructed for the modern depth of the Rand fault (Cheadle et al., 1986; Li et al., 1992; Malin et al., 1995; Yan et al., 2005). The Rand fault operated as a unique segment of the southern Cordillera Late Cretaceous subduction megathrust system, having followed a shallow flat trajectory over an ~500-km-long stretch of the southern California convergent margin (Grove et al., 2003; Saleeby, 2003). The structure contours that show the megathrust flat are folded into a broad Quaternary syncline beneath the western Mojave plateau. The Garlock fault coincides with the northern margin of this expansive megathrust flat. The structure contours further show the megathrust to descend sharply to mid-crustal depths beneath the Tehachapi Range and Tejon Embayment (seismic-reflection line of Malin et al., 1995). The northward-deepening contours define a lateral ramp between the Rand megathrust and the Coast Range subduction megathrust that underlies the Great Valley and daylights in the central California Coast Ranges (Saleeby et al., 2013a). The (Rand) shallow segment of the southern Cordillera subduction megathrust system formed in the Late Cretaceous in response to the collision and subduction of a major oceanic plateau that was embedded in the Farallon plate (Saleeby, 2003; Liu et al., 2010; Sun et al., 2017). Collision-driven shallowing of the megathrust resulted in the shearing off and down-dip displacement of the mantle lithosphere that formed as the mantle wedge beneath the southernmost Sierra Nevada batholith and its extension into the southern California batholith (Saleeby, 2003; Luffi et al., 2009; Shields and Chapman, 2016). Mantle xenolith studies from the central Sierra Nevada batholith show that the Cretaceous mantle wedge was left intact beneath the greater Sierra Nevada region (Ducea and Saleeby, 1998), further defining the megathrust lateral ramp. Late in the displacement history of the Rand fault, it inverted to a regional low-angle normal fault as its subduction accretion assemblage was partially extruded back out the subduction channel to the southwest (Chapman et al., 2010, 2012).

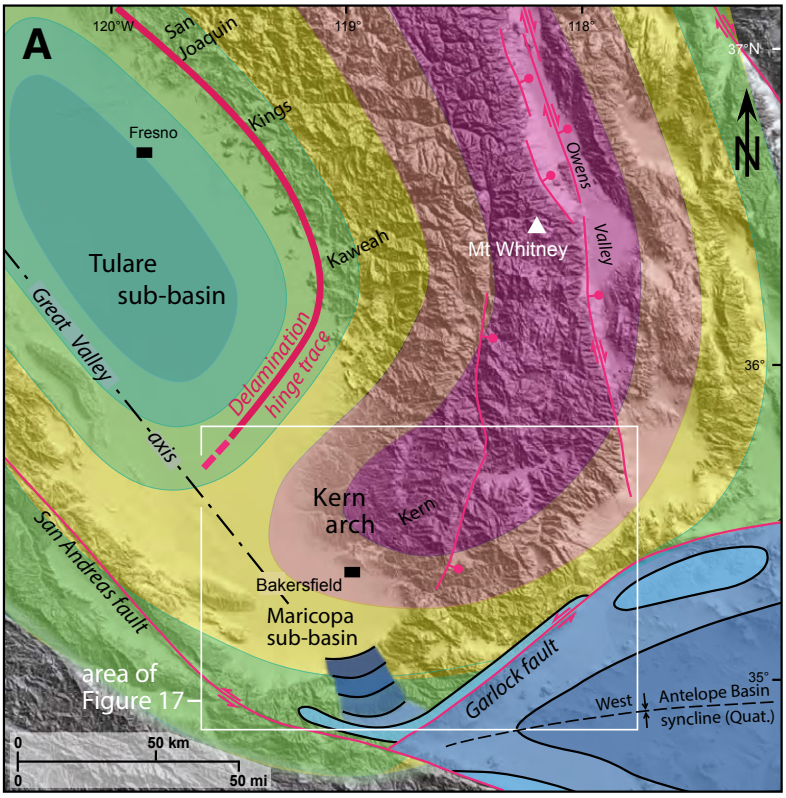

Modeled surface displacement resulting from the progression of mantle lithosphere delamination as rendered in image B below (contours terminated at Garlock fault)

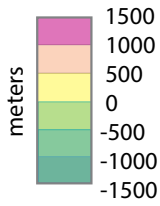

Structure contours on the Late Cretaceous Rand subduction megathrust defining the southern boundary of the residual mantle lithosphere that progressively delaminated in late Miocene to Quaternary time as rendered in image B below

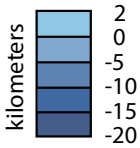

Major active faults as in Figure 2

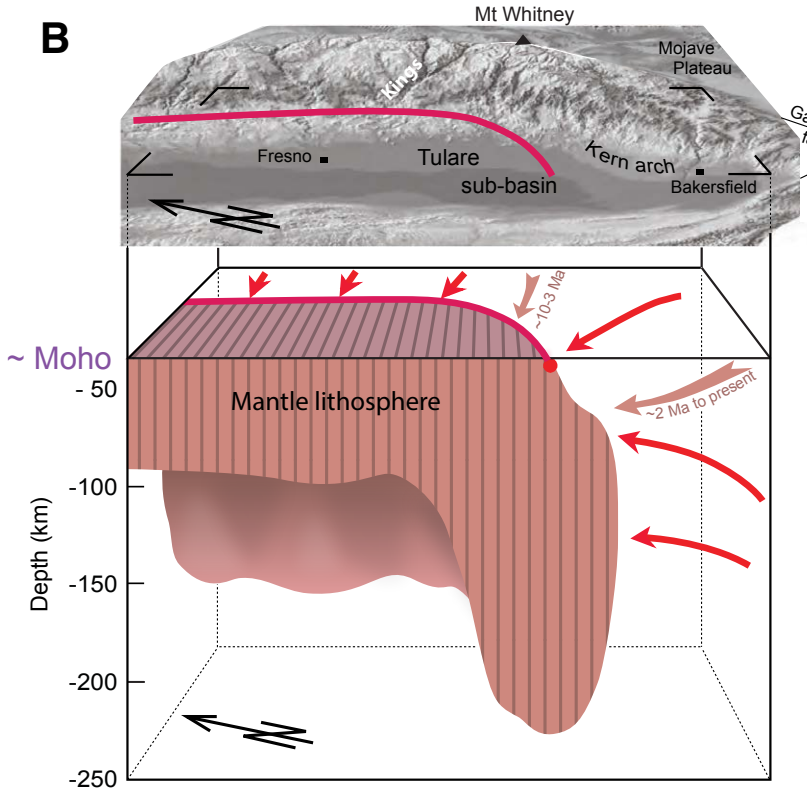

Oblique digital elevation model registered to mantle block diagram below

Model results predict slow east to west delamination initiating at ca. 10 Ma, accelerating from 6 to 1 Ma, and then subsequent vertical stretch of the delaminated slab

Inflow of asthenosphere

Delamination through time

Delamination hinge and its surface trace on digital elevation models above

100 km V=H

Figure 16. Select geodynamic features of southern Sierra Nevada region. (A) Digital elevation model with shaded contours plotted showing the modeled Quaternary surface uplift and coupled tectonic subsidence resulting from mantle lithosphere delamination (Le Pourhiet and Saleeby, 2013; Saleeby et al., 2012); and in southeast structure contours on the Rand fault, which, by low-angle subduction, sheared off the Mesozoic mantle lithosphere of the southernmost Sierra Nevada and adjacent Mojave region (Cheadle et al., 1986; Li et al., 1992; Malin et al., 1995; Yan et al., 2005). (B) Idealized block diagram for contemporary upper-mantle structure of southern Sierra Nevada region registered to oblique digital elevation model (after Saleeby et al., 2013a). The partially delaminated slab of sub-Sierran mantle lithosphere constitutes the Isabella high seismic wave speed anomaly (Jones et al., 2014). V=H—vertical scale equals horizontal scale.

The Late Cretaceous plate tectonic regime summarized above had several important impacts on the Cenozoic tectonics of the region: (1) The late Cenozoic Garlock fault nucleated precisely along the axis of the principal inflection of the subduction megathrust lateral ramp (Fig. 16A). (2) The southernmost Sierra Nevada batholith and adjacent Great Valley forearc were stripped of their mantle lithosphere leaving the crust in a poorly coupled state to the underlying mantle. (3) The southernmost Sierra Nevada–Great Valley region crust was severely weakened by pervasive extensional faulting and fracturing due to its coupling to the southwest extrusion of subduction accretion assemblages as the Rand fault inverted to a regional low-angle normal fault (Wood and Saleeby, 1998; Chapman et al., 2010, 2012, 2017). (4) The White Wolf–Kern Canyon fault system developed as a crust-penetrating ductile shear and fault zone that partitioned the crust into differentially deforming extensional panels (Nadin and Saleeby, 2008; Saleeby et al., 2009b). (5) The Owens–Indian Wells Valley fault system developed as a dextral fault zone that further partitioned upper-crustal extensional panels in the southern Sierra region (Bartley et al., 2007). (6) Large-magnitude extensional faulting exhumed the southernmost Sierra Nevada batholith from mid- to lower-crustal levels over the southern ~75 km of the batholith and imparted a regional topographic gradient that descended southward to sea level by the end of Cretaceous time (Wood and Saleeby, 1998; Nadin and Saleeby, 2008; Chapman et al., 2012, 2017). (7) Southwest extrusion of the Rand subduction channel material and coupled crustal extension deformed the southernmost Sierra Nevada batholith into a dextral-sense orocline (Wood and Saleeby, 1998; Chapman et al., 2010), which is traditionally interpreted as a Miocene feature (McWilliams and Li, 1985; Goodman and Malin, 1992; Reid, 2009). (8) The initial exhumation of the Sierra Nevada batholith in the Late Cretaceous promoted upper-crustal cooling that coupled low-temperature thermochronometers of the basement to regional geomorphic patterns and landscape evolution (House et al., 2001; Clark et al., 2005; Cecil et al., 2006; Saleeby et al., 2007; Mahéo et al., 2009; Sousa et al., 2016b). The disrupted state of the southern Sierra region mantle lithosphere and crust resulting from the Late Cretaceous events summarized above rendered the region more highly susceptible to deforming during subsequent tectonic episodes than the greater Sierra Nevada to the north—episodes that we will now discuss.

Early Tertiary Faulting and Exhumation

The Late Cretaceous events outlined above left the southern Sierra Nevada batholith crust south of ~35.7°N in a fragmented state and with much of its underlying mantle lithosphere removed. Peripheral structural and rapid exhumation signatures resulting from this tectonic regime are observed as far north in the Sierra Nevada as ~37°N (Nadin et al., 2016; Sousa et al., 2016b). Earlier we discussed evidence for Eocene activity along the western Sierra normal fault system (Fig. 1) and for at least local Eocene to Oligocene activity along the principally Neogene southern Sierra normal fault system, as well as cover strata erosional phases along the eastern Basin margin. Within the Walker graben area, the early Paleogene Witnet Formation underwent tilting and extensive erosion prior to Kinnick deposition and Cache Peak volcanism, leaving isolated Witnet patches adjacent to, and along the base of, the Kinnick (Figs. 2 and 6 B–B′). Upper Paleogene shoaling and erosional phases are also recorded within the greater San Joaquin Basin stratigraphy (Reid, 1988; Reid and Cox, 1989; Bartow, 1992) and in the northern Great Valley, where normal growth faulting and submarine canyon incision accent the late Paleogene history (Imperato, 1995; Unruh at al., 2007; Sullivan and Sullivan, 2013).

Regional epeirogenic deformation is well expressed for the early Cenozoic of the southern Cordillera by the rise of the Nevadaplano with its north-south drainage divide that runs along the eastern Nevada region (DeCelles, 2004; Henry and John, 2013). In terms of potential plate tectonic forcing mechanisms, the subduction of progressively younger aged oceanic lithosphere of the Farallon plate through early Cenozoic time (Atwater and Stock, 1998; Seton et al., 2012) conceivably provided the dynamic framework for such epeirogeny. Late Eocene regional uplift of the Sierra Nevada region and complementary east-up high-angle normal faulting along the western Sierra are in line with regional surface uplift along the western margin of the Nevadaplano. The more distal western reaches of this uplift reached the Great Valley basin, promoting submarine canyon incision, shoaling phases, and depositional hiatuses. The extent to which this epeirogenic regime continued into, or through, Oligocene time is poorly constrained. Plate tectonic reconstructions show that the Mendocino Triple Junction began its northward trajectory along southern Sierra latitudes at ca. 25 Ma (Atwater and Stock, 1998), initiating a new tectonic and geodynamic regime for the region.

Early Miocene Normal Faulting and Volcanism

Figure 17A shows the normal faults and the attendant volcanism and sedimentation patterns for early Miocene time focused on the time interval of 19–17 Ma. Early Miocene time was characterized by the northward passage of the Mendocino Triple Junction and the opening of the Pacific-Farallon slab window (Atwater and Stock, 1998). We track this on Figure 17A by a Mendocino edge reference line. This line tracks the migration of the Mendocino plate edge (northern border of the slab window) through the area of Figure 17A, as well as the derivative rolling hinges of uplift and subsidence (Table 3). Early attempts to relate epeirogenic pulses driven by the subduction and northward migration of the Mendocino plate edge to San Joaquin Basin stratigraphy (Glazner and Schubert, 1985; Loomis and Glazner, 1986) have been improved upon by subsequent plate kinematic studies (Atwater and Stock, 1998) and dynamic analysis of the Mendocino Triple Junction leading to the "crustal conveyor model" (Furlong and Govers, 1999). This model asserts that as the triple junction migrates northward, isostatic uplift related to transient crustal thickening, followed by thinning, in conjunction with dynamic topography resulting from asthenosphere flow into the slab window, produces a double rock uplift signal with an intervening tectonic subsidence signal (Table 3).

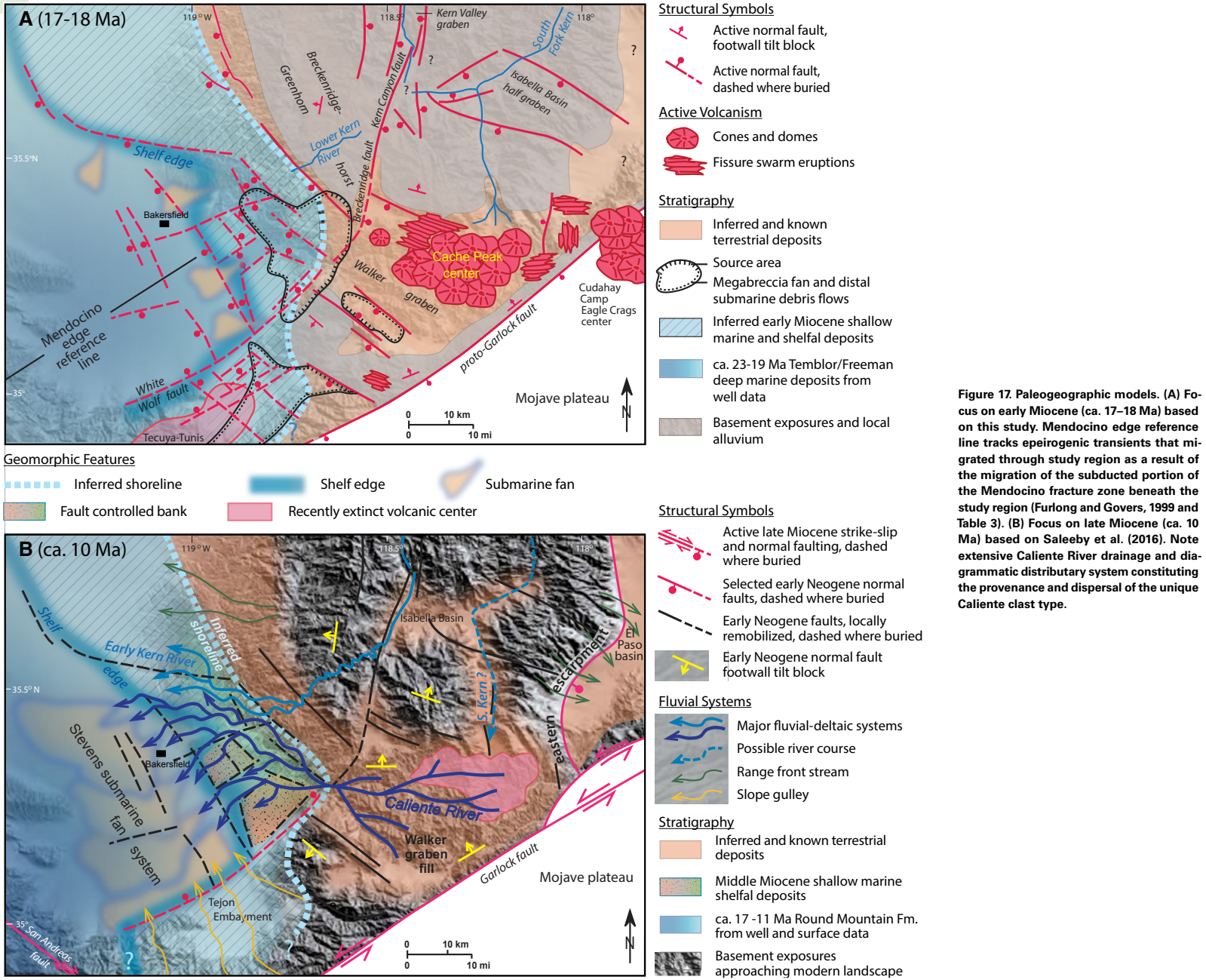

Figure 17. Paleogeographic models. (A) Focus on early Miocene (ca. 17–18 Ma) based on this study. Mendocino edge reference line tracks epeirogenic transients that migrated through study region as a result of the migration of the subducted portion of the Mendocino fracture zone beneath the study region (Furlong and Govers, 1999 and Table 3). (B) Focus on late Miocene (ca. 10 Ma) based on Saleeby et al. (2016). Note extensive Caliente River drainage and diagrammatic distributary system constituting the provenance and dispersal of the unique Caliente clast type.

TABLE 3. TEMPORAL SEQUENCE OF EPEIROGENIC TRANSIENTS THAT MIGRATED ACROSS MENDOCINO EDGE REFERENCE LINE OF FIGURE 17A BASED ON MENDOCINO TRIPLE JUNCTION CRUSTAL CONVEYOR MODEL; AND POSSIBLE STRATIGRAPHIC EXPRESSIONS ALONG EASTERN SAN JOAQUIN BASIN MARGIN

Age (Ma)	Mendocino Plate Edge Signal	Stratigraphic Expression
24	Position of subducted Mendocino plate edge	*Extensive erosion along SE Basin margin (ca. 26–20 Ma)*
26–22	First rock uplift phase	Vedder shallow-marine–alluvial facies; shallow-marine lower Jewett sands
22–20.5	First tectonic subsidence phase	Freeman-Jewett bathyal marine silts
20.5–17	Second rock uplift phase	Olcese shallow-marine and alluvial sands
17–13	Second tectonic subsidence phase	Round Mountain–Fruitvale bathyal marine silts and shale

Sources: Atwater and Stock (1998); Furlong and Govers (1999); Wilson et al. (2005); Lock et al. (2006); Table 1 and Figure 3A.
Note: Italics denotes hiatuses developed along basin margin during triple junction migration.

Vertical displacements of uplift and subsidence are at kilometer scale and thus are more significant on basin stratigraphy than the 50–100-m-scale eustatic sea-level changes for the Neogene (Haq et al., 1987). Table 3 summarizes the stratigraphic expression of the uplift and subsidence transients that occurred along the southeastern San Joaquin Basin margin as a result of triple junction migration. Correlations with the crustal conveyor model are good to within ±1 m.y., although early Oligocene shoaling recorded by the lower Vedder sands (Fig. 3 and Table 1) also correlates with an ~200 m drop in eustatic sea level (Haq et al., 1987; Tye et al., 1993).

During the 20.5–17 Ma rock uplift phase (Table 3), and continuing partly into the subsequent tectonic subsidence phase, the southern Sierra Nevada and eastern San Joaquin Basin underwent high-angle normal faulting, diffuse basaltic volcanism, and focused growth of the mafic to felsic Cache Peak volcanic center (Fig. 17A). High-angle normal faulting of the southern Sierra system extended as far north as the Isabella Basin and Kern Valley region and well into the eastern part of the Tulare sub-basin (Fig. 1). The Walker graben sediment accommodation space formed by displacement along inward-facing normal scarps of the Walker Basin, Breckenridge, and Bear Mountains faults, and by the footwall tilt block of the proto-Garlock fault. The early Miocene Breckenridge and White Wolf normal faults formed along the southern half of the Late Cretaceous Kern Canyon–White Wolf basement shear zone, with W-up motion along the Breckenridge segment being an integral part of the Walker graben and SE-up motion of the White Wolf segment initiating the Neogene sediment accommodation space that subsequently became the Maricopa sub-basin (Davis, 1983; Goodman and Malin, 1992; Saleeby et al., 2013a). Despite the widespread distribution of southern Sierra system normal faults, the magnitude of extension appears modest, with the rectilinear pattern of faulting suggesting a strong component of vertical flattening and horizontal pure shear. Such an integrated strain pattern is consistent with the associated cycles of epeirogenic uplift and subsidence and the terminal crustal thinning phase predicted by the Mendocino crustal conveyor model (Furlong and Govers, 1999). Many of the Neogene faults of the southern Sierra system followed Late Cretaceous basement structures, and along the eastern margin of the San Joaquin Basin, the faults exhibit complex Paleogene subsurface growth patterns. Additionally, some of the stratigraphic complexities documented across growth faults along the eastern San Joaquin Basin margin (Figs. 6, 8, and 11; Supplemental File 6 [footnote 1]) conceivably resulted from transient reversals in sense of motion as the axes of uplift and subsidence nodes migrated through the region (Table 3).

Regional tectonic forcing for the incision of major westward-flowing Sierra Nevada river channels diminished during the early Miocene, compared to Late Cretaceous through Eocene time (House et al., 2001; Sousa et al., 2016a), as well as late Neogene–Quaternary time (discussed below). Consequently, coarse clastic sedimentation was restricted to a complexly faulted shelf with only local small turbiditic fans lapping off the shelf onto the basin floor (Tye et al., 1993; Reid, 2009; Fig. 17A).

The Cache Peak volcanic center is shown on Figure 17A nested within the Walker graben and in its principal phase of basalt-andesite stratocone and felsic dome construction. Dense swarms of dikes adjacent to the center (Fig. 2) are shown feeding fissure eruptions. The Cache Peak center and adjacent fissure eruptions to the east formed a near continuous volcanic field with the Cudahay Camp volcanic center, which lapped across the scarp of the proto-Garlock fault to subsequently be displaced by the sinistral Garlock fault as the Eagle Crags center of the northern Mojave plateau (Monastero et al., 1997). Olivine basalts in the Cache Peak center are presumed to have a depleted mantle source from asthenosphere that filled into the slab window. The more felsic rocks of the Cache Peak center are too voluminous to be directly related to the basalts by differentiation processes. In the crustal conveyor model, initial slab window opening is coincident with a crustal thickening transient that lasts ~4 m.y., over the past ~2 m.y. of which asthenosphere flow into the slab window starts. This is followed by ~5 m.y. of crustal thinning, during which, asthenosphere ascent accelerates and then ceases. The coincidence of maximum crustal thickening with underlying asthenosphere ascent presents an ideal setting for synchronous generation of primitive basaltic magmas from the asthenosphere and more felsic magmas from deep-level thickened crust. In a review of late Cenozoic volcanism of coastal California, Dickinson (1997) resolves an ~3 m.y. time lag

between the migratory position of the Mendocino plate edge and the corresponding eruption of "slab window" volcanic rocks. This relationship holds for the Cache Peak volcanic center, noting the position of the Mendocino edge at 24 Ma (Table 3) and the initiation of Cache Peak volcanism at ca. 20 Ma (Fig. 3B). This magma genesis regime offers a mechanism for the few zircon grains extracted from the Cache Peak–derived felsic rocks that give aberrant ages as old as 24 Ma (Supplemental Items 1 and 2 [footnote 1]). In this scenario, lower-crustal partial melting began in small domains as crustal thickening progressed, some partially freezing and crystallizing zircon, subsequently to be incorporated into larger partial melt channels that formed during the 20–17.5 Ma principal flux of felsic magma and ash eruptions (Fig. 3B). Isotopic data on the Ilmon basalt and related dikes (Fig. 10G and Table 2) show that asthenosphere-derived melts continued to erupt as late as ca. 17 Ma (Table 2).

In the Tejon Embayment–San Emigdio Mountains area, the Tunis-Tecuya volcanic center shed basaltic and dacitic lavas across near-shore terrestrial and shallow-marine environments in earliest Miocene time (Figs. 3C and 17A). Isotopic data show that the basalts were derived from ascended asthenosphere, and the dacites were derived from lower-crustal sources (Sharma et al., 1991; Fig. 10G). We interpret the genesis of these volcanic rocks to be similar to that of the Cache Peak center, discussed above. The ~2 m.y. older age of the Tunis-Tecuya lavas may reflect its more southerly position, relative to the Cache Peak center, also taking into account Quaternary clockwise rotation of the San Emigdio Tertiary section in the upper plates of the active thrust belt (Chapman et al., 2010; Fig. 2).

The intersection zone between the W-up Breckenridge and SE-up White Wolf faults produced a breach in the western wall of the Walker graben, providing a structural channel for fluvial, ash-flow, and lahar dispersal from the Cache Peak center into the Edison and range front graben system. Rapid relief generation on the Breckenridge and West Breckenridge faults destabilized a large hanging-wall complex in their intersection area; this complex collapsed to move downslope as the Bealville fanglomerate and its submarine debris-flow runout deposits (Figs. 7, 8, 12, and 13). Distal fines sourced from the Bealville runouts were shed into the deeper part of the southern San Joaquin Basin as the Nozu sands and grits (Figs. 3A and 8 D–D′). Rapid relief generation along the Bear Mountain and Tejon Creek faults is hypothesized to have generated similar megabreccias that ran out onto the western Kinnick lacustrine-ash sequence (Fig. 5C), as well as the shoreline and offshore environments of the Tejon Embayment (unnamed conglomerate of Nilsen et al., 1973, and Goodman and Malin, 1992). Stratigraphic truncations along the base of the unnamed conglomerate (Nilsen et al., 1973) and Bealville (Figs. 7 and 8) indicate local erosion of the basin margin section in conjunction with the generation of structural and topographic relief that drove megabreccia dispersal.

The reconstruction of sediment overburden thicknesses that have been eroded off of the Kern arch and adjacent Sierran basement, as well as the Walker graben (Fig. 6), indicate that much of the basement of the region was buried by sediment in the early to middle Miocene. The Kern Gorge fault and faults that controlled the Edison graben are shown as active growth structures for this time interval. The lower Kern River canyon between the West Breckenridge and Kern Canyon faults is characterized by a broad deep canyon that resembles in form the older Eocene and perhaps Late Cretaceous paleolandscape regime that characterizes the greater Sierra Nevada to the north (House et al., 2001; Stock et al., 2004; Sousa et al., 2016a). The West Breckenridge fault formed the local range front, with the lower Kern drainage incised deeply through its footwall. Sediment overburden constraints for the fault's hanging wall (Fig. 6B) indicate sediment aggradation up into the footwall river channel. It is possible that aggradation extended up into the Isabella Basin half graben, and that the graben was alluviated deeply, hosting ephemeral lakes; but there are few constraints on this. Based on geomorphic and basement rock weathering patterns, we speculate that the South Fork of the Kern River transected the Isabella half graben to debouch into the northern Walker graben. The course of the North Fork Kern River is uncertain as to where it exited the Kern Valley graben. Conceivably it flowed into the Isabella Basin half graben to join the South Fork course into the Walker graben.

Late Miocene Microplate Break-Off and Regional West Tilting

By late Miocene time, the Mendocino Triple Junction and its epeirogenic welts and troughs had migrated to northern Sierra latitudes beyond its influence along southern Sierra latitudes (Atwater and Stock, 1998). At ca. 10 Ma, the Sierran microplate broke off from the western edge of the Nevadaplano and underwent regional west tilting that forced profound changes in erosion and sediment dispersal and accumulation patterns (Fig. 17B). The principal controlling structural system for this tectonic regime was the eastern Sierra escarpment system, which followed the Late Cretaceous Owens–Indian Wells Valley dextral fault system (Bartley et al., 2007). A number of regional factors indicate that microplate break-off occurred between 8 and 10 Ma (Loomis and Burbank, 1988; Busby and Putirka, 2009; Saleeby et al., 2009a), although distinct changes in the depositional patterns of the San Joaquin Basin (Saleeby et al., 2016) suggest this forcing regime could have started in the south as early as ca. 12 Ma. Stratigraphic complexity along the eastern Basin margin was compounded by an ~200 m drop in eustatic sea level between 14 and 11 Ma (Haq et al., 1987). This eustatic sea-level change plausibly explains the erosional unconformity at the base of the upper Bena Formation along which alluvial gravels channeled into the Round Mountain and lower Bena marine units (Fig. 3A). Alternatively, erosion of these marine units and the progradation of the upper Bena alluvium extended across the northeastern (uplifted) side of the regional west-tilt axis of the newly formed microplate producing the unconformities. Subsequent Pliocene–Quaternary subsidence along the eastern edge of the Tulare sub-basin and en masse uplift of the Kern arch and Breckenridge-Greenhorn horst (Saleeby and Foster, 2004; Saleeby et al., 2013a) have deformed the southern reaches of the tilt axis to the extent that it cannot be accurately recognized in the field, as it is along the northern reaches of the microplate (Fig. 1 inset).

The west tilt of the Sierran microplate initiated the deepening of major west-flowing river channels in Sierran basement (Unruh, 1991; Stock et al., 2005; Busby and Putirka, 2009). At this time, the Walker graben fill also began a period of vigorous erosion with fluvial transport of the derivative detritus into the southeastern San Joaquin Basin along a major fluvial system called the Caliente River (Saleeby et al., 2016). The Caliente River was funneled through the breach in the western wall of the Walker graben that formed along the intersection zone of the White Wolf and Breckenridge faults, and it was further channeled along the Edison and range front graben system. This structural control promoted the northwestward growth of a fluvial fan and deltaic system that crossed and thereby deflected northward the course of the lower Kern River. Sediment load in the Caliente River is hypothesized to have greatly exceeded that of the Kern River as a result of the former being sourced in an actively eroding Miocene sedimentary basin while the latter was sourced primarily by basement channel incision (Saleeby et al., 2016). Kern arch stratigraphic units that record the Caliente fluvial-deltaic regime include the upper Bena, Chanac, and parts of the Santa Margarita formations (Fig. 3A). Northward progradation of this fan-delta system was mimicked in the deeper parts of the basin by the northward sequential growth of submarine fan lobes of the Stevens fan system, which was sourced primarily from the Caliente River delta front (MacPherson, 1977; Harrison and Graham, 1999; Saleeby et al., 2016).

Continued displacement along the southern Sierra fault system into late Miocene time has not been documented for faults exposed in the Sierran uplands, but local continued growth is documented along some members within the eastern San Joaquin Basin (Figs. 6 A–A′ and 8 D–D′ and EE′; Reid, 2009). Relief generation along the southernmost eastern Sierra escarpment system also resulted in a westerly-derived sediment flux that was shed into the El Paso Basin (Loomis and Burbank, 1988). Beyond the eastern escarpment system, the Sierran microplate was further defined during this time frame by the initiation of left slip along the Garlock fault (Monastero et al., 1997) and the integration of right slip along the San Andreas transform system into its current kinematic regime (Dickinson and Wernicke, 1997; Atwater and Stock, 1998).

Quaternary Epeirogenic Rise of the Kern Arch

Latest Miocene and Pliocene time were characterized by continued erosion of the Walker graben fill and the progradational growth of the Caliente River fan across much of the future Kern arch region by the northwest-directed braided stream system of the "Kern River" Formation (Miller, 1986; Saleeby et al., 2016). To the west within the axial San Joaquin Basin and to the north in the area of the northern Kern arch, the Kern River Formation is in facies relations with the Etchegoin and San Joaquin formations that record shoaling in the basin to shallow-marine and estuary facies (Fig. 3A and Table 1). Up-dip stratigraphic projections of the erosional truncations of the Kern River Formation and its northern facies equivalents (Mahéo et al., 2009; Saleeby et al., 2009a, 2013a; Fig. 6B) and low-temperature thermochronometry from Kern arch strata (Cecil et al., 2014) indicate that maximum sediment burial of the Sierran range front area occurred near the end of Kern River Formation deposition, in the earliest Pleistocene (Fig. 3A).

During the Quaternary, an epeirogenic uplift migrated into the study area as a result of the delamination of the residual sub–Sierra Nevada batholith mantle lithosphere that was left intact above the lateral ramp in the Rand–Coast Range subduction megathrust system (Figs. 16A and 16B). The region of this uplift extended far beyond the map area of Figure 17, affecting the axial to eastern Sierra Nevada as far north as ~38°N (Saleeby et al., 2013a). On Figure 16A, the area affected by this phase of uplift is shown for the region south of ~37°N by surface and rock uplift and coupled tectonic subsidence contours that are constructed by the integration of two-dimensional thermomechanical models of the Sierran delamination process and three-dimensional models of the flexural anomaly resulting from the modern mantle lithosphere load that is still attached to the base of the crust (Le Pourhiet et al., 2006; Saleeby et al., 2012; Le Pourhiet and Saleeby, 2013). The total predicted uplift shown by the contours developed primarily during the Pliocene along the eastern to axial Sierra and Quaternary for the region of the Breckenridge-Greenhorn horst and Kern arch. Predicted tectonic subsidence shown for the Tulare sub-basin includes Pliocene and Quaternary time and matches well with observed subsidence (Saleeby et al., 2013a). Also shown on Figure 16A is the current surface trace of the delamination hinge (Saleeby et al., 2012, 2013a), which demarks the locus of separation of mantle lithosphere from the crust (Fig. 16B). The hinge runs obliquely northeastward along the northern margin of the Kern arch and then turns to a northwest trend along the western Sierra Foothills, east of the Tulare sub-basin. The northwest-trending hinge trace segment migrated from the Owens Valley region (locus of Sierran microplate break-off) to its current position mainly during the Pliocene by a westward progression in delamination, while the northeast-trending segment migrated from the (Rand fault) truncated southern edge of the mantle lithosphere to its current position in the Quaternary (Saleeby et al., 2013a).

The axis of the northeast-trending segment of the modeled uplift welt corresponds to the topographic axis of the Kern arch (Figs. 16A and 16B). This uplift welt continues eastward through basement exposures of the Breckenridge-Greenhorn horst; these exposures are anomalously elevated relative to basement exposures along the entire western Sierra (Saleeby et al., 2013a; Fig. 1). The principal Neogene normal faults that resulted in horst structural relief, as well as growth faults along the eastern Basin margin, were epeirogenically uplifted en masse with local fault remobilizations plausibly resulting from flexure-related fiber stresses. At the position of the arch topographic axis, proximal to the cover strata-basement contact, the uplift model predicts ~1000 m of surface and rock uplift. Regional surface uplift of the eastern and axial Sierra basement forced the deepening of major river channels and their proximal side creeks mainly in the Pliocene (Stock et al., 2004; Figueroa and Knott, 2010; Krugh and Foreshee, 2018) but drove very little erosion of the regional low-relief upland surface (Clark et al., 2005; Stock et al., 2005). In contrast, feebly- to non-lithified Neogene strata of the Kern arch and adjacent western Sierra were vigorously eroded by fluvial activity dispersed across

the low-relief surface as the region rose in the Quaternary. Quaternary uplift along the eastern Kern arch forced ~1800 m of sediment erosion (Mahéo et al., 2009; Cecil et al., 2014; Fig. 6 B–B′), which is on order with the modeled ~1000 m of delamination-forced uplift. This can be demonstrated by simply considering the first-order relationship between erosion and resultant flexural isostatic uplift. Gilchrist and Summerfield (1991) show that for the scale of the crustal load imposed by the Isabella anomaly (Fig. 16B), the flexural isostatic response to progressive denudation is continuous in time and space. This is consistent with Quaternary deposits in the Tulare and Maricopa sub-basin; these deposits record continuous Quaternary sedimentation as the adjacent arch rose and was eroded (Miller, 1999; Saleeby and Foster, 2004, their supplemental file; Saleeby et al., 2013a). The first-order relationship between denudation (D) and rebound (R) is: $D = R(\rho_m/\rho_c)$, where ρ_m = upper-mantle density (~3.3) and ρ_c = crustal density (~2.7) (Gallagher, 2012, Equations 8A and 8B). The 1000 m uplift contour on Figure 16A closes around the Kern arch topographic crest at an elevation of ~450 m (~1500 ft), which approximates local Quaternary surface uplift referenced to the shallow-marine and estuary San Joaquin Formation, the deposition of which was terminated by the rise of the arch (Fig. 3A). Total uplift of ~1450 m multiplied by the rock density quotient of 1.22 results in denudation of 1770 m, which for a first-order calculation is close to the observed 1800 m of erosion referenced above.

Emergence of the Kern arch partitioned the eastern San Joaquin Basin into the Tulare and Maricopa sub-basins. The early Quaternary onset of this episode is recorded to the northwest of the arch by ~1–2-m.y.-old subsurface foresets that record fluvial reworking of arch detritus into the adjacent Tulare sub-basin (Miller, 1999) and by pronounced thickening of Pleistocene strata to the south of the arch in the Maricopa sub-basin (Saleeby et al., 2013a; Fig. 6 A–A′). As the Kern arch rose, its erosional detritus was reworked northwestward into the Tulare sub-basin, westward into the axial trough of the Great Valley and southward into the Maricopa sub-basin. This pattern is clearly expressed in the modern geomorphology of the arch by the generally radial orientation of drainages that disperse off it, including that of the lower Kern channel (Fig. 1). The lower Kern channel shows evidence of its southward migration away from the topographic axis of the arch by its subdued northern wall and steep, high-relief segments along its southern wall. Demise of the Caliente River also entailed the deflection of its lower trunk channel southward into the Maricopa sub-basin, with the creation and ultimate demise of its terminal channel (Figs. 2 and 7). Terminal channel demise is interpreted to have resulted from the changes in tectonic forcing entailing the waning of eastern Sierra escarpment faulting in the southernmost Sierra region and the epeirogenic rise of the Breckenridge-Greenhorn horst and Kern arch (Saleeby et al., 2009a). Near exhaustion of the Walker graben fill detrital source for the Caliente River (Figs. 6B and 6C) is also likely to have contributed to the demise of the once expansive river system.

On Figures 1 and 4, we show two color tones for areas of Sierran basement that have had extensive sections of Neogene strata eroded off: (1) teal for the eastern margin of the Kern arch in Quaternary time and (2) beige for the Walker graben fill in late Neogene–Quaternary time. The exhumed nonconformity surface along the southeast Basin margin maps in near continuity, although with minor erosional modification, into the low-relief upland surface of Clark et al. (2005) and Mahéo et al. (2009). Study of Figure 1, as well as relations depicted in Figure 17, reveal that the West Breckenridge fault scarp bounded the southeast San Joaquin Basin margin through much of the Neogene as well as early Quaternary time. Quaternary erosion of the Neogene section off of the footwall of the Kern Gorge fault left the lower Kern River trunk channel to superimpose its meandering course steeply into footwall basement. Sharp meanders in the steep basement channel of the Kern Gorge fault footwall consequently resemble in wavelength and amplitude current meanders in the lower Kern trunk channel that are incising through Kern arch Neogene section (Fig. 1).

The oblique digital elevation model (DEM) that is used in the block diagram of Figure 16B demonstrates the critical first-order geomorphic patterns that resulted from the various phases of tectonic forcing discussed above. The profound regional topographic gradient that descends southward from the Mount Whitney region to the Mojave plateau developed in the Late Cretaceous as a result of large-magnitude extensional faulting linked to the Rand megathrust extrusion channel (Wood and Saleeby, 1998; Saleeby, 2003; Chapman et al., 2012, 2017). To the north of this topographic gradient, the Sierran highlands exhibit large-wavelength topographic variations with large west-flowing river channels that mark the initiation of Sierran landscape evolution off the western margin of the Nevadaplano (House et al., 2001; Sousa et al., 2016a). Deepening of the large west-flowing river channels may be linked to the ca. 10 Ma breakoff of the Sierran microplate from the Nevadaplano and west tilting (Unruh, 1991; Stock et al., 2005; Busby and Putirka, 2009) and to Pliocene epeirogenic uplift driven by mantle lithosphere delamination (Stock et al., 2004; Figueroa and Knott, 2010; Saleeby et al., 2013a; Krugh and Foreshee, 2018). In contrast, the southern ~100 km of the block diagram reveals much more local relief than regions to the north regardless of its lower position on the regional southward topographic gradient. This local relief pattern has developed in response to early Neogene normal faulting of the southern Sierra Nevada system (Figs. 1 and 17A). Finally, the oblique DEM of Figure 16B, as well as the DEM base for Figure 16A, clearly show the anomalous topographic relief of the Kern range front region and adjacent Kern arch relative to the greater western Sierra Foothills to the north. The spatial correspondence of this anomalous uplift zone, as well as the anomalous subsidence in the Tulare sub-basin to the underlying anomalous upper-mantle structure is clearly rendered in Figure 16B.

Contemporary Deformation Field

Seismicity within the southern Sierran microplate is concentrated to the east and south of the delamination hinge shown on Figure 16 (Nadin and Saleeby, 2010; Brossy et al., 2012; Unruh et al., 2014). Larger events, or event clusters, indicate dextral slip along the eastern Sierra escarpment, east-west extension along the northern Kern Canyon fault, sinistral slip along the eastern White Wolf fault, and reverse slip along the western White Wolf fault (Jones and

Dollar, 1986; Bawden, 2001; Clinton et al., 2006; Goebel et al., 2016). Reverse slip along the western White Wolf fault is readily related to the Quaternary Tehachapi–San Emigdio fold-thrust belt (Goodman and Malin, 1992; Gordon and Gerke, 2009; Goebel et al., 2016) and dextral slip along the eastern escarpment system to the Walker Lane Belt (Unruh et al., 2003, 2014; Fig. 1 inset), with these seismic zones in part defining the Sierran microplate boundaries. Seismicity within the southern microplate arises from both localized body forces related to ongoing mantle lithosphere delamination and plate tectonic forces propagating into the internally broken crust of the southern Sierra, where it has lost its mantle lithosphere. Integrated microseismic strain to the east and southeast of the delamination hinge arises from horizontal plain strain and vertical flattening resulting from crustal thinning above asthenosphere that has filled in behind the delaminated mantle lithosphere (Frassetto et al., 2011; Jones et al., 2014; Unruh et al., 2014) and east-west extension driven by asthenosphere flow driven by the westward retreat of the delaminated mantle lithosphere slab (Le Pourhiet et al., 2006; Saleeby et al., 2012).

Superimposed on the east-west extension and horizontal plane strain microseismic strain field are zones of distributed dextral (±extensional) shear interpreted to be the incipient propagation of Walker Lane Belt deformation into the weakened and basally detached crust of the southern Sierra (Unruh et al., 2014). The zones of distributed shear for the most part trend northwestward through the Walker graben between the Bear Mountain and Walker Basin faults and continue northwestward in a zone between the Edison graben and the Kern Gorge and Pond-Poso faults (Fig. 2). We have yet to observe any surface geologic expression of dextral slip along any of these NW-striking members of the southern Sierra system. Holocene sinistral slip along the eastern White Wolf fault and late Quaternary normal scarps along the Breckenridge–Kern Canyon system die out rapidly within the northwest-trending zone of microseismic dextral shear. This is consistent with the orientation of the microseismic dextral shear zone being such that it interferes with, and thus nullifies, the normal extensional strain field of the southern Breckenridge fault, while being antithetic to sinistral slip along the eastern White Wolf fault.

The most current northwestward progression in mantle lithosphere delamination (Fig. 16B) could be working in concert with San Andreas plate margin dynamics in the incipient rerouting of Walker Lane Belt dextral shear components through the Kern arch area as resolved by Unruh et al. (2014). The inflow of asthenosphere into the northwestward-retreating mantle lithosphere slab is kinematically compatible with the overall displacement pattern along the west wall of the San Andreas fault (Fig. 16B). This is consistent with recent geodynamic modeling suggesting that the asthenosphere plays a more active role in lithospheric displacements and deformation than traditionally thought (Semple and Lenardic, 2018). Together, asthenosphere flow into the northwestward delamination zone and northwestward asthenosphere flow and lithosphere displacement along the western wall of the San Andreas fault appear to be enhancing NW-SE shortening across the Tehachapi–San Emigdio fold-thrust belt. Basement and cover strata relationships show greater components of NW-SE shortening westward along the belt (Goodman and Malin, 1992; Gordon and Gerke, 2009; Chapman and Saleeby, 2012). This strain gradient along the belt is imparting a clockwise rotation to the Tertiary section of the San Emigdio Mountains, which, like the Late Cretaceous basement distortion discussed above, is traditionally interpreted as Miocene in age (McWilliams and Li, 1985; Goodman and Malin, 1992; Reid, 2009).

Geodetic studies of the southern Sierra Nevada utilizing GPS monuments show a combination of E-W extension and right shear, consistent with microseismicity studies reviewed above (Nadin and Saleeby, 2010; Hammond et al., 2012). These studies are too early in their data acquisition phases to confidently resolve high-precision vertical displacements. Nevertheless, a synthesis of these and other geodetic data (Saleeby et al., 2013a; Fig. 6) shows a strong spatial correspondence in the pattern of contemporary surface uplift to the surface uplift model of Figure 16A. Significantly, the surface uplift rates currently resolved by the GPS data show the transition from the Breckenridge-Greenhorn horst to the Kern arch to be the fastest uplift rates of the entire Sierran microplate. These geodetic vertical rates (~2 mm/yr) are nearly identical to the geologic rates of Quaternary erosion determined in thermochronologic samples from oil well cores along the eastern Kern arch (Cecil et al., 2014).

CONCLUSIONS

The southern Sierra Nevada and adjacent eastern San Joaquin Basin display a number of features that are globally significant in terms of tectonic, geodynamic, and geomorphic analysis. Owing to a large published database on basement structural geometry and deformational history and on geophysical imaging and modeling, clear patterns in both mantle lithosphere dynamics and basement structure dating back to the Late Cretaceous are shown to have strongly influenced the region's crustal responses to superposed late Cenozoic tectonic regimes. Most significant of these are the early Miocene passage of the Mendocino Triple Junction and the related opening of the Pacific-Farallon slab window and the Pliocene–Quaternary delamination of the region's mantle lithosphere. During the early Miocene, basement faults and areas of dispersed structural disruption were extensively remobilized as high-angle normal and related transfer faults, while, at depth, convective mantle that filled into the slab window drove a transverse zone of basaltic and felsic volcanism. Such faulting and volcanism are lacking in the triple junction migration path along the Sierran microplate to the north, as a result of the main more northern reaches of the microplate having escaped the intense basement and mantle lithosphere disruptions that characterize the southernmost reaches.

Neogene basinal conditions extended continuously from the San Joaquin Basin across the southernmost Sierra Nevada. Distinct phases in late Miocene and Pliocene–Quaternary tectonic forcing denuded the southernmost Sierra Nevada of its Neogene basinal cover and redistributed the derivative detritus into the adjacent San Joaquin Basin. These phases of tectonic forcing can be correlated to the distinct mantle dynamic regimes of the late Miocene break-off of the Sierran microplate from the western margin of the Nevadaplano and to

the Pliocene–Quaternary delamination of the southern Sierra Nevada region mantle lithosphere. These regimes were governed by lithospheric structures that developed in the Late Cretaceous.

The geomorphology of the southernmost Sierra Nevada and the structural and facies relations of the southeastern San Joaquin Basin were strongly influenced by the early Miocene fault system. This fault system created and accentuated sediment accommodation spaces across the entire Neogene basinal track by syndepositional normal growth. As the southern Sierra Nevada was denuded of its early Neogene basinal cover, normal fault structural relief of Miocene age on the basement surface emerged as modern topographic relief. These local relief patterns dominate the modern southernmost Sierra Nevada geomorphology. This has left the southernmost Sierra Nevada and the adjacent southeastern San Joaquin Basin in stark morphologic contrast to each other, in spite of their closely related late Cenozoic geologic history.

ACKNOWLEDGEMENTS

We gratefully acknowledge support from the Gordon and Betty Moore Foundation and the Division of Geological and Planetary Sciences, California Institute of Technology. We acknowledge helpful discussions, sharing of resources, and field excursions with Timothy Elam, Jan Gillespie, A.F. Glazner, S.A. Graham, W.D. Kleck, Larry Knauer, J.S. Lewis, S.A. Reid, F.J. Sousa, and J.R. Unruh. Analyses performed in the isotope geochemistry laboratories of K.A. Farley (California Institute of Technology), G.E. Gehrels and Mihai Ducea (University of Arizona, Tucson), and M. Cosca (U.S. Geological Survey, Denver, Colorado) were of critical importance for this study. We also acknowledge the California Division of Oil and Gas online oil well file database and the California State University, Bakersfield oil well core repository. Co-author J.S. acknowledges J.C. Crowell's influence on pursuing in detail basement-cover strata relationships in working out the Cenozoic tectonics of the southern California region.

REFERENCES CITED

Addicott, W.O., 1965, Miocene macrofossils of the southeastern San Joaquin Valley, California: U.S. Geological Survey Professional Paper 525-C, p. 101–109.

Addicott, W.O., 1970, Miocene Gastropods and biostratigraphy of the Kern River area, California: U.S. Geological Survey Professional Paper 642, 174 p., 21 plates.

Andrew, J.E., Walker, J.D., and Monastero, F.C., 2014, Evolution of the central Garlock fault zone, California: A major sinistral fault embedded in a dextral plate boundary: Geological Society of America Bulletin, v. 127, no. 1–2, p. 227–249, https://doi.org/10.1130/B31027.1.

Argus, D.F., and Gordon, R.G., 1991, Current Sierra Nevada–North America motion from very long baseline interferometry: Implications for the kinematics of the western United States: Geology, v. 19, no. 11, p. 1085–1088, https://doi.org/10.1130/0091-7613(1991)019<1085:CSNNAM>2.3.CO;2.

Atwater, T., and Stock, J., 1998, Pacific–North American plate tectonics of the Neogene southwestern United States: An update: International Geology Review, v. 40, p. 375–402, https://doi.org/10.1080/00206819809465216.

Bandy, O.L., and Arnal, R.E., 1969, Middle Tertiary basin development, San Joaquin Valley, California: Geological Society of America Bulletin, v. 80, p. 783–820, https://doi.org/10.1130/0016-7606(1969)80[783:MTBDSJ]2.0.CO;2.

Baron, D., Negrini, R.M., Golob, E.M., Miller, D.D., Sarna-Wojcicki, A., Fleck, B., Hacker, B., and Erendi, A., 2007, Geochemical correlation and $^{40}Ar/^{39}Ar$ dating of the Kern River ash bed related tephra layers: Implications for the stratigraphy of petroleum-bearing formations in the San Joaquin Valley, California: Quaternary International, v. 178, p. 236–260.

Bartley, J.M., Glazner, A.F., Coleman, D.S., Kylander-Clark, A.R.C., and Friedrich, A.M., 2007, Large Laramide dextral offset across Owens Valley, California, and its possible relation to tectonic unroofing of the southern Sierra Nevada, *in* Till, A.B., Roeske, S.M., Foster, D.A., and Sample, J.C., eds., Exhumation Processes along Major Continental Strike-Slip Fault Systems: Geological Society of America Special Paper 434, p. 129–148, https://doi.org/10.1130/2007.2434(07).

Bartow, J.A., 1984, Geologic map and cross sections of the southeastern margin of the San Joaquin Valley, California: U.S. Geological Survey Miscellaneous Investigations Series Map I-1496, scale 1:125,000.

Bartow, J.A., 1992, Cenozoic stratigraphy of the northern San Joaquin Valley, central California: Field Guide to the Tectonics of the Boundary between the California Central Coast Ranges and the Great Valley of California: American Association of Petroleum Geologists, Pacific Section, p. 512.

Bartow, J.A., and McDougall, K.A., 1984, Tertiary stratigraphy of the southeastern San Joaquin Valley, California: U.S. Geological Survey Bulletin 1529-J, 41 p.

Bartow, J.A., and Pittman, G.M., 1983, The Kern River Formation, Southeastern San Joaquin Valley, California: U.S. Geological Survey, Bulletin 1529-D, 17 p.

Bawden, G.W., 2001, Source parameters for the 1952 Kern County earthquake, California: A joint inversion of leveling and triangulation observations: Journal of Geophysical Research, v. 106, p. 771–785, https://doi.org/10.1029/2000JB900315.

Bedrossian, T.L., Roffers, P.D., Lancaster, J.T., and Short, W.R., 2012, Geologic compilation of Quaternary surficial deposits in southern California: California Geological Survey Special Report 217 (Tehachapi and east half Taft 1:100,000 sheets).

Blythe, A.E., and Longinotti, N., 2013, Exhumation of the southern Sierra Nevada/eastern Tehachapi Mountains constrained by low-temperature thermochronology: Implications for the initiation of the Garlock fault: Lithosphere, v. 5, no. 3, p. 321–327, https://doi.org/10.1130/L252.1.

Brossy, C.C., Kelson, K.I., Amos, C.B., Baldwin, J.N., Kozlowicz, B., Simpson, D., Ticci, M.G., Lutz, A.T., Kozaci, O., Strig, A., Turner, R., and Rose, R., 2012, Map of the late Quaternary active Kern Canyon and Breckenridge faults, southern Sierra Nevada, California: Geosphere, v. 8, no. 3, p. 581–591, https://doi.org/10.1130/GES00663.1.

Busby, C.J., and Putirka, K., 2009, Miocene evolution of the western edge of the Nevadaplano in the central and northern Sierra Nevada: Palaeocanyons, magmatism and structure: International Geology Review, v. 51, p. 670–701, https://doi.org/10.1080/00206810902978265.

Callaway, D.C., 1990, Organization of stratigraphic nomenclature for the San Joaquin Basin, California, *in* Kuespert, J.G., and Reid, S.A., eds., Structure, Stratigraphy, and Hydrocarbon Occurrences of the San Joaquin Basin, California: Bakersfield, California, Pacific Sections, Society of Economic Paleontologists and Mineralogists and American Association of Petroleum Geologists, v. 64, p. 5–21.

Cecil, M.R., Ducea, M.N., Reiners, P.W., and Chase, G.C., 2006, Cenozoic exhumation of the northern Sierra Nevada, California, from (U-Th)/He thermochronology: Geological Society of America Bulletin, v. 118, p. 1481–1488, https://doi.org/10.1130/B25876.1.

Cecil, R., Saleeby, Z., Saleeby, J., and Farley, K., 2014, Pliocene–Quaternary subsidence and exhumation of the southeastern San Joaquin Basin, California, in response to mantle lithosphere removal: Geosphere, https://doi.org/10.1130/GES00882.1.

Chapman, A.D., and Saleeby, J.B., 2012, Geologic map of the San Emigdio Mountains, southern California, Geological Society of America Map and Chart Series MCH101, 1:40,000 scale.

Chapman, A.D., Kidder, S., Saleeby, J.B., and Ducea, M.N., 2010, Role of extrusion of the Rand and Sierra de Salinas schists in Late Cretaceous extension and rotation of the southern Sierra Nevada and vicinity: Tectonics, v. 29, no. 5, 21 p., https://doi.org/10.1029/2009TC002597.

Chapman, A.D., Saleeby, J., Wood, D.J., Piasecki, A., Kidder, S., Ducea, M.N., and Farley, K.A., 2012, Late Cretaceous gravitational collapse of the southern Sierra Nevada batholith, California: Geosphere, v. 8, no. 2, p. 314–341, https://doi.org/10.1130/GES00740.1.

Chapman, A.D., Wood, D.J., Saleeby, J., and Saleeby, Z., 2017, Late Cretaceous to Neogene assembly and disaggregation of the southern Sierra Nevada region, *in* Kraatz, B., Lackey, J.S., and Fryxell, J.E., eds., Field Excursions in Southern California: Field Guides to the 2016 GSA Cordilleran Section Meeting: Geological Society of America Field Guide 45, p. 187–228, https://doi.org/10.1130/2017.0045(05).

Cheadle, M.J., Czuchra, B.L., Byrne, T., Ando, C.J., Oliver, J.E., Brown, L.D., Kaufman, S., Malin, P.E., and Phinney, R.A., 1986, The deep crustal structure of the Mojave Desert, California, from COCORP seismic reflection data: Tectonics, v. 5, p. 293–320, https://doi.org/10.1029/TC005i002p00293.

Clark, M.K., Maheo, G., Saleeby, J., and Farley, K.A., 2005, The non-equilibrium landscape of the southern Sierra Nevada, California: GSA Today, v. 15, no. 9, p. 4–10, https://doi.org/10.1130/1052-5173(2005)015[4:TNLOTS]2.0.CO;2.

Clinton, J.F., Hauksson, E., and Solanki, K., 2006, An evaluation of the SCSN moment tensor solutions: Robustness of the Mw magnitude scale, style of faulting, and automation of the method: Bulletin of the Seismological Society of America, v. 96, p. 1689–1705, https://doi.org/10.1785/0120050241.

Coles, S., Prothero, D.R., Quinn, J.P., and Swisher, C.C., III, 1997, Magnetic stratigraphy of the middle Miocene Bopesta Formation, southern Sierra Nevada, California, *in* Girty, G.H., Hanson, R.E., and Cooper, J.D., eds., Geology of the Western Cordilleran: Perspectives from Undergraduate Research, Pacific Section: Society of Economic Paleontologists and Mineralogists, v. 82, p. 21–34.

Davis, T.L., 1983, Late Cenozoic Structure and Tectonic History of the Western "Big Bend" of the San Andreas Fault and Adjacent San Emigdio Mountains, University of California, Santa Barbara [Ph.D. dissertation]: 578 p., 4 plates.

Davis, T.L., and Lagoe, M.B., 1988, A structural interpretation of major tectonic events affecting the western and southern margins of the San Joaquin Valley, California: Field Trip Guidebook—Pacific Section: Society of Economic Paleontologists and Mineralogists, v. 60, p. 65–87.

Davis, T.L., and Namson, J.S., 2017, Field excursion: Petroleum traps and structures along the San Andreas convergent strike-slip plate boundary, California: American Association of Petroleum Geologists Bulletin, v. 101, no. 4, p. 607–615, https://doi.org/10.1306/011817DIG17040.

DeCelles, P.G., 2004, Late Jurassic to Eocene evolution of the Cordilleran thrust belt and foreland basin system, western USA: American Journal of Science, v. 304, p. 105–168, https://doi.org/10.2475/ajs.304.2.105.

Dibblee, T.W., Jr., and Louke, G.P., 1970, Geologic map of the Tehachapi quadrangle, Kern County, California: U.S. Geological Survey, Miscellaneous Geologic Investigations Map I-607, scale 1:62,500.

Dibblee, T.W., Jr., and Warne, A.H., 1986, Inferred relation of the Oligocene to Miocene Bealville Fanglomerate to the Edison fault, Caliente Canyon area, Kern County, California, *in* Studies of the Geology of the San Joaquin Basin: Pacific Section Society of Economic Paleontologists and Mineralogists, p. 223–232.

Dickinson, W.R., 1997, Tectonic implications of Cenozoic volcanism in coastal California: Geological Society of America Bulletin, v. 109, p. 936–954, https://doi.org/10.1130/0016-7606(1997)109<0936:OTIOCV>2.3.CO;2.

Dickinson, W.R., and Wernicke, B.P., 1997, Reconciliation of San Andreas slip discrepancy by a combination of interior Basin and Range extension and transrotation near the coast: Geology, v. 25, no. 7, p. 663–665, https://doi.org/10.1130/0091-7613(1997)025<0663:ROSASD>2.3.CO;2.

Ducea, M.N., and Saleeby, J.B., 1998, The age and origin of a thick mafic-ultramafic keel from beneath the Sierra Nevada Batholith: Contributions to Mineralogy and Petrology, v. 133, p. 169–185, https://doi.org/10.1007/s004100050445.

Figueroa, A.M., and Knott, J.R., 2010, Tectonic geomorphology of the Sierra Nevada Mountains, California: Evidence for uplift and basin formation: Geomorphology, v. 123, p. 34–45, https://doi.org/10.1016/j.geomorph.2010.06.009.

Flowers, R.M., Shuster, D.L., Wernicke, B.P., and Farley, K.A., 2007, Radiation damage control on apatite (U-Th)/He dates from the Grand Canyon region, Colorado Plateau: Geology, v. 35, no. 5, p. 447–450, https://doi.org/10.1130/G23471A.1.

Flowers, R.M., Ketcham, R.A., Shuster, D.L., and Farley, K.A., 2009, Apatite (U-Th)/He thermochronometry using a radiation damage accumulation and annealing model: Geochimica et Cosmochimica Acta, v. 73, no. 8, p. 2347–2365, https://doi.org/10.1016/j.gca.2009.01.015.

Fox, L.S., 1929, Structural features of the east side of the San Joaquin Valley, California: American Association of Petroleum Geologists Bulletin, v. 13, p. 101–108.

Frassetto, A.M., Zandt, G., Gilgert, H., Owens, T.J., and Jones, C.H., 2011, Lithospheric structure of the Sierra Nevada from receiver functions and implications for lithospheric foundering: Geosphere, v. 7, p. 898–921, https://doi.org/10.1130/GES00570.1.

Furlong, K.P., and Govers, R., 1999, Ephemeral crustal thickening at a triple junction: The Mendocino crustal conveyor: Geology, v. 27, p. 127–130, https://doi.org/10.1130/0091-7613(1999)027<0127:ECTAAT>2.3.CO;2.

Gallagher, K., 2012, Uplift, denudation, and their causes and constraints over geological timescales, *in* Roberts, D.G., and Bally, A.W., eds., Regional Geology and Tectonics: Principles of Geologic Analysis: The Netherlands, Elsevier, p. 608–644, https://doi.org/10.1016/B978-0-444-53042-4.00022-4.

Gilbert, G.K., 1928, Studies of Basin and Range Structure: U.S. Geological Survey Professional Paper 153, 92 p., https://doi.org/10.3133/pp153.

Gilchrist, A.R., and Summerfield, M.A., 1991, Denudation, isostasy and landscape evolution: Processes and Landforms, v. 16, p. 555–562, https://doi.org/10.1002/esp.3290160607.

Glazner, A.F., and Schubert, G., 1985, Flexure of the North American lithosphere above subducted Mendocino fracture zone and formation of east-west faults in the Transverse Ranges: Journal of Geophysical Research, v. 90, p. 5405–5409, https://doi.org/10.1029/JB090iB07p05405.

Goebel, T.H.W., Hosseini, S.M., Cappa, F., Hauksson, E., Ampuero, J.P., Aminzadeh, F., and Saleeby, J.B., 2016, Wastewater disposal and earthquake swarm activity at the southern end of the Central Valley, California: Geophysical Research Letters, v. 43, no. 3, p. 1092–1099, https://doi.org/10.1002/2015GL066948.

Goodman, E.D., and Malin, P.E., 1992, Evolution of the southern San Joaquin Basin and mid-Tertiary transitional tectonics, central California: Tectonics, v. 11, p. 478–498, https://doi.org/10.1029/91TC02871.

Gordan, S.A., and Gerke, H.J., 2009, Controls on petroleum occurrence and exploration prospectiveness in the southernmost San Joaquin Basin, California, *in* Contributions to the Geology of the San Joaquin Basin, California: Pacific Section American Association of Petroleum Geologists, Miscellaneous Publication 48, p. 19–50.

Grove, M., Jacobson, C.E., Barth, A.P., and Vucic, A., 2003, Temporal and spatial trends of Late Cretaceous–early Tertiary underplating of Pelona and related schist beneath southern California and southwestern Arizona, *in* Johnson, S.E., Paterson, S.R., Fletcher, J.M., Girty, G.H., Kimbrough, D.L., and Martín-Barajas, A., eds., Tectonic Evolution of Northwestern México and the Southwestern USA: Geological Society of America Special Paper 374, p. 381–406, https://doi.org/10.1130/0-8137-2374-4.381.

Hake, B.F., 1928, Scarps of the Southwestern Sierra Nevada, California: Geological Society of America Bulletin, v. 39, p. 1017–1030, https://doi.org/10.1130/GSAB-39-1017.

Hammond, W.C., Blewitt, G., Li, Z., Plag, H.P., and Kreemer, C., 2012, Contemporary uplift of the Sierra Nevada, western U.S. from GPS and InSAR measurements: Geology, v. 40, no. 7, p. 667–670, https://doi.org/10.1130/G32968.1.

Haq, B.U., Hardenbol, J., and Vail, P.R., 1987, Chronology of fluctuating sea levels since the Triassic: Science, v. 235, p. 1156–1167, https://doi.org/10.1126/science.235.4793.1156.

Harrison, C.P., and Graham, S.A., 1999, Upper Miocene Stevens Sandstone, San Joaquin Basin, California: Reinterpretation of a petroliferous, sand rich, deep-sea depositional system: American Association of Petroleum Geologists Bulletin, v. 83, no. 6, p. 898–924.

Henry, C.D., and John, D.A., 2013, Magmatism, ash-flow tuffs, and calderas of the ignimbrite flareup in the western Nevada volcanic field, Great Basin, USA: Geosphere, v. 9, p. 951–1008, https://doi.org/10.1130/GES00867.1.

Hewlett, J.S., and Jordon, D.W., 1993, Stratigraphic and combination traps within a seismic sequence framework, Miocene Stevens turbidites, Bakersfield arch, California, *in* Weimer, P., and Posamentier, H.W., eds., Siliciclastic Sequence Sratigraphy: American Association of Petroleum Geologists Memoir 58, p. 135–162.

Hirst, B., 1986, Tectonic development of the Tejon and adjacent areas, Kern County, California, *in* Bell, P., ed., Structure and Stratigraphy of the East Side San Joaquin Valley: Pacific Section American Association of Petroleum Geologists Guidebook, p. 2–8.

Hirst, B.M., 1988, Early Miocene tectonism and associated turbidite deposystems of the Tejon area, Kern County, California, *in* Graham, S.A., ed., Studies of the Geology of the San Joaquin Basin Pacific Section: Los Angeles, California, Society of Economic Paleontologists and Mineralogists, Pacific Section, v. 60, p. 207–222.

Hoffman, A.W., 2004, Sampling mantle heterogeneity through oceanic basalts: Isotopes and trace elements, *in* Carson, R.W., ed., Treatise on Geochemistry, v. 2, The Mantle and Core: Amsterdam, Elsevier Pergamon, p. 61–101.

Hoots, H.W., Bear, L.T., and Kleinpell, W.D., 1954, Geological summary of the San Joaquin Valley, California, *in* Jahns, R.H., ed., Geology of southern California: California Division of Mines Bulletin, v. 170, p.113–129.

Hosford Scheirer, H., and Magoon, L.B., 2003, Age, distribution, and stratigraphic relationship of rock units in the San Joaquin Basin province, California, *in* Hosford Scheirer, H., ed., Petroleum Systems and Geologic Assessment of Oil and Gas in the San Joaquin Basin Province, California: U.S. Geological Survey Professional Paper 1713, chap. 5, 107 p., https://doi.org/10.3133/pp17135.

House, M.A., Wernicke, B.P., and Farley, K.A., 2001, Paleo-geomorphology of the Sierra Nevada, California, from (U-Th)/He ages in apatite: American Journal of Science, v. 301, p. 77–102, https://doi.org/10.2475/ajs.301.2.77.

Imperato, D.P., 1995, Studies of the stratigraphy and structure of the Great Valley of California and implications for plate tectonics [Ph.D. dissertation]: University of California, Santa Barbara, 271 p.
Jennings, C.W., and Bryant, W.A., 2010, Fault activity map of California, California Department of Conservation, California Geological Survey, scale 1:750,000.
Jones, C.H., Reeg, H., Zandt, G., Gilbert, H., Owens, T.J., and Stachnik, J., 2014, P-wave tomography of potential convective downwellings and their sources, Sierra Nevada, California: Geosphere, v. 10, p. 505–533, https://doi.org/10.1130/GES00961.1.
Jones, L.M., and Dollar, R.S., 1986, Evidence of Basin and Range extensional tectonics in the Sierra Nevada: The Durrwood Meadows swarm, Tulare County, California (1983–1984): Bulletin of the Seismological Society of America, v. 76, p. 439–461.
Kistler, R.W., and Ross, D.C., 1990, A strontium isotopic study of plutons and associated rocks of the southern Sierra Nevada and vicinity, California: U.S. Geological Survey Bulletin 1920, 20 p.
Klausing, R.L., and Lohman, K.E., 1964, Upper Pliocene marine strata on the east side of the San Joaquin Valley, California: U.S. Geological Survey Professional Paper 475-D, p. 14–17.
Krugh, W.C., and Foreshee, B.C., 2018, Geomorphic constraints on the incision history of the lower Kern River, southern Sierra Nevada, California: Geosphere, v. 14, no. 3, p. 1101–1118, https://doi.org/10.1130/GES01603.1.
Le Pourhiet, L., and Saleeby, J., 2013, Lithospheric convective instability could induce creep along the San Andreas fault: Geology, v. 41, no. 9, p. 999–1002, https://doi.org/10.1130/G34244.1.
Le Pourhiet, L., Gurnis, M., and Saleeby, J., 2006, Mantle instability beneath the Sierra Nevada Mountains in California and Death Valley extension: Earth and Planetary Science Letters, https://doi.org/10.1016/j.epsl.2006.08.028.
Lettis, W.R., and Unruh, J.R., 1991, Quaternary geology of the Great Valley, California, *in* Dupre, W.R., et al., eds., Quaternary Geology of the Pacific Margin: The Geology of North America, Quaternary Nonglacial Geology: Conterminous U.S.: Boulder, Colorado, The Geological Society of America, v. K-2, p. 164–176.
Li, Y.G., Henyey, T.L., and Silver, L.T., 1992, Aspects of the crustal structure of the western Mojave Desert, California, from seismic reflection and gravity data: Journal of Geophysical Research, v. 97, no. B6, p. 8805–8816, https://doi.org/10.1029/91JB02119.
Liu, L., Gurnis, M., Seton, M., Saleeby, J., Muller, D., and Jackson, J., 2010, The role of oceanic plateau subduction in the Laramide orogeny: Nature Geoscience, v. 3, p. 353–357, https://doi.org/10.1038/ngeo829.
Lock, J., Kelsey, H., Furlong, K., and Woolace, A., 2006, Late Neogene and Quaternary landscape evolution of the northern California Coast Ranges: Evidence for Mendocino triple junction tectonics: Geological Society of America Bulletin, v. 118, no. 9–10, p. 1232–1246, https://doi.org/10.1130/B25885.1.
Loomis, D.P., and Burbank, D.W., 1988, The stratigraphic evolution of the El Paso basin, southern California: Implications for the Miocene development of the Garlock fault and uplift of the Sierra Nevada: Geological Society of America Bulletin, v. 100, p. 12–28, https://doi.org/10.1130/0016-7606(1988)100<0012:TSEOTE>2.3.CO;2.
Loomis, D.P., and Glazner, A.F., 1986, Middle Miocene tectonic uplift of southern San Joaquin Basin, California: The American Association of Petroleum Geologists Bulletin, v. 70, no. 8, p. 1003–1007.
Luffi, P., Saleeby, J.B., Lee, C.A., and Ducea, M.N., 2009, Lithospheric mantle duplex beneath the central Mojave Desert revealed by xenoliths from Dish Hill, California: Journal of Geophysical Research, v. 114, B03202, https://doi.org/10.1029/2008JB005906.
MacPherson, B.A., 1977, Sedimentation and trapping mechanism in upper Miocene Stevens and older turbidite fans of the southeastern San Joaquin Valley, California, *in* Bazeley, B., Steinert, B., and Hancock, S., eds., Late Miocene Geology and New Oil Fields of the Southern San Joaquin Valley: Pacific Section, American Association of Petroleum Geologists, p. 5–36.
Mahéo, G., Saleeby, J., Saleeby, Z., and Farley, K.A., 2009, Tectonic control on southern Sierra Nevada topography, California: Tectonics, v. 28, TC6006, https://doi.org/10.1029/2008TC002340.
Malin, P.E., Goodman, E.D., Henyey, T.L., Li, Y.G., Okaya, D.A., and Saleeby, J.B., 1995, Significance of seismic reflections beneath a tilted exposure of deep continental crust, Tehachapi Mountains, California: Journal of Geophysical Research, v. 100, p. 2069–2087, https://doi.org/10.1029/94JB02127.
McSaveney, M., and Davies, T., 2006, Inferences from the morphology and internal structure of rockslides and rock avalanches rapid rock mass flow with dynamic fragmentation, *in* Evans, S.G., Mugnozza, G.S., Strom, A., and Hermanns, R.L., eds., Landslides from Massive Rock Slope Failure: NATO Science Series, v. 49, Dordrecht, Springer, Netherlands, p. 285–304, https://doi.org/10.1007/978-1-4020-4037-5_16.
McWilliams, M., and Li, Y., 1985, Oroclinal bending of the southern Sierra Nevada batholith: Science, v. 230, p. 172–175, https://doi.org/10.1126/science.230.4722.172.
Michael, E.D., 1960, The geology of the Cache Creek area, Kern County, California [M.S. thesis]: University of California, Los Angeles, 145 p., 5 plates.
Miller, D.D., 1999, Sequence stratigraphy and controls on deposition of the upper Cenozoic Tulare Formation, San Joaquin Valley [Ph.D. dissertation]: Stanford, California, Stanford University, 179 p.
Miller, G.E., 1986, Sedimentology, depositional environment and reservoir characteristics of the Kern River Formation, southeastern San Joaquin Basin, California [M.S. thesis]: Stanford, California, Stanford University, 80 p.
Monastero, F.C., Sabin, A.E., and Walker, J.D., 1997, Evidence for post-early Miocene initiation of movement on the Garlock fault from offset of the Camp Formation, east-central California: Geology, v. 25, p. 247–250, https://doi.org/10.1130/0091-7613(1997)025<0247:EFPEMI>2.3.CO;2.
Nadin, E.S., and Saleeby, J.B., 2008, Disruption of regional primary structure of the Sierra Nevada batholith by the Kern Canyon fault system, California, *in* Wright, J.E., and Shervais, J.W., eds., Ophiolites, Arcs, and Batholiths: A Tribute to Cliff Hopson: Geological Society of America Special Paper 438, p. 429–454, https://doi.org/10.1130/2008.2438(15).
Nadin, E.S., and Saleeby, J., 2010, Quaternary reactivation of the Kern Canyon fault system, southern Sierra Nevada, California: Geological Society of America Bulletin, v. 122, p. 1671–1685, https://doi.org/10.1130/B30009.1.
Nadin, E.S., Saleeby, J., and Wong, M., 2016, Thermal evolution of the Sierra Nevada batholith, California, and implications for strain localization: Geosphere, v. 12, no. 2, p. 377–399, https://doi.org/10.1130/GES01224.1.
Nilsen, T.H., Dibblee, T.W., and Addicott, W.O., 1973, Lower and Middle Tertiary Stratigraphic Units of the San Emigdio and Western Tehachapi Mountains, California: U.S. Geological Survey Bulletin 1372-H, p. H1–H23.
Nugent, L.E., Jr., 1942, The genesis of subordinate conjugate faulting in the Kern River salient, California: The Journal of Geology, v. 50, p. 900–913, https://doi.org/10.1086/625090.
Olson, H.C., 1988, Middle Tertiary stratigraphy, depositional environments, paleoecology, and tectonic history of the southeastern San Joaquin Basin, California [Ph.D. dissertation]: Stanford, California, Stanford University, 353 p.
Olson, H.C., 1990, Early and middle Miocene Foraminiferal paleoenvironments, southeastern San Joaquin Basin, California: Journal of Foraminiferal Research, v. 20, p. 289–311, https://doi.org/10.2113/gsjfr.20.4.289.
Olson, H.C., Miller, G.E., and Bartow, J.A., 1986, Stratigraphy, paleoenvironment and depositional setting of Tertiary sediments, southeastern San Joaquin Basin, *in* Structure and Stratigraphy of the Eastside of the San Joaquin Valley: Pacific Section, American Association of Petroleum Geologists Guidebook, p. 18–56.
Pickett, D.A., and Saleeby, J.B., 1993, Thermobarometry of Cretaceous rocks of the Tehachapi Mountains, California: Plutonism and metamorphism in deep levels of the Sierra Nevada batholith: Journal of Geophysical Research, v. 98, p. 609–629, https://doi.org/10.1029/92JB01889.
Pickett, D.A., and Saleeby, J.B., 1994, Nd, Sr and Pb isotopic characteristics of Cretaceous intrusive rocks from deep levels of the Sierra Nevada batholith, Tehachapi Mountains, California: Contributions to Mineralogy and Petrology, v. 118, p. 198–215, https://doi.org/10.1007/BF01052869.
Pyenson, N.D., Irmis, R.B., Lipps, J.H., Barnes, L.G., Mitchell, E.D., Jr., and McLeod, S.A., 2009, Origin of a widespread marine bonebed deposited during the middle Miocene Climatic Optimum: Geology, v. 37, p. 519–522, https://doi.org/10.1130/G25509A.1.
Quinn, J.P., 1987, Stratigraphy of the middle Miocene Bopesta Formation, southern Sierra Nevada, California, Natural History Museum of Los Angeles, Contributions in Science, v. 393, p. 1–31, 1 plate.
Reid, S.A., 1988, Late Cretaceous and Paleogene sedimentation along the east side of the San Joaquin Basin: Field Trip Guidebook: Pacific Section: Society of Economic Paleontologists and Mineralogists, v. 60, p. 157–171.
Reid, S.A., 2009, Implications of Miocene rotation in the Tehachapi and San Emigdio Mountains on the structure and stratigraphy of the southeastern San Joaquin Basin, *in* Contributions to the Geology of the San Joaquin Basin, California: Pacific Section, American Association of Petroleum Geologists, Miscellaneous Publication 48, p. 1–18.

Reid, S.A., and Cox, B.F., 1989, Early Eocene uplift of the southernmost San Joaquin basin, California: Palm Springs, California, Pacific Section, American Association of Petroleum Geologists Annual Meeting.

Ross, D.C., 1989, The metamorphic and plutonic rocks of the southernmost Sierra Nevada, California and their tectonic framework: U.S. Geological Survey Professional Paper 1381, 159 p., 2 plates.

Saleeby, J., 2003, Segmentation of the Laramide slab-evidence from the southern Sierra Nevada region: Geological Society of America Bulletin, v. 115, p. 655–668, https://doi.org/10.1130/0016-7606(2003)115%3C0655:SOTLSF%3E2.0.CO;2.

Saleeby, J., and Foster, Z., 2004, Topographic response to mantle lithosphere removal, southern Sierra Nevada region, California: Geology, v. 32, p. 245–248, https://doi.org/10.1130/G19958.1.

Saleeby, J., Farley, K.A., Kistler, R.W., and Fleck, R.J., 2007, Thermal evolution and exhumation of deep-level batholithic exposures, southernmost Sierra Nevada, California: Geological Society of America Special Paper, v. 419, p. 39–66, https://doi.org/10.1130/2007.2419(2).

Saleeby, J., Ducea, M., Busby, C., Nadin, E., and Wetmore, P., 2008, Chronology of pluton emplacement and regional deformation in the southern Sierra Nevada batholith, California, *in* Wright, J.E., and Shervais, J.W., eds., Ophiolites, Arcs, and Batholiths: A Tribute to Cliff Hopson: Geological Society of America Special Paper 438, p. 397–427, https://doi.org/10.1130/2008.2438(14).

Saleeby, J., Saleeby, Z., Nadin, E., and Maheo, G., 2009a, Step over in the structure controlling the regional west tilt of the Sierra Nevada microplate: Eastern escarpment to Kern Canyon system, *in* Ernst, W.G., ed., Special Volume on the Nevada Plano: International Geology Review, v. 51, no. 7–8, p. 634–669.

Saleeby, J., Saleeby, Z., Chapman, A.D., and Nadin, E., 2009b, Origin and evolution of the White Wolf fault and the Maricopa basin, southernmost California Great Valley: Geological Society of America Abstracts with Programs, v. 41, no. 7, p. 180.

Saleeby, J., Le Pourhiet, L., Saleeby, Z., and Gurnis, M., 2012, Epeirogenic transients related to mantle lithosphere removal in the southern Sierra Nevada region, Part I: Implications of thermal-mechanical modeling: Geosphere, v. 8, no. 6, p. 1286–1309, https://doi.org/10.1130/GES00746.1.

Saleeby, J., Saleeby, Z., and Le Pourhiet, L., 2013a, Epeirogenic transients related to mantle lithosphere removal in the southern Sierra Nevada region, California, Part II: Implications of rock uplift and basin subsidence relations: Geosphere, v. 9, no. 3, p. 394–425, https://doi.org/10.1130/GES00816.1.

Saleeby, J., Saleeby, Z., and Sousa, F., 2013b, From deep to modern time along the western Sierra Nevada Foothills of California, San Joaquin to Kern River drainages, *in* Putirka, K., ed., Geologic Excursions from Fresno, California, and the Central Valley: Geological Society of America Field Guide 32, p. 37–62, https://doi.org/10.1130/2013.0032(03).

Saleeby, J., Saleeby, Z., Robbins, J., and Gillespie, J., 2016, Sediment Provenance and Dispersal of Neogene–Quaternary Strata of the Eastern San Joaquin Basin and Its Transition into the Southern Sierra Nevada, California: Geosphere, v. 12, no. 6, p. 1744–1773, https://doi.org/10.1130/GES01359.1.

Saleeby, J.B., and Sharp, W.D., 1980, Chronology of the structural and petrologic development of the southwest Sierra Nevada Foothills, California: Geological Society of America Bulletin, Part I, v. 91, p. 317–320; Part II, v. 91, p. 1416–1535.

Saleeby, J.B., Sams, D.B., and Kistler, R.W., 1987, U/Pb zircon, strontium, and oxygen isotopic and geochronological study of the southernmost Sierra Nevada batholith, California: Journal of Geophysical Research, v. 92, p. 10,443–10,466, https://doi.org/10.1029/JB092iB10p10443.

Semple, A.G., and Lenardic, A., 2018, Plug flow in the Earth's asthenosphere: Earth and Planetary Science Letters, v. 496, no. 29, p. 29–36, https://doi.org/10.1016/j.epsl.2018.05.030.

Seton, M., Müller, R.D., Zahirovic, S., Gaina, C., Torsvik, T., Shepard, G., Talsma, A., Gurnis, M., Turner, M., Maus, S., and Chandler, M., 2012, Global continental and ocean basin reconstructions since 200 Ma: Earth-Science Reviews, v. 113, p. 212–270, https://doi.org/10.1016/j.earscirev.2012.03.002.

Sharma, M., Basu, A.R., Cole, R.B., and DeCelles, P.G., 1991, Basalt-rhyolite volcanism by MORB-continental crust interaction: Nd, Sr-isotopic, and geochemical evidence from southern San Joaquin Basin, California: Contributions to Mineralogy and Petrology, v. 109, p. 159–172, https://doi.org/10.1007/BF00306476.

Shields, J.E., and Chapman, A.D., 2016, Late Cretaceous tectonic displacement of sub-continental mantle lithosphere beneath the SW U.S. Cordillera: Mantle xenolith constraints from the Colorado Plateau transition zone (central Arizona): Geological Society of America Abstracts with Programs, v. 48, no. 7, https://doi.org/10.1130/abs/2016AM-285152.

Shuster, D.L., Flowers, R.M., and Farley, K.A., 2006, The influence of natural radiation damage on helium diffusion kinetics in apatite: Earth and Planetary Science Letters, v. 249, no. 3–4, p. 148–161, https://doi.org/10.1016/j.epsl.2006.07.028.

Sousa, F.J., Farley, K.A., Saleeby, J., and Clark, M.K., 2016a, Eocene activity on the western Sierra fault system and its role incising Kings River Canyon: Earth and Planetary Science Letters, https://doi.org/10.1016/j.epsl.2016.01.020.

Sousa, F.J., Saleeby, J., Farley, K.A., Unruh, J.R., and Lloyd, M.K., 2016b, The southern Sierra Nevada pediment, central California: Geosphere, v. 13, no. 2, p. 369–390, https://doi.org/10.1130/GES01389.1.

Stein, R.S., King, G.C.P., and Rundle, J.B., 1988, The growth of geologic structures by repeated earthquakes 2. Field Examples of continental dip-slip faults: Journal of Geophysical Research, v. 93, p. 13,319–13,331, https://doi.org/10.1029/JB093iB11p13319.

Stock, G.M., Anderson, R.S., and Finkel, R.C., 2004, Pace of landscape evolution in the Sierra Nevada, California, revealed by cosmogenic dating of cave sediments: Geology, v. 32, p. 193–196, https://doi.org/10.1130/G20197.1.

Stock, G.M., Anderson, R.S., and Finkel, R.C., 2005, Rates of erosion and topographic evolution of the Sierra Nevada, California, inferred from cosmogenic ^{26}Al and ^{10}Be concentrations: Earth Surface Processes and Landforms, v. 30, p. 985–1006, https://doi.org/10.1002/esp.1258.

Sullivan, R., and Sullivan, M.D., 2013, Markley submarine canyon or something different?: A new Eocene canyon in the Sacramento Basin, northern California: Monterey California, Pacific Section American AAPG-SEG-SEPM Joint Technical Conference, American Association of Petroleum Geologists Search and Discovery article #30275.

Sun, D., Gurnis, M., Saleeby, J., and Helmberger, D., 2017, A dipping, thick segment of the Farallon Slab beneath central U.S.: Journal of Geophysical Research. Solid Earth, v. 122, no. 4, p. 2911–2928, https://doi.org/10.1002/2016JB013915.

Tye, R.S., Goodman, D.K., Hewlett, J.S., and Thompson, P.R., 1993, Integrated stratigraphic and depositional facies analysis of parasequences in a transgressive systems tract, San Joaquin Basin, California, *in* Weimer., P., and Posamentier, H.W., eds., Siliciclastic Sequence Stratigraphy: Recent Developments and Applications: American Association of Petroleum Geologists Memoir, p. 99–133.

Unruh, J., Humphrey, J., and Barron, A., 2003, Transtensional model for the Sierra Nevada frontal fault system, eastern California: Geology, v. 31, p. 327–330, https://doi.org/10.1130/0091-7613(2003)031<0327:TMFTSN>2.0.CO;2.

Unruh, J., Hauksson, E., and Jones, C., 2014, Internal deformation of the southern Sierran microplate associated with foundering lower lithosphere, California: Geosphere, v. 10, p. 107–128, https://doi.org/10.1130/GES00936.1.

Unruh, J.R., 1991, The uplift of the Sierra Nevada and implications for late Cenozoic epeirogeny in the western Cordillera: Geological Society of America Bulletin, v. 103, p. 1395–1404, https://doi.org/10.1130/0016-7606(1991)103<1395:TUOTSN>2.3.CO;2.

Unruh, J.R., Dumitru, T.A., and Sawyer, T.L., 2007, Coupling of early Tertiary extension in the Great Valley forearc basin with blueschist exhumation in the underlying Franciscan accretionary wedge at Mount Diablo, California: Geological Society of America Bulletin, v. 119, p. 1347–1367, https://doi.org/10.1130/B26057.1.

Warhaftig, C., 1965, Stepped topography of the southern Sierra Nevada, California: Geological Society of America Bulletin, v. 76, p. 1165–1172, https://doi.org/10.1130/0016-7606(1965)76[1165:STOTSS]2.0.CO;2.

Wentworth, C.M., Fisher, G.R., Levine, P., and Jachens, R.C., 1995, The Surface of Crystalline Basement, Great Valley and Sierra Nevada, California: A Digital Map Database: U.S. Geological Survey Open-File Report 95-96, 18 p.

Wilson, D.S., McCrory, P.A., and Stanley, R.G., 2005, Implications of volcanism in coastal California for the Neogene deformation history of western North America: Tectonics, v. 24, TC3008, https://doi.org/10.1029/2003TC001621.

Wilson, E.L., and Prothero, D.R., 1997, Magnetic stratigraphy of the upper Miocene "Santa Margarita" and Chanac Formations, Tejon Hills, Kern County, California: Bulletin of the American Association of Petroleum Geologists, v. 81, no. 4, p. 694.

Wolf, R.A., Farley, K.A., and Silver, L.T., 1996, Helium diffusion and low temperature thermochronometry of apatite: Geochimica et Cosmochimica Acta, v. 60, p. 4231–4240, https://doi.org/10.1016/S0016-7037(96)00192-5.

Wood, D.J., and Saleeby, J.B., 1998, Late Cretaceous–Paleocene extensional collapse and disaggregation of the southernmost Sierra Nevada batholith: International Geology Review, v. 39, p. 289–325.

Yan, Z., Clayton, R.W., and Saleeby, J., 2005, Seismic refraction evidence for steep faults cutting highly attenuated continental basement in the central Transverse Ranges, California: Geophysical Journal International, v. 160, p. 651–666, https://doi.org/10.1111/j.1365-246X.2005.02506.x.